

# **Evaluation of small molecule inhibitors of Pin1 for their effects on tissue factor within tumour cells**

**[Oluremi Isola Adeniran]  
[MSc. BSc. (Hons)]**

Thesis submitted for the degree of

Doctor of Philosophy

at

University of Hull

School of Mathematics and Physical Science

Department of Chemistry

University of Hull

December 2019

## Abstract

Most standard anticancer drugs are non-selective in their cytotoxicity towards cancerous versus normal cells. Therefore, there is a need for the development of selective and targeted anticancer agents. Previous studies have reported upregulation of tissue factor (TF) as a regularly observed phenomenon in cancer cells. Others have also identified the *cis-trans* isomerization of pSer-Pro dipeptides by Pin1, controlled by the proline-directed phosphorylation motif, as an essential mechanism in tumor growth and metastasis. The inhibition of the activity of prolyl-protein *cis-trans* isomerase 1 (Pin1) has been reported to preclude TF release. This prevention therefore results in TF accumulation within the cancer cell. The intracellular TF accumulation consequently results in localisation of p53 within the nucleus of the cell, Bax protein overexpression and apoptotic cell death. The aim of this study is to explore the ability of synthetic pSer-Pro motif organic compounds to inhibit Pin1 and to prepare and test some new derivatives of a known small molecule Pin1 inhibitor, with a view to investigating their interference with the proliferative mechanisms specific to cancer cells and the outcome on TF activity and cellular apoptosis. The subsequent self-poisoning of the tumor cells, through the apoptotic mechanism would discriminate between normal and cancerous cells. The synthesis of the target proline-based dipeptide involved a one-pot *in situ* activation and coupling using a carbodiimide while preparation of its *N*-analogue involved a Hofmann-type oxidative decarboxylation of asparagine. An exploration of alternative, non-peptidic molecules for inhibition of Pin1 resulted in design of a class of structure-guided molecules derived from 5-(*p*-methoxyphenyl)-2-methylfuran-3-carbonyl amide. The derivatives were synthesised with modification to the original structure possibly to improve the efficiency. The derivatization resulted in compounds differing in the amino acid moiety whereby the 3-(2-naphthyl)-D-alanine moiety in (**30**), was replaced with D-phenylalanine in (**31**), D-tyrosine in (**32**) and D-tryptophan in (**33**). Using a chromogenic TUNEL assay, cellular

apoptosis was analysed 18 h post-treatment of MDA-MB-231 cells with vehicle control or each of the compounds (100  $\mu$ M). Furthermore, localisation of p53 protein to the nucleus was analysed with a fluorescence microscope while Bax protein and *bax* mRNA expressions were measured by western blot analysis and RT-PCR respectively. Compared to the control sample, compound **32** demonstrated a reduction in number of cells and activity of TF while it demonstrated an increase in both p53 localisation within the nucleus and expression of Bax protein. Additionally, both **30** and **33** exhibited reduced activity towards the analysed parameters in the cells, whereas **31** was substantially inactive. The observed trend can be explained by the degree of ligand potency (efficiency) of the molecules in the active site of Pin1. Compound **32** is highly potent; compounds **30** and **33** are moderately potent whereas compound **31** is less potent. The result of this study suggests that these molecules may function possibly as potential small molecule Pin1 inhibitors and moderators of procoagulant activity of TF hence preventing the consequent growth of tumor cells.

# Acknowledgements

I would like to give all praise and thanks to God Almighty for the grace and privilege to carry out this PhD study.

I would like to thank Dr Andrew Boa (my supervisor), for his patience, guidance, encouragement, and enthusiasm. I am grateful to you for your affability. My thanks also go to Dr Camille Ettelaie (my co-supervisor), for her encouragement, patience and support; I count myself privileged to have enjoyed the tutelage of an experienced academic. My gratitude equally goes to the following people and group of people for their contributions in various ways in the course of this study. Professor Anthony Maraveyas and Dr Grahame Mackenzie, for all their valuable suggestions. My colleagues in Chemistry laboratory: Sunday Abimbade, Arundhasa, Aimilia and Alberto. My colleagues in Biology laboratory: Sophie, Yahaya, Muhammed and Ali. My colleagues in the Department of Chemistry, University of Abuja. The analytical team especially Carol Kenedy for elemental analysis. Pastors Victor and Bothwell as well as all my brethren in the UK and Nigeria for their prayers and moral supports. To my parents, I am highly grateful for your constant prayers and support. I am highly indebted to my uncle, Late 'Femi Adekunle Adeniran, who was responsible for my early education. My sponsors, University of Abuja and TETFund, Nigeria. A million thanks to my friend, Ojo Joel Adeola, you are a friend in need and indeed. I appreciate my children, Jerry, John, Joses and Jemima specially for learning to cope with daddy's absence without complaints during the study period. I am exceptionally grateful to my darling wife, Adebola Victoria, who was always there for me.

Thank you all for your contributions towards the achievement of "the goal".

*Oluremi*

# Table of Contents

Abstract .....	i
Acknowledgements.....	iii
Table of Contents .....	iv
List of Figures .....	viii
List of Schemes .....	x
List of Tables .....	xii
List of Abbreviations .....	xiii
Presentations from this thesis .....	xvii
<b>Chapter 1: Introduction .....</b>	<b>1</b>
1.1 Background .....	1
1.1.1 Cancer.....	1
1.1.2 The cell cycle.....	2
1.1.3 The hallmarks of cancer .....	4
1.1.4 Chemical carcinogenesis.....	8
1.2 Stages involved in carcinogenesis.....	12
1.2.1 Tumor initiation .....	13
1.2.2 Tumor promotion .....	13
1.2.3 Tumor progression .....	15
1.3 Classification of chemical carcinogens.....	15
1.4 Tissue factor .....	18
1.4.1 Structure of tissue factor.....	19
1.4.2 Tissue factor and cancer .....	20
1.5 Small molecule inhibitors .....	20
1.6 Pin1 as a molecular timer .....	24
1.6.1 Modular domain architecture of Pin1 .....	25
1.6.2 Expression of Pin1 in cancer .....	28
1.6.3 Inhibition of Pin1 for cancer therapy.....	28

1.6.4 Structures and Biological Data of Some Known Pin1 Inhibitors .....	29
1.7 Aims and Objectives .....	33
<b>Chapter 2: Materials and methods .....</b>	<b>34</b>
2.1 General (Chemistry) .....	34
2.2 Materials (biology) .....	35
2.3 Chemical Synthesis .....	38
2.3.1 Preparation of amino acid methyl esters .....	39
2.3.2 Synthesis of proline-based dipeptides (peptide coupling) .....	42
2.3.3 Synthesis of amino ( $\beta$ -aminoalanine) derivatives of serylprolyl motif ... ..	44
2.3.4 The Merrifield procedure for peptide synthesis .....	48
2.4 Attempted Phosphorylation Reactions .....	50
2.4.1 Attempted synthesis of <i>O</i> -phosphorylserylproline motif.....	50
2.4.2 Attempted synthesis of <i>N</i> -phosphoryl amino derivatives of the serylprolyl motif.....	51
2.4.3 Attempted preparation of non-hydrolysable phosphonates .....	52
2.4.4 Attempted preparation of diallyl phosphite (19).....	53
2.5 Synthesis of <i>N</i> -Substituted Sulphamic Acids.....	53
2.6 Synthesis of New Derivatives of a Non-peptide PIN1 Inhibitor .....	54
2.6.1 Preparation of ethyl phenacylacetoacetate (22) .....	54
2.6.2 Preparation of Ethyl 2-methyl-5-aryl-3-furoate (23) .....	56
2.6.3 Preparation of 2-Methyl-5-aryl-3-furoic acids (24) .....	57
2.6.4 Preparation of methyl ester of 3-(2-naphthyl)- <i>D</i> -alanine (25) .....	58
2.6.5 Coupling of 2-methyl-5-aryl-3-furoic acid with amino acid esters .....	59
2.6.6 Hydrolysis of methyl ester of the coupled amide .....	62
2.7 Biological protocols.....	65
2.7.1 Cell culture .....	65
2.7.2 Subculturing, harvesting and counting the cells .....	65
2.7.3 Cryopreservation of cells .....	66
2.7.4 Estimation of protein concentration using the Bradford assay.....	66
2.7.5 SDS-polyacrylamide gel electrophoresis (SDS-PAGE) .....	67
2.7.6 Western blot analysis.....	68
2.7.7 Determination of optimum concentration for assay .....	68
2.7.8 Crystal Violet Staining (CVS) Assay .....	69

2.7.9	Determination of cell number by crystal violet assay .....	70
2.7.10	Measurement of cellular apoptosis using the TiterTACS™ chromogenic TUNEL assay. ....	70
2.7.11	Standard Curve for MDA-MB-231 cell count measurement .....	71
2.7.12	Measurement of p53 expression mediated by the synthesized molecules .....	72
2.7.13	Examination of the effect of the synthetic molecules on nuclear localisation of p53 by fluorescence microscopy .....	73
2.7.14	Investigation of the effect of the synthesized molecules on expression of Bax protein by western blot.....	73
2.7.15	Total RNA isolation.....	74
2.7.16	Measurement of mRNA expression by Real-time RT-PCR.....	75
<b>Chapter 3: Discussion – synthetic mimics of Pin1 substrate .....</b>		<b>77</b>
3.1	Synthetic Mimics of Serine-proline motif .....	77
3.1.1	Aims .....	78
3.2	Preparation of Seryl-Proline Dipeptide Derivatives .....	79
3.2.1	Amino acid methyl ester synthesis.....	79
3.2.2	Preparation of seryl-proline derivatives .....	83
3.3	Preparation of Amino Analogues of the Seryl-Prolyl Motif .....	88
3.3.1	N-protection of L-asparagine .....	89
3.3.2	Amide coupling of Z-asparagine (9) with methyl proline (1).....	90
3.3.3	Oxidative decarboxylation of Z-Asn-Pro-OMe (10).....	91
3.4	Phosphoesters of Ser-Pro and related dipeptides: the prodrug approach. ....	94
3.4.1	Proposed phosphoesters of Ser-Pro dipeptide .....	96
3.4.2	Proposed phosphoesters of amino analogues of the seryl-prolyl motif .....	97
3.5	Phosphorylation of Seryl-Proline Dipeptide Derivatives .....	99
3.5.1	Proposed O-phosphoryl serine-proline dipeptide by phosphoramidite approach .....	99
3.5.2	Attempted preparation of O-phosphoryl serine-proline molecule.....	102
3.6	Phosphorylated $\beta$ -aminoalanyl-proline dipeptides .....	103
3.6.1	Proposed N-phosphoryl $\beta$ -aminoalanine-proline dipeptide.....	103
3.6.2	Attempted preparation of N-phosphoryl $\beta$ -aminoalanine-proline dipeptide.....	105

3.7	New Derivatives of a Non-peptide Pin1 Inhibitor .....	106
3.7.1	Aims .....	107
3.7.2	Synthesis of 2-methyl-5-arylfuroic acid .....	107
3.7.3	Preparation of ethyl phenacylacetoacetate (22) .....	107
3.7.4	Preparation of Ethyl 2-methyl-5-aryl-3-furoate (23) .....	110
3.7.5	Preparation of 2-Methyl-5-aryl-3-furoic acids (24) .....	112
3.8	Amide Coupling of (24) with Aromatic D-Amino Acids.....	113
3.8.1	Preparation of methyl ester of 3-(2-naphthyl)-D-alanine (25) .....	113
3.9	Biological evaluation of synthesized potential Pin1 inhibitors .....	117
3.9.1	Examination of the influence of synthesized molecules on MDA-MB-231 cell proliferation .....	117
3.9.2	Cellular apoptosis measured 24 h post-treatment using TUNEL assay.....	118
3.9.3	Analysis of nuclear localisation of p53 following treatment with synthesized molecules.....	120
3.9.4	Synthesized molecules upregulate Bax protein expression in cancer cells .....	123
3.10	Conclusion.....	127
	<b>Bibliography .....</b>	<b>131</b>



# List of Figures

<b>Figure 1.1.</b> The cell cycle. ....	3
<b>Figure 1.2.</b> Metabolism of DNA-reactive carcinogens. ....	10
<b>Figure 1.3.</b> Metabolic activation of benzo[a]pyrene and formation of DNA-adduct.....	11
<b>Figure 1.4.</b> Structure of some examples of polycyclic aromatic hydrocarbons (PAHs) and polycyclic aromatic amines (PAA) and their DNA adducts. ....	11
<b>Figure 1.5.</b> Stages of carcinogenesis.....	13
<b>Figure 1.6.</b> Mechanism of tumor promotion.....	15
<b>Figure 1.7.</b> Structure of Tissue Factor.....	19
<b>Figure 1.8.</b> Energy profile for peptidyl prolyl cis-trans isomerases-catalysed cis-trans isomerization of proline.....	25
<b>Figure 1.9.</b> A barrel representation of the domains of human Pin1. ....	26
<b>Figure 1.10.</b> The ribbon representation of human Pin1 domain architecture. ....	26
<b>Figure 1.11.</b> Pin1 PPlase domain showing the active site bound to a phosphoryl-peptide substrate.....	27
<b>Figure 2.1.</b> Standard curve for the Bradford assay.....	67
<b>Figure 2.2.</b> Standard curve for determination of cell number. ....	72
<b>Figure 3.1.</b> Basic structural skeleton of proposed Pin1 substrate.....	77
<b>Figure 3.2.</b> <sup>1</sup> H NMR spectrum of <b>4</b> in DMSO-d <sub>6</sub> . ....	82
<b>Figure 3.3.</b> Structures of Z-Ser-Pro-OMe and its amino analogue .....	91
<b>Figure 3.4.</b> A diagram showing the concept of prodrug for phosphate esters. ....	95
<b>Figure 3.5</b> Structure of the literature Pin1 inhibitor .....	106

<b>Figure 3.6.</b> $^1\text{H}$ NMR spectrum of <b>22a</b> in $\text{CDCl}_3$ .....	110
<b>Figure 3.7.</b> $^1\text{H}$ NMR spectrum of <b>23a</b> in $\text{DMSO-d}_6$ . ....	111
<b>Figure 3.8.</b> $^1\text{H}$ NMR spectrum of <b>24a</b> in $\text{CDCl}_3$ .....	112
<b>Figure 3.9.</b> $^1\text{H}$ NMR spectrum for <b>27</b> in $\text{CDCl}_3$ . ....	115
<b>Figure 3.10.</b> Assessment of reduction in cell number by the synthesized small molecules.....	118
<b>Figure 3.11.</b> Measurement of induced cellular apoptosis by small molecule Pin1 inhibitors. ....	119
<b>Figure 3.12.</b> Analysis of the effect of the synthetic molecules on nuclear localisation of p53.....	121
<b>Figure 3.13.</b> Molecular structure of compound <b>30</b> .....	122
<b>Figure 3.14.</b> Crystal structure of a model molecule bound to Pin1 active site.....	122
<b>Figure 3.15</b> Examination of expression of Bax protein in cells treated with compounds <b>30</b> , <b>31</b> , <b>32</b> , and <b>33</b> .....	124
<b>Figure 3.16.</b> Analysis of influence of test molecules on bax mRNA expression.....	126

# List of Schemes

<b>Scheme 3.1.</b> Retrosynthetic pathway of phosphoserine-proline molecule. .....	78
<b>Scheme 3.2.</b> Preparation of methyl ester of proline analogues. ....	79
<b>Scheme 3.3.</b> A proposed mechanism for preparation of methyl proline. .....	80
<b>Scheme 3.4.</b> Amide coupling of serine and proline derivatives. ....	83
<b>Scheme 3.5.</b> Formation of oxazolone and racemisation reaction. ....	84
<b>Scheme 3.6.</b> Mechanism of peptide coupling mediated by EDC and HOBt. ....	86
<b>Scheme 3.7.</b> Preparation of serine-proline-based dipeptide <b>6</b> . ....	86
<b>Scheme 3.8.</b> Proposed pathway for synthesis of the amino analogue of serine-proline dipeptide. ....	88
<b>Scheme 3.9.</b> Preparation of amino derivative of serine-proline motif. ....	89
<b>Scheme 3.10.</b> N-protection of asparagine. ....	89
<b>Scheme 3.11.</b> Amide coupling of Z-asparagine with methyl proline. ....	91
<b>Scheme 3.12.</b> Oxidative decarboxylation of Z-Asn-Pro-OMe. ....	92
<b>Scheme 3.13.</b> Synthetic pathway for Z-( $\beta$ -Boc-amino)Ala-Pro-OMe. ....	93
<b>Scheme 3.14.</b> Proposed preparation of phosphoester of Ser-Pro using di-tert-butylphosphorochloridate. ....	97
<b>Scheme 3.15.</b> Preparation of phosphoester of Ser-Pro using the phosphoramidite approach. ....	97
<b>Scheme 3.16.</b> Preparation of phosphoesters of $\beta$ -aminoalanyl-proline using phosphoramidate approach. ....	98
<b>Scheme 3.17.</b> Preparation of phosphoester of $\beta$ -aminoalanylproline using dibenzylphosphorochloridate. ....	98

<b>Scheme 3.18.</b> Preparation of phosphoester of $\beta$ -aminoalanylproline using bis(9-fluorenylmethyl)phosphite.....	99
<b>Scheme 3.19.</b> Preparation of O-phosphoryl serine-proline dipeptide by phosphoramidite approach.....	100
<b>Scheme 3.20.</b> Proposed mechanism of the tetrazole-catalysed O-phosphitylation of the serine-proline dipeptide. ....	101
<b>Scheme 3.21.</b> Planned preparation of O-phosphoryl serine-proline dipeptide by phosphoramidite approach using 4,5-dicyanoimidazole.....	101
<b>Scheme 3.22.</b> Attempted preparation of dialkyl N,N-diisopropylphosphoramidite.....	102
<b>Scheme 3.23.</b> Attempted preparation of di-tert-butyl phosphorochloridate.....	102
<b>Scheme 3.24.</b> Phosphorylation of the $\beta$ -aminoalanyl-proline dipeptide. ....	103
<b>Scheme 3.25.</b> A proposed mechanism of the Atherton-Todd reaction for preparation of N-phosphoryl $\beta$ -aminoalanine-proline derivative. ....	104
<b>Scheme 3.26.</b> Phosphorylation of the $\beta$ -aminoalanylproline dipeptide. ....	104
<b>Scheme 3.27.</b> Attempted synthesis of N-phosphoryl- $\beta$ -aminoalanine-proline dipeptide.....	105
<b>Scheme 3.28.</b> Synthesis of 2-methyl-5-arylfuroic acid.....	107
<b>Scheme 3.29.</b> Formation of the enolate ion from ethyl acetoacetate.....	108
<b>Scheme 3.30.</b> Preparation of alkylated ethyl acetoacetate.....	108
<b>Scheme 3.31.</b> Cyclisation of the intermediate <b>22</b> (ethyl 2-(p-methoxyphenyl)acetoacetate) through Paal-Knoor synthesis. ....	111
<b>Scheme 3.32.</b> Amide coupling of moieties of target Pin1 inhibitor.....	113

# List of Tables

<b>Table 1.1.</b> Categorization of chemical carcinogens based on chemical class.....	17
<b>Table 1.2.</b> Examples of various classes of small molecule inhibitors for treatment of cancer .....	22
<b>Table 1.3.</b> Structures and biological data of some known Pin1 inhibitors .....	30
<b>Table 2.1.</b> C-terminal protected proline and its analogues .....	38
<b>Table 2.2.</b> Synthesized amino acid methyl esters.....	40
<b>Table 2.3.</b> Amount of component amino acids required for 200 mg resin.....	49
<b>Table 3.1.</b> Summary of some important peaks for the methyl ester hydrochlorides.....	81
<b>Table 3.2.</b> Summary of product yield with or without sodium ethoxide. ....	109
<b>Table 3.3.</b> Summary of the characteristic $^1\text{H}$ NMR and $^{13}\text{C}$ NMR signals for the amide-coupled esters of the literature Pin1 inhibitor and its new derivatives. ....	115
<b>Table 3.4.</b> A summary of yield and molecular ion peaks of the new derivatives of the non-peptide inhibitor.....	116
<b>Table 3.5.</b> Analysis of bax mRNA expression in samples treated with synthesized compounds.....	125

# List of Abbreviations

AhR	Arylhydrocarbon receptor
APL	Acute promyelocytic leukaemia
ARNT	AhR nuclear translocator
asTF	Alternatively spliced TF
ATP	Adenosine triphosphate
ATRA	All trans retinoic acid
BAX	Bcl-2 associated X protein
Bcl-2	B-cell CLL/lymphoma 2
BCME	Bis(chloromethyl) ether
BCR-ABL	BCR-ABL fusion gene
BSA	Bovine serum albumin
CD133	Prominin-1
CDK	Cyclin-dependent protein kinase
cDNA	complementary DNA
CSCs	Cancer stem cells
C <sub>T</sub>	Threshold cycle
CVS	Crystal violet staining
CYP	Cytochrome P450
Cyr61	Cysteine-rich angiogenic inducer 61
DAPI	4',6-Diamidino-2-phenylindole dihydrochloride
DIPEA	Diisopropylethylamine
DMEM	Dulbecco's modified eagle's medium
DMF	<i>N,N</i> -Dimethylformamide
DMSO	Dimethylsulfoxide

DNA	Deoxyribonucleic acid
ECM	Extracellular matrix
EDTA	Ethylenediaminetetraacetic acid
EGCG	Epigallocatechin-3-gallate
EGFR	Epidermal growth factor receptors
FACS	Fluorescence-activated cell sorting
FCS	Foetal calf serum
FVII	Factor VII
FVIIa	Activated Factor VII
FX	Factor X
GEF	Guanine nucleotide exchange factor
GLUT 1	Glucose transporter 1
HEF	Human enhancer of filamentation
HSP40	Heat shock protein 40
IL-1	Interleukin-1
KRAS	Kirsten rat sarcoma
LPS	Lipopolysaccharides
mAbs	Monoclonal antibodies
MDM2	Mouse double minute 2
MMP	Matrix metalloproteinase
MT-II	Metallothionein II
NEK2	Never in Mitosis (NIMA) Related Kinase 2
NF- $\kappa$ B	Nuclear factor kappa-light-chain-enhancer of activated B cells
NIMA	Never in mitosis A
NK	Natural killer

NSCLC	Non-small cell lung cancer
PAA	polycyclic aromatic amine
PAH	Polycyclic aromatic hydrocarbon
PAI	Plasminogen-activator inhibitor
PBS	Phosphate buffered saline
PDGF	Platelet-derived growth factor
PERP	p53 apoptosis effector related to PMP-22
PIN1	Peptidyl-prolyl cis-trans isomerase NIMA-interacting 1
PPIases	Peptidyl-prolyl cis/trans isomerases
pRB	retinoblastoma protein
PUMA	P53-upregulated modulator of apoptosis
RNA	Ribonucleic acid
SDS-PAGE	Sodium dodecyl sulfate polyacrylamide gel electrophoresis
SKOV-3	Ovarian cancer cells
SMI	Small molecule inhibitor
TBST	Tris buffered saline with Tween 20
TCCD	2,3,7,8-tetrachlorodibenzo-p-dioxin
TF	Tissue factor
TFA	Trifluoroacetic acid
TMEDA	Tetramethylethylenediamine
TNF	Tissue necrosis factor
TP53	Tumour protein p53
TUNEL	Terminal deoxynucleotidyl transferase dUTP Nick End Labeling
VEGF	Vascular endothelial growth factor



XREs

Xenobiotic-responsive elements

## **Presentations from this thesis**

Adeniran OI, Boa AN, Ettelaie C, Maraveyas A. (2018) Studies towards design of a potential therapeutic anticancer agent (Poster). Presented at RSC Chemical Biology and Bio-organic Postgraduate Symposium. University of Leeds, UK.

Adeniran OI, Mohammad AM, Maraveyas A, Boa AN, Camille Ettelaie C. (2018) Design and analysis of small compounds to restrain the functions of tissue factor within tumor cells (poster). Presented in BSHT Annual Scientific Meeting. University of Warwick, UK.

# Chapter 1: Introduction

---

## 1.1 BACKGROUND

Cancer represents a group of malignant diseases that distinctively exhibits uninhibited proliferation and metastasis of abnormal cells. Universally, it ranks high among chief causes of death.<sup>1</sup> Though the causes of cancer remain to be understood in detail, many known risk factors increase its incidence, including use of tobacco, excess body weight and congenital genetic mutations.

One observation regarding this complex disease comes in the reports of induction and high levels of a protein called tissue factor (TF) in numerous types of cancer, such as breast and lung cancers.<sup>2</sup> Many factors are indicated in the enhancement of expression of TF in tumor tissues, including hypoxia and genetic mutations of oncogenes, such as viral oncogene homologue of Kirsten rat sarcoma (KRAS), or tumor suppressor proteins such as tumor protein p53 (TP53).<sup>3</sup> Therefore, TF has been identified as a molecule of interest in development of new ways for treating cancers. This introduction will describe briefly the cell division cycle, identify the hallmarks of cancer, and explain the key stages of the carcinogenesis process. Later it will explain the role of tissue factor in cells, and in doing this will then explain the role of the enzyme Pin1 in controlling the release of tissue factor microvesicles from cells, and the consequence of what occurs when Pin1 inhibitors block this process.

### 1.1.1 Cancer

Occurring worldwide, cancer constitutes a major health challenge with high rate of mortality. It is a disease with characteristic features including aberrant proliferation and spread of abnormal cells. It is rated only second after cardiovascular disorders among the leading cause of death.<sup>4</sup> The frequency of cancer has dramatically increased over the past century due to changes in economic and social status.<sup>5</sup> It has also been projected that by 2025 there will be an increase in occurrences of this disease to 19.3 million cases per annum

worldwide.<sup>6</sup> Cancer is a multi-step process involving cells undergoing metabolic and behavioural alterations resulting in their excessive and premature proliferation.<sup>7</sup> These alterations are consequences of modifications to the mechanisms regulating cell propagation, lifespan and capability for immune system evasion. For proper structure and function of tissue, cell proliferation occurs in an ordered sequential molecular and cellular process known as the cell cycle. This is a process involving replication and segregation of genetic materials between two daughter cells produced newly through mitotic process, as described in section 1.1.2. In cancer, however, aberrant activation of cell division occurs because of loss of cell cycle control over some genetic programs including inactivation of tumor suppressor genes e.g. TP53 and activation of oncogenes e.g. KRAS.<sup>8</sup>

### **1.1.2 The cell cycle**

The typical cell cycle model comprises a succession of transition phases where cells meet certain requirements prior to progression to the next stage. The phases of the cell cycle include the S phase (DNA synthesis) and the M phase (mitosis); two gap phases separate both stages. The S phase is preceded by the G<sub>1</sub> phase while the M phase is preceded by the G<sub>2</sub> phase (Figure 1.1). Subsequent to completion of a cell cycle, the cells that have temporarily stopped dividing or non-dividing cells such as the nerve cells enter into a resting quiescent state, G<sub>0</sub> phase. The Gap 0 phase (G<sub>0</sub>) represents a resting stage whereby cells that have stopped dividing move out of the cycle and remain in a state of quiescence. They may maintain this state for a long time until they receive growth factor signals and enter the G<sub>1</sub> phase in preparation for cell division. In eukaryotes, the cells generally enter quiescence from G<sub>1</sub>. Epithelial cells however do not enter the G<sub>0</sub>, and therefore they continue to divide all through the lifetime of the cell. The G<sub>1</sub> phase is the first within interphase; it is a phase for protein synthesis, cell growth and increasing the number of organelles including mitochondria and ribosomes for the newly divided cells. In this phase, the cell may enter the S phase to continue the cell cycle or enter quiescence to undergo differentiation or, following arrest in G<sub>1</sub> phase, may enter G<sub>0</sub> or re-enter cell cycle. The S phase is characterized by replication of DNA whereby the amount of DNA in the cell is doubled. The G<sub>2</sub>

phase follows the DNA duplication and involves protein synthesis as well as rapid cell growth in preparation of cells for division in the M phase. The cell then divides into two morphologically identical daughter cells during mitosis (M phase).

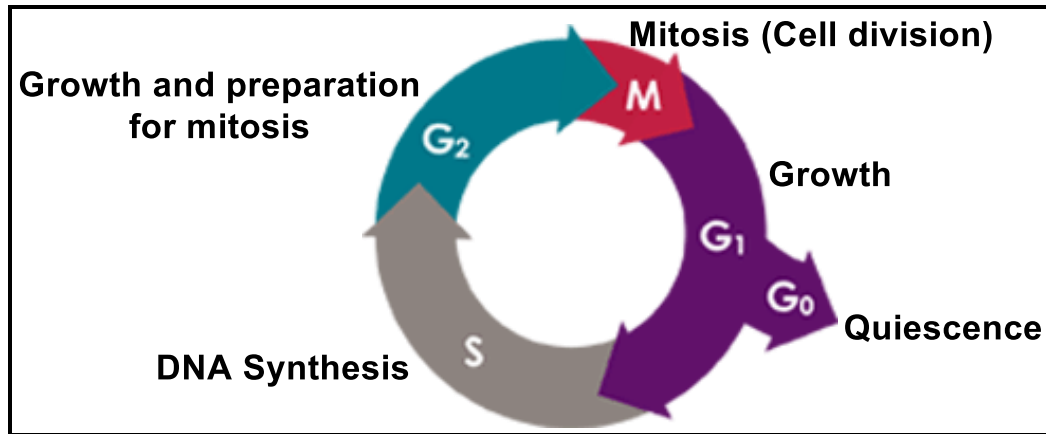


**Figure 1.1.** The cell cycle. In cell cycle, no cell division occurs in the G<sub>0</sub> phase so the cells are quiescent. These cells prepare for division by entering G<sub>1</sub> following stimulation by the growth factor signals. In the G<sub>1</sub> phase, the size increased and everything within the cell except the DNA is duplicated. Duplication of the chromosomes (DNA) takes place in the synthesis (S) phase, prior to cell division. The G<sub>1</sub>/S checkpoint (restriction point) is a checkpoint where cells with damaged DNA, or oncogenic expressions are interrupted from progressing to the S phase by cyclins and tumor suppressor proteins including pRB and p53 pending the repair of the damage. Alternatively, the cell will induce apoptosis (programmed cell death) if the damage is extensive. Defects in the tumor suppressor genes can result in unchecked cell proliferation and cancer. (Adapted from Cooper<sup>9</sup>)

There are points in the cycle, known as checkpoints, for monitoring and regulating the progress of the cell cycle.<sup>10</sup> These checkpoints function to ensure the fidelity of the cell cycle process. The two major checkpoints occur before S and M phases and are known as G<sub>1</sub>/S and G<sub>2</sub>/M checkpoints respectively. The G<sub>1</sub>/S checkpoint (restriction point),<sup>11</sup> functions in checking if the cells have adequate materials for full DNA replication; it is regulated by cyclin D-1 and cyclin E. Similarly, the G<sub>2</sub>/M checkpoint is responsible for ensuring that the cells have enough cytoplasmic materials to be able to

undergo mitosis. Cyclin B-CDK1 complex regulates the progression through this G<sub>2</sub>/M phase transition.

For cell cycle regulation, the level of peptidyl-prolyl isomerase Pin1 expression is vital for cell cycle progression. Pin1 modulates various functions of the cell cycle regulatory proteins via Pin1-mediated *cis-trans* isomerization of key prolyl-serine amide linkages. In addition, it regulates different mitotic proteins for coordination of proper condensation of chromosomes, segregation of chromatids and cell division. Overexpression of Pin1 therefore results in deregulation of cell cycle and malignant cell mutation that may eventually lead to cancer.

Although, cancer is a multifactorial disease, its well-defined hallmarks have been described including achievement of proliferative independence, evasion of growth suppressors, suppression of apoptosis, facilitating limitless replication, invasion and metastasis, sustained angiogenesis, deregulation of metabolic pathways and evasion of immunological destruction.<sup>12,13</sup>

### **1.1.3 The hallmarks of cancer**

In the year 2000 Hanahan and Weinberg<sup>13</sup> described six common traits shared by all cancers. These characteristic and complementary potentials promote tumor growth and metastatic propagation. These hallmarks simplified the understanding of complexities of cancer and some of them are highlighted below.

#### ***Achievement of proliferative independence***

The growth in normal cells and maintenance of tissue homeostasis is controlled by growth signaling produced in a tightly-regulated cell cycle. In contrast, cancer cells deregulate these signals and multiply without stimulation from external signals such as growth factors.<sup>14,15</sup> The capability for growth factor independence and sustaining of proliferative signaling can be achieved by cancer cells in a number of ways, including self-production of growth factor ligands and responding to the same by expressing cognate receptors in order to promote autocrine proliferative signaling. In the alternative, it may be derived from stimulation of the epithelial or stromal cells to aberrantly produce growth-promoting ligands in high levels and shutting down braking signals to growth-inhibiting receptors to allow tumors to escape.<sup>14</sup> In addition, deregulation of cell

cycle processes through oncogenic mutations of oncoproteins such as RAS and its regulatory proteins can also result in enhancement of growth and proliferation.<sup>16</sup>

### ***Evasion of growth suppressor***

In the cell cycle (Figure 1.1), the process of cell division and growth is tightly regulated by mechanisms involving the activities of tumor suppressor proteins such as retinoblastoma (RB) and p53 proteins. For example, on exposure of cells to cellular stress, such as hypoxia, DNA damage and radiation, p53 induces cell cycle arrest or apoptosis to prevent propagation of defective cells. In cancer, these mechanisms are subverted to permit unrestricted proliferation of cells with severe abnormalities. Another mechanism for preventing unchecked cell division is through contact inhibition, (a mechanism involving coupling of cells by E-cadherin with consequent transmission of antigrowth signals) which is a regulatory mechanism whereby normal cells stop dividing when they have fully occupied the entire substrate space available and a monolayer of cells is formed. Typically, this property is lost in cancerous cells and consequently they divide and grow irrepressibly over each other despite being in contact with other cells.<sup>13</sup> Subsequently, the cancer cells invade the surrounding tissues, metastasize to the neighbouring organs and eventually undergo tumorigenesis.

### ***Suppression of apoptosis***

Apoptosis is a coordinated process through which defective cells are programmed for death. The apoptosed cells are subsequently removed from circulation for maintenance of healthy tissue homeostasis. The process involves two pathways. The extrinsic pathway receives and processes external death-inducing signals and involves interaction of death receptors on cell surfaces with their corresponding ligands, for example the Fas ligand/Fas receptor. The other is the intrinsic pathway, which involves detecting and integrating intracellular signals activated through cellular stress including DNA damage and hypoxia. Each of these culminates in activation of cysteine-proteases (caspases) responsible for progressive disassembling of cells through degradation of cellular proteins and eventual consumption by phagocytic cells. Cancer cells evolve various mechanisms to evade apoptosis

including inactivation of mutations involving tumor-suppressor protein p53 thereby rendering the cell unresponsive to apoptotic inducements. Likewise, cancer cells can either upregulate anti-apoptotic proteins including Bcl-X<sub>L</sub> and Bcl-2 or downregulate pro-apoptotic proteins such as Bax, Puma, and Bim through genetic or epigenetic process. Occasionally, tumor cells also short-circuit extrinsic (ligand-induced) cell death pathway by inhibiting caspase activity.<sup>17,18</sup>

### ***Facilitating limitless replication***

Normal cells of the body usually do not undergo successive cell growth and divisions indefinitely, they stop dividing after only a certain number of cycles. Subsequently, they enter into a viable but non-proliferative state (senescence) and then a phase involving cell death (crisis).<sup>19</sup> A body of evidence suggests that the factor responsible for these phenomena is the protective DNA at the end of chromosomes (telomeres).<sup>20</sup> Each cell division results in shortening of telomeric DNA until when critically short and it induces senescence, so cell replication is halted. The enzyme telomerase is known to be responsible for lengthening of telomeric DNA by adding repeat segments of telomere. Cancer cells enable replicative immortality by maintaining telomeric DNA at lengths adequate for preventing induction of senescence or crisis by upregulating telomerase. A small fraction of human tumors (approximately 15%) uses alternative telomere-lengthening pathway which mechanism is yet uncertain.<sup>21</sup>

### ***Sustained angiogenesis***

The process of angiogenesis addresses the need for provision of oxygen and nutrients along with removal of metabolic wastes and carbon dioxide from a tumor. It is a process involving production of new endothelial cells, their arrangement into tubes and sprouting of new vessels from existing ones. The growth and metastasis of tumors depends on angiogenesis.<sup>22</sup> Under physiological conditions, angiogenesis (vasculature) remains essentially quiescent in the adult, except in female reproductive cycle and wound healing when it is transiently turned on. However, in tumor progression, cancer cells obtain the aptitude to activate the 'angiogenic-switch' and keep it on for continuous tumor vascularization in order to address the need of adequate oxygen and nutrients for the expanding tumor.<sup>23</sup> Convincing evidence indicates



that sustained angiogenesis is achieved by overexpressing stimulatory angiogenic regulators of angiogenesis including vascular endothelial growth factor-A (VEGF-A) and decreasing expression of inhibitory angiogenic modulators such as thrombospondin-1 (TSP-1) that bind to the corresponding receptors on vascular endothelial cell surfaces.<sup>24</sup>

### ***Invasion and metastasis***

Essentially, cancer's capability to invade adjacent tissues and those that occur at distant sites is one of its distinctiveness. It involves a sequence of distinct events known as 'invasion-metastasis cascade'.<sup>25</sup> The discrete steps involved in this cascade include local invasion through the extracellular matrix (ECM), by crossing the basement membrane and stromal cells. Others include intravasation by direct migration into adjacent vessels; survival in the circulation by tumor cell-induced platelet aggregation, extravasation into the parenchyma of distant tissues, survival and manipulation of foreign microenvironments to form micrometastases and proliferation to form macroscopic tumors (macrometastases), this last phase of the process is known as 'colonisation'.<sup>26</sup>

### ***Deregulation of energy metabolism***

Normal cells convert glucose under aerobic conditions to pyruvate then to carbon dioxide, and under anaerobic conditions convert the glycolytic pyruvate to lactate. In contrast, cancer cells even in aerobic conditions reprogram their glucose metabolism preferentially to "aerobic glycolysis", a condition involving transformation of glucose in the presence of oxygen to lactate (Warburg effect).<sup>27</sup> Although this metabolic alteration is less efficient than oxidative phosphorylation with respect to production of ATP, it results in increased production of extra metabolites mainly beneficial to proliferating cells.<sup>27</sup> In exhibition of the Warburg effect, cancer cells upregulate the cytosolic glycolysis and prevent mitochondrial oxidation of pyruvate. The pyruvate thus formed is converted by cancer cells to produce the precursors for various biosynthetic pathways such as those producing amino acid and nucleosides. This subsequently facilitate biosynthetic generation of organelles and macromolecules essential for assembly of new cells.<sup>28,29</sup> To compensate for the low ATP production in this process, cancer cells upregulate glucose

transporters particularly GLUT1; this is responsible for the elevated glucose import into the cytosol.<sup>30</sup>

### ***Evasion of immune destruction***

Concrete evidence on transplanted tumors in mice show immune-mediated rejection of the transplantation, thereby supporting the 'cancer immune surveillance' theory.<sup>31</sup> In spite of immune surveillance, tumors continue to grow in bodies where the immune system remains intact. The clones that escape immune surveillance through genetic and epigenetic mutations grow uncontrollably to the point it is detectable clinically. The various escape mechanisms have been categorized broadly under three concepts: (i) prevention of recognition of tumor-antigen mediated by mutation or downregulation of expression of essential molecules for recognition and immune system activation, (ii) resistance to apoptosis, and (iii) induction of immune dysfunction through paralysis of cytotoxic mechanisms of immune system by secreting immunosuppressive factors.<sup>32</sup> Through these mechanisms, the tumor cells enjoy less recognition by the natural killer cells (NK cells) and T-cells as well as less susceptibility to the effector molecules of the immune system.

A recent review of important crosstalk between chemicals and evasion of tumor from immune destruction (a hallmark of cancer), revealed that many chemicals might contribute to carcinogenesis via this mechanism.<sup>33</sup> The following section presents the general mechanisms and stages of carcinogenesis.

#### **1.1.4 Chemical carcinogenesis**

Carcinogenesis can be defined as a process involving uncontrolled cell growth following activation of oncogenes and/or deactivation of tumor suppressor genes. Several factors are responsible for development of cancer and are categorized into exogenous and endogenous factors.<sup>34</sup> The exogenous factors include dietary habits (involving preparation and preservation of foods), lifestyle factor (e.g. consumption of alcohol and tobacco smoking), socio-economic status and chemical substances (natural and synthetic compounds). They also include physical agents (exposure to ionizing radiation and ultraviolet radiation from natural, industrial, medical and other sources) and

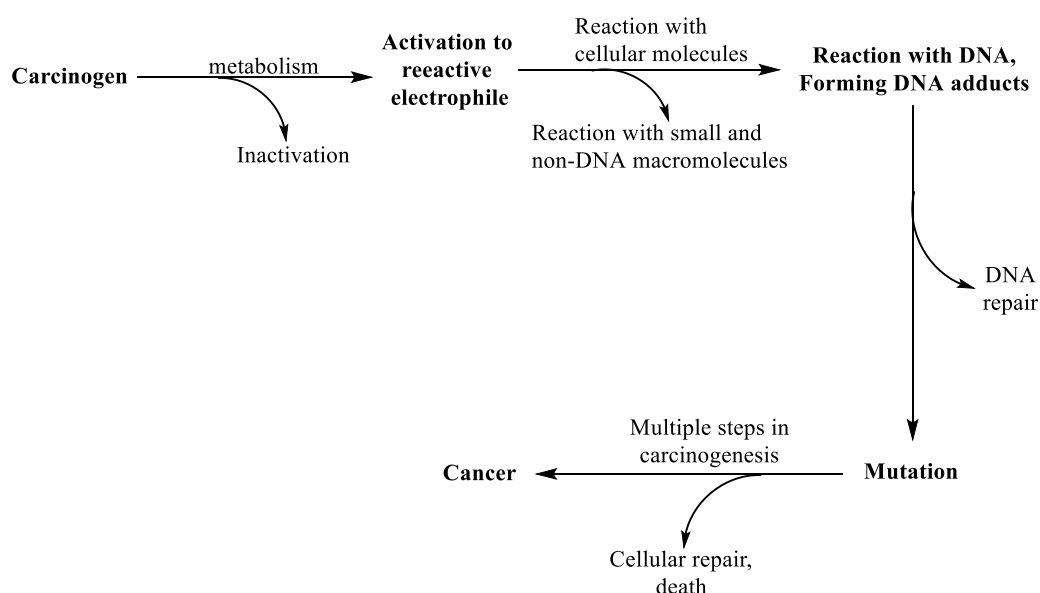
biological agents including various infectious agents such as bacteria or viruses (e.g. *Helicobacter pylori*, hepatitis B virus and human papilloma virus) and parasites (e.g. *Opisthorchis vivarium* and *Schistosoma haematobium*).<sup>35,36</sup> The causal factors for cancer in the endogenous group include genetic susceptibility, endocrine balance, age, inflammation induced by indeterminate aetiology (e.g. pancreatitis and ulcerative colitis), physiological conditions and damage to the immune system.<sup>37,38</sup> Strikingly, viruses have been implicated as a causal element of an estimated 5% of cancers in man and another 5% by radiation, while the remaining 90% are associated with chemicals.<sup>39</sup> There is evidence of a relationship between chemicals and carcinogenesis as discussed in the following sections.

Man has benefited in a number of ways from the use of chemicals, for example, pesticides have been employed in production of adequate quantities of foodstuffs to meet the needs of a large populace thereby increasing levels of life expectancy.<sup>40</sup> However, the side effects resulting from exposure to these chemicals can range from a gradual progression of chemical carcinogenesis to instantaneous death. Association of development of cancer with exposure to chemicals dates back to the time of John Hills' observation of more frequent incidence of nasal cancer among snuff users than the general population.<sup>41</sup> There are essentially two mechanisms involved in chemical carcinogenesis which are DNA-reactive procedure leading to generation of DNA reactivity and genetic abnormalities (genotoxic mechanism) and non-DNA reactive process whereby the risk of cancer is increased by increasing cell proliferation (epigenetic mechanism).<sup>42</sup>

### ***DNA-reactive mechanism***

Development of a common carcinogenic mechanism for chemicals from a variety of classes was not reported until 1970.<sup>43</sup> This report suggested that metabolic activation of an aromatic amide, 2-acetylaminofluorene, resulted in a reactive electrophile capable of establishing adducts with DNA, by binding to DNA, with consequent mutations. Ever since the establishment of this seminal mechanism, the mainstay of carcinogenesis research has been metabolic activation. Apparently, almost all chemicals are metabolised through numerous competing enzyme pathways.<sup>44</sup> The cytochrome P450 isozymes

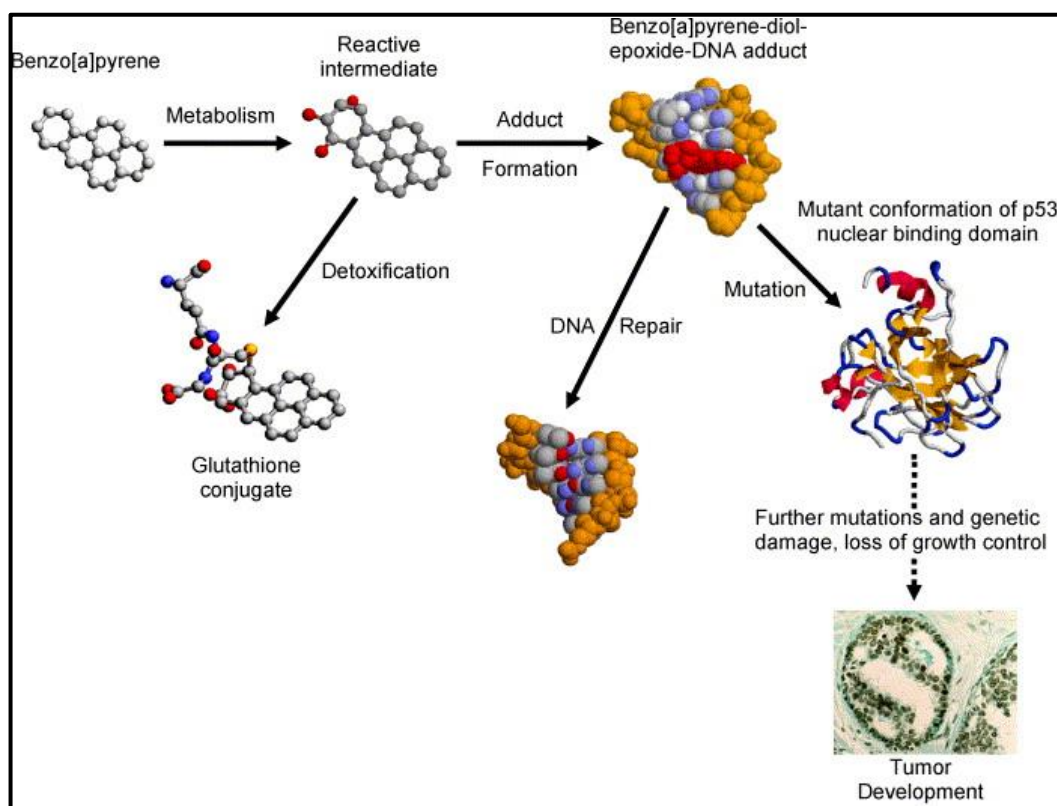
are a common group of enzymes primarily involved in metabolism of carcinogens through participation in oxidation, reduction and hydrolysis reactions. In this process, the enzymes convert the carcinogen into a strong electrophile capable of forming adducts with DNA by introducing into the chemical a reactive polar group thereby making it lipophilic.<sup>45</sup> The high electrophilic reactivity of all chemical carcinogens (or their derivatives), depends on the presence of electron-deficient (electrophilic) atoms in the species, which are capable of reacting with electron-rich (nucleophilic) centres within the cell. The damaging agents particularly form adducts with deoxyribonucleic acid (DNA) through one or more covalent bonds at the nucleophilic sites. However, in metabolism of a range of classes of carcinogens, involvement of several other enzyme systems has also been identified.<sup>46</sup> Although many of the metabolic processes originally result in detoxification of chemicals by promoting their aqueous solubility and subsequent excretion in urine or feces, some were involved in their activation to reactive electrophiles (Figure 1.2, Figure 1.3 and Figure 1.4). Invariably, competing activation and deactivation metabolic pathways are initiated on exposure to any chemicals.



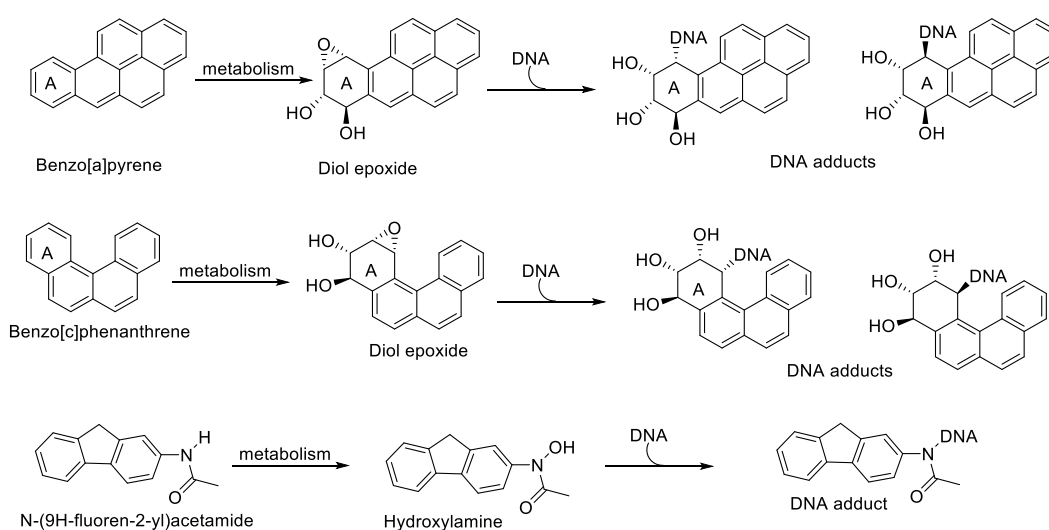
**Figure 1.2.** Metabolism of DNA-reactive carcinogens. A scheme showing competing processes of activation and inactivation of carcinogens (adapted from Cohen<sup>47</sup>).

Figure 1.3 shows a pictorial representation of metabolic activation of a polycyclic aromatic hydrocarbon (PAH) -benzo[a]pyrene- and its formation of

DNA-adduct. In addition, Figure 1.4 shows the general schemes for formation of DNA adducts by polycyclic aromatic amines and polycyclic aromatic hydrocarbons.



**Figure 1.3.** Metabolic activation of benzo[a]pyrene and formation of DNA-adduct. (Source *Runde*<sup>48</sup>).



**Figure 1.4.** Structure of some examples of polycyclic aromatic hydrocarbons (PAHs) and polycyclic aromatic amines (PAA) and their DNA adducts.

*The active mutagenic forms of polycyclic hydrocarbons are epoxide derivatives and the reactive products of aromatic amines are hydroxylamine derivatives.*

### ***Non-DNA-reactive mechanisms***

The non-DNA-reactive or epigenetic mechanism involves modulating cell proliferation by either increasing cell production or decreasing cell deaths.<sup>49</sup> In this process, the carcinogen acts by interacting with specific cellular receptors including nuclear receptors and growth factor receptors. This interaction induces damage to the chromosome and DNA through such mechanisms that interfere with cell cycle control and DNA repair or production of reactive oxygen species.<sup>50</sup> These epigenetic alterations are achieved through specific mechanisms for example, methylation of DNA and histone modifications such as phosphorylation, methylation and acetylation. Further evidence now reveals that carcinogenicity of some chemicals involves hypermethylation of DNA or deacetylation of histone leading to epigenetic silencing of cell cycle regulators or tumor suppressor genes.<sup>51</sup>

Although the hallmarks of cancer have helped tremendously in simplifying the complexities associated with cancer, research is yet to produce an undisputed theory of carcinogenesis. The humoralist and cellular theories are the two main theories in the field. The humoralist theory conceptualises cancer as evolving from an individual's genetic characteristics associated with vulnerability to contract the disease. The cellular theory, however, viewed cancer as originating from a form of chronic irritation. The advocates of the cellular theory supported their claim with experimental studies showing the tumorigenic role of wounding in mouse skin. A body of studies over the years have confirmed carcinogenicity of thousands of chemicals and their transformation of normal cells to tumor cells *in vitro* in animal studies.<sup>39</sup> Therefore, the popular mechanism of carcinogenesis are presented in the following section.

## **1.2 STAGES INVOLVED IN CARCINOGENESIS**

The process of chemical carcinogenesis reasonably divides into three phases namely tumor initiation, tumor promotion and tumor progression stages (Figure 1.5).<sup>52</sup>

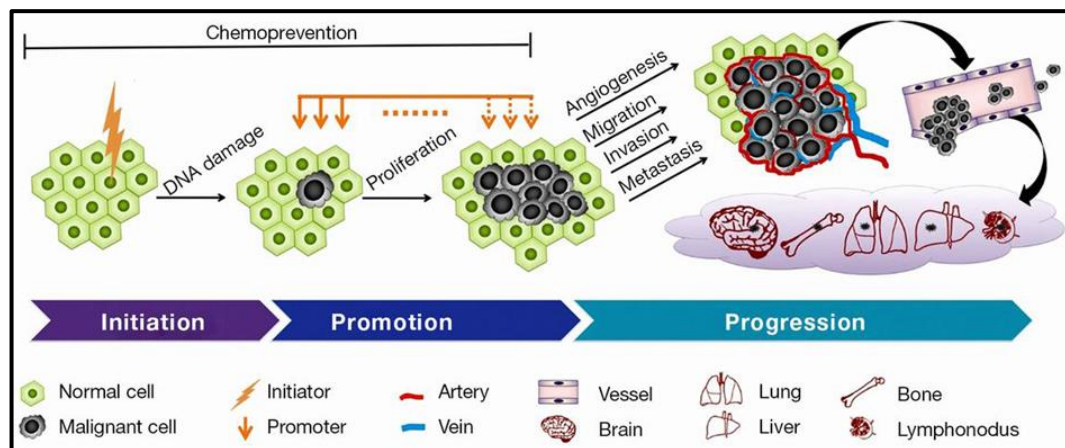


**Figure 1.5.** Stages of carcinogenesis. A diagram showing the stages involved in carcinogenesis (adapted from Liu et al.<sup>53</sup>).

### 1.2.1 Tumor initiation

Tumor initiation results from predisposition of susceptible normal cells to irreversible genetic changes leading to a permanent alteration in the DNA.<sup>54</sup> During tumor initiation phase of chemical carcinogenesis, susceptible normal cells are predisposed to irreversible genetic changes characterized by an intrinsic ability to grow autonomously. These initiated cells can maintain a latency period and ability to grow autonomously for a long period (weeks, months or years) and throughout this period may be indistinguishable phenotypically from the remaining parenchymal cells in that tissue.<sup>55</sup> The initiation process ensures that the initiated cells expands clonally by increasing the number of new cells through inhibition of apoptosis thereby preventing death of initiated cells.<sup>52</sup> The initiating event can be either induced or spontaneous whereby the specific agent responsible for the initiation is unidentified. The spontaneous initiation, which is less frequently occurring than induced initiation may result from compromised DNA polymerase activity during normal processes such as cell division or in the process of DNA repair.<sup>56</sup>

### 1.2.2 Tumor promotion

Tumor promotion is a stage during which the initiated cells are selectively multiplied clonally thus producing a larger population of cells that are susceptible to further genetic mutations and malignant transformations. The mutations in genetic expression and development of benign neoplasia occur

through increase in selective proliferation of initiated cells.<sup>57</sup> In the promotion stage of carcinogenesis, there is no molecular alteration in the DNA structure but changes in the genome expression. The mechanisms of promotion therefore involve expression of genome mediated by information transduction from environmental signals<sup>58</sup>. The promoting agents mediate their effects by binding as ligands to the receptor molecules. The resulting complex then binds to specific DNA regions in a noncovalent mode typically from definite genes. Consequently, the interaction of the receptor-promoter complex with the DNA alters the expression of genes responsible for transduction of signals.<sup>59</sup> Specifically, chemicals e.g. 2,3,7,8-tetrachlorodibenzo-p-dioxin (TCDD) or benzo[a]pyrene (BP) promote tumor through signal transduction mediated by arylhydrocarbon-receptor (AhR) complex. The complex formed between TCDD or BP and AhR is translocated into the cell nucleus following its activation.<sup>60</sup> The AhR nuclear translocator (ARNT) and the AhR complex heterodimerizes within the nucleus. Then xenobiotic-responsive elements (XREs) bind to the heterodimer leading to induction of expression of various types of carcinogen metabolism genes.<sup>61</sup> Such genes include cytochrome P450 (CYPs) such as CYP1A1, CYP1A2 and CYP1B1. In addition, it alters the pattern of expression of some factors that regulate growth and differentiation of cells including metallothionein II (MT-II), plasminogen-activator inhibitor-1 (PAI-1), human enhancer of filamentation 1 (HEF1), guanine nucleotide exchange factors (GEFs), KRAS and COT.<sup>62</sup> Furthermore, pro-apoptosis factors including HSP40 (heat shock protein 40) and TNFs (tissue necrosis factors) are downregulated, however, genes regulating the cell cycle may either be downregulated (e.g. NEK2) or upregulated (e.g. cyclin B2)<sup>63</sup> as illustrated in Figure 1.6.



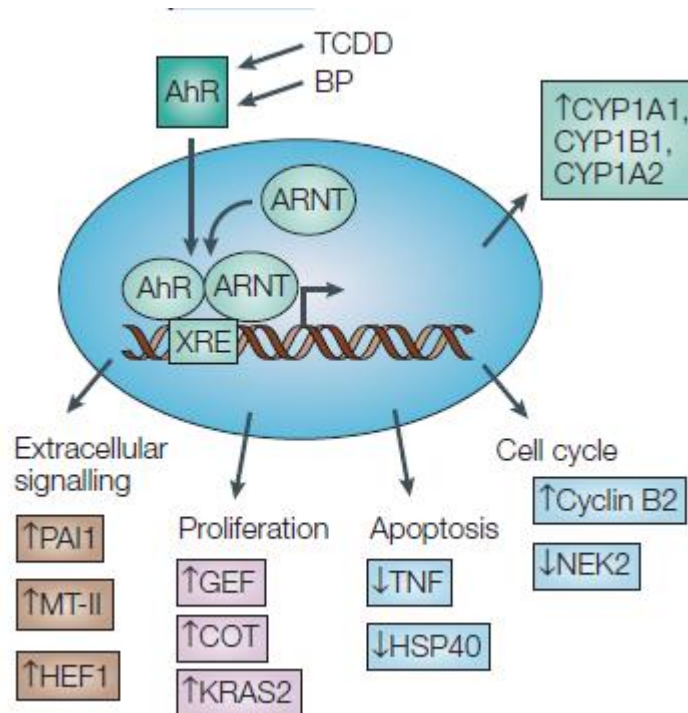


**Figure 1.6.** Mechanism of tumor promotion. Arrows indicate the pattern of gene expression: downregulation (↓) and upregulation (↑) (Adapted from Luch<sup>58</sup>).

### 1.2.3 Tumor progression

In carcinogenesis, the progression stage is that during which initiated cells develop into a population of biologically malignant cells, or a benign neoplasia is transformed into a malign neoplasia. Tumor progression involves a phenotypic acquisition of neoplasia through genotoxic and non-genotoxic mechanisms.<sup>55</sup> It is an irreversible process characterized by progressively increased invasion by neoplasms, development of metastatic ability, genetic perturbation and modifications in biochemical, metabolic and morphologic cellular characteristics.<sup>64</sup> Angiogenesis is a vital epigenetic occurrence to progression of neoplasms. Angiogenic phenotype is acquired prior to the development of contributory characteristics to malignancy and neoplastic development is delayed when it is inhibited.<sup>65</sup>

## 1.3 CLASSIFICATION OF CHEMICAL CARCINOGENS

Categorization of chemical carcinogens based on their mechanism of action remains controversial; however, several other ways of classification have been proposed including grouping based on class of chemicals and as genotoxic

and non-genotoxic compounds. Table 1.1 presents a classification based on chemical class reflecting the group of the carcinogens, specific examples of compounds in the group, mode of action of the group and organs affected by the carcinogens.

**Table 1.1.** Categorization of chemical carcinogens based on chemical class

<b>Group</b>	<b>Specific compound</b>	<b>Mode of action</b>	<b>Target organs</b>
Aminoazo dyes	N,N-dimethyl-4-aminobenzene, o-Aminoazotoluene <sup>66</sup>	Forms adducts with DNA and with haemoglobin	Liver, lungs, Liver, lungs, bladder
Anticancer drugs	Altretamine, Cisplatin, Melphalan, Thiotepa <sup>58</sup>	Interstrand and/or intrastrand cross links	Leukaemia
Aromatic amines/amides	2-Acetylaminofluorene, 4-Aminobiphenyl, 2-Naphthylamine <sup>58</sup>	Increase the rate of cell duplication, Genotoxic compounds.	Liver, bladder Bladder Bladder
Carbamates	Carbofuran, Fenobucarb, Methiocarb, Propoxur <sup>67</sup>	Chromosome aberration, gene mutation, cell transformation	Experimental results showed liver, kidneys and tests degeneration
Halogenated compounds	Chloroethene, Chloroprene, Trichloroethylene <sup>68</sup>	Somatic mutations, modification of cell cycle pathways	Experimental results showed kidney, liver and lung cancer
Metals	Arsenic <sup>69-71</sup>  Cadmium  Nickel	Inhibition of DNA repair pathways, Inhibition of nucleotide excision repair. Acetylation of histone, hypermethylation of DNA and oxidative stress	Liver, lungs, Skin  Kidneys, lungs, prostate,  Nasal cavity, lungs
Natural carcinogens	Aflatoxin B1 <sup>58,72</sup>  Asbestos	React with proteins and RNA, produces adducts with guanine,	Liver  Lungs
N-nitroso compounds	4-(Methylnitrosamino)-1-(3-pyridyl)-1-butanone, N-Nitrosodimethylamine <sup>73</sup>	Form adducts at N- and O-atoms in DNA bases	Liver, lungs, kidneys
Polycyclic aromatic hydrocarbons	Anthanthrene, Benzo[a]pyrene, Dibenzo(a,h)acridine, Polychlorinated biphenyls <sup>58</sup>	Form adducts with purine bases of DNA, mainly resulting on transversions	Skin, lungs, stomach Liver, skin

Another classification of chemicals based on their mechanism of action grouped them into mutagens (initiators), promoters and complete carcinogens. A mutagen typically causes genetic mutations to induce the tumor initiation stage. An initiator may be either itself chemically reactive or a substance that is transformed into a chemically reactive species with the DNA. For example, alkylating agents such as bis(chloromethyl) ether (BCME), cause mutation by reacting with DNA or biological molecules without prior metabolic process whereas 2-naphthylamine must first be metabolised into the hydroxylamine derivative which is the mutagenic agent. Interestingly, Millsom et al.,<sup>74</sup> reported TF overexpression in certain forms of cancer cells that harbour makers of cancer stem cells (CSCs) that is, CD133. It was also postulated that the formation of vascular niche for tumor initiating CSCs might be mediated by TF through its procoagulant and signaling effects. Therefore, therapeutic blockade of TF pathway may inhibit processes of tumor initiation that are CSC-dependent and are involved in onset of tumor, drug resistance, metastasis and recurrence.<sup>75</sup>

#### **1.4 TISSUE FACTOR**

A number of studies have established overexpression of tissue factor (TF) in many tumor cells and detection of its circulation within the bloodstream of cancer patients.<sup>76</sup> In physiologic situations, TF is known principally to initiate blood coagulation and to function as a receptor for cell signaling. Involvement of TF signaling has been reported in processes such as wound healing, angiogenesis and cell migration.<sup>77</sup> However, TF-mediated signaling has also been implicated in disease processes including tumor metastasis.<sup>78</sup> These mechanisms of TF-signaling and release of TF as microvesicles into the bloodstream are controlled by the TF cytoplasmic domain post-translational modifications.<sup>79</sup> Furthermore, it has been shown that the release of TF into microparticles is regulated by phosphorylation of Ser253 and Ser258 within TF cytoplasmic domain.<sup>80</sup> A recent study has identified Pin1 as a crucial moderator that controls the phosphorylation state of TF through a mechanism that modulates its function by interacting with its cytoplasmic domain.<sup>81</sup> The focus of this study is on inhibition of Pin1 to prevent TF release with a view to hindering growth of cancer cells.

### 1.4.1 Structure of tissue factor

Tissue factor is an integral transmembrane receptor and a member of the superfamily of cytokine receptor protein. Structurally, it is a 47kDa single-chain polypeptide comprising 263 amino acids. Its constituent amino acids are divided into three domains as follows: the extracellular domain (first 219 amino acids), the transmembrane domain (the next 23 amino acids) and the cytoplasmic domain (the last 21 amino acid residues) (Figure 1.7). The extracellular domain represents the NH<sub>2</sub>-terminal of the molecule. It binds with factor VIIa in complex formation and in a membrane-dependent manner activates FVII, FIX and FX by increasing the protease activity toward its natural substrates by several orders of magnitude.<sup>82</sup> The transmembrane domain functions in TF pro-coagulant activity and in attaching the bi-complex (TF-FVIIa) to the membrane; the intracellular domain, which represents the COOH-terminal<sup>83</sup> is responsible for signal transduction.<sup>80</sup>

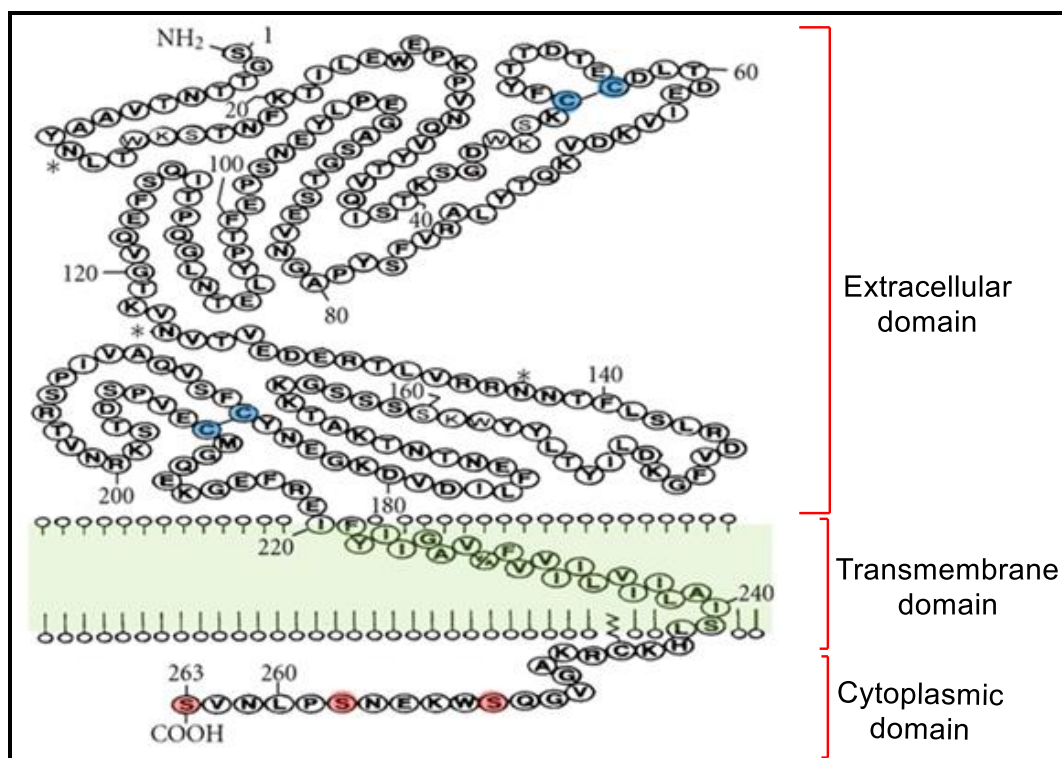


**Figure 1.7.** Structure of Tissue Factor. TF is a single chain 46-kDa membrane-bound polypeptide comprising three domains extracellular, transmembrane, and cytoplasmic domains. In the cytoplasmic domain, the three serine residue that undergo phosphorylation are coloured red (adapted from Chu<sup>84</sup>).

### **1.4.2 Tissue factor and cancer**

Under physiological conditions, the clotting factors contained in the circulating blood are prevented from coming in contact with extravascular TF by a physical barrier (the vascular endothelium) comprising a monolayer of endothelial cells, which act as a semi-permeable membrane. However, in endothelial dysfunction or pathological states such as angiogenesis, inflammation and tumorigenesis, proinflammatory cytokines including TNF- $\alpha$  and TIL-1 cause upregulation of TF expression in endothelial cells, neutrophils and monocyte and macrophages. Yu et al.,<sup>3</sup> suggested that tumor-specific oncogenic events such as loss of p53 and Ras mutation cause expression of TF particularly in cancer. In angiogenic endothelial cells and monocytes, expression of TF is induced by hypoxia through tumor cell-derived VEGF.<sup>85</sup>

Extreme TF expression in numerous tumors and circulation in cancer patient's blood has been discovered. There has been report of expression of TF in cancer cells in various forms of cancer such as colorectal, breast, pancreatic, prostate, hepatocellular and non-small cell lung cancers, glioma, melanoma and leukemia.<sup>86-88</sup> In malignant tumors, increased TF expression corresponds to microvascular density and increased expression of the proangiogenic protein, VEGF, thus implicating TF in tumor angiogenesis.<sup>89</sup> Local factors produced by the tumor probably control the induction of TF in angiogenic endothelium. Furthermore, serine/threonine-specific protein kinases are among the cancer targets that play critical roles in signal transduction pathway. For example, Sánchez-Solana et al.<sup>90</sup> reported that stimulation of p21-activated kinase-1 (PAK1) regulates the procoagulant activity of TF in epithelial cancer cells. In addition, convincing evidence in the area of molecular targeted cancer therapy showed that there are small molecule drugs that target and inhibit these cell-signaling molecules.<sup>6</sup>

## **1.5 SMALL MOLECULE INHIBITORS**

In traditional management of cancer, chemotherapy, surgery and radiotherapy have been widely used for many years.<sup>91</sup> Both single agent and combination chemotherapy when applied have shown some undesirable side effects because of their non-selective action on cancer and normal cells.<sup>91</sup> In addition,

the concomitant adverse side effects of surgery in preventing spread of cancer that commonly include damage to surrounding tissue, surgery-associated bleeding and drug reactions from drugs such as cisplatin, docetaxel and oxaliplatin are some of the drawbacks of this approach.<sup>6</sup> Furthermore, application of radiotherapy for destruction of cancer cells can produce inflammation of soft tissues, damaging of epithelial surfaces and a variety of intestinal discomforts. Therefore, these unwanted side effects have hampered the efficiency of the traditional therapeutic agents and necessitated the search for an effective targeted therapy.<sup>91,92</sup> Clinically, the two effective and most acceptable specific molecular targeting agents are monoclonal antibodies (mAbs) and small molecule inhibitors (SMIs).<sup>93</sup> A comparison of both agents showed that small molecule therapeutic agents are of much reduced size ( $\leq 500$ Da) than the high molecular weight monoclonal antibodies ( $\approx 150$ kDa proteins). The small size of the small molecule inhibitors, which allows for their easy translocation through the plasma membrane, their cost effectiveness and amenability to administration orally made them more preferable than the mAbs that are often intravenously administered and can only interact with cell surface-expressed molecules.<sup>94</sup>

SMIs have been effective in blocking the activity of intracellular key molecules including different proteins involved in cell signaling and tyrosine kinases as well as suppressing biological functions of cancer cells such as differentiation and proliferation.<sup>95</sup> Specific critical cancer targets that are inhibited by most of these agents include heat shock proteins, matrix metalloproteinase, proteasomes and serine/threonine/tyrosine kinases. The indispensable role of protein kinases in almost all signal transduction pathways has made them to gain particular attention as crucial drug targets.<sup>96</sup>

Following the effectiveness of this model drug, new classes of SMIs for targeting cancer of various types have been produced.<sup>92</sup> However, only a few candidates have been able to scale through various stages of clinical trials for approval by FDA. A list of some examples of FDA-approved drugs for cancer therapy is shown overleaf (Table 1.2).

**Table 1.2.** Examples of various classes of small molecule inhibitors for treatment of cancer

<b>Molecular target</b>	<b>Name</b>	<b>Trade name</b>	<b>Particular target</b>	<b>Malignancy</b>	<b>IC<sub>50</sub> (nM)</b>
<b>Tyrosine and Serine/threonine kinases</b>	Axitinib <sup>97</sup>	Inlyata	VEGFR1-3, cKIT, PDGFR,	Renal cell carcinoma	0.1-0.3, 1.7, 1.6
	Bosutinib <sup>98</sup>	Bosulif	Src, Bcr-Abl	CML	No data
	Crizotinib <sup>99</sup>	Xalkori	HGFR	NSCLC	No data
	Everolimus <sup>100</sup>	Afinitor	mTOR	RCC	1.6-2.4
	Gefitinib <sup>101</sup>	Iressa	EGFR	NSCLC	37
	Imatinib <sup>102</sup>	Gleevec	Bcr-Abl	CML	600
	Lapatinib <sup>103</sup>	Tykerb	EGFR, HER2/neu	Breast cancer	10.8, 9.2
	Nilotinib <sup>104</sup>	Tasigna	Bcr-Abl	CML	<30
	Pazopanib <sup>105</sup>	Votrient	VEGFR,PDGFR,FGFR and c-KIT	RCC, soft-tissue sarcoma	140, 74, 84, 10
	Ruxolitinib <sup>105</sup>	Jafaki	Jak1, Jak2	Primary Myelofibrosis	No data
Sorafenib <sup>106</sup>	Nexavar	RAF-1, B-RAF, VEGFR-2	Hepatocellular carcinoma	6, 22, 90	
<b>Proteasomes</b>	Bortezomib <sup>107</sup>	Velcade	26S proteasome	Multiple myeloma	No data
	Carfilzomib <sup>108</sup>	Kyprolis	20S proteasome	Multiple myeloma	No data
	Marizomib	NPI-0052	20S proteasome	Multiple myeloma	No data



**Table 1.2.** Examples of various classes of small molecule inhibitors for treatment of cancer (cont.)

	<b>Name</b>	<b>Trade name</b>	<b>Particular target</b>	<b>Malignancy</b>	<b>IC<sub>50</sub> (nM)</b>
<b>MMPs and HSPs</b>	Batimastat <sup>109</sup>	BB-94	Broad spectrum MMPs	Various tumors	No data
	Neovastat <sup>110</sup>	AE-941	VEGFR-2; MMPs 2,9,12	RCC, NSCL	No data
	Prinomastat <sup>111</sup>	AG-3340	MMPs 2, 3, 9, 13 and 14	RCC	No data
	Rebimastat <sup>112</sup>	BMS-275291	MMPs 1, 2, 8, 9, and 14	NSCLC	No data
<b>Apoptosis</b>	Obatoclax <sup>113</sup>	GX15-070	Bcl-2 family of proteins	Myelofibrosis, lymphoma, leukemia	No data
	Navitoclax <sup>114</sup>	ABT-263	Bcl-w,Bcl-2 and Bcl-xL	Chronic lymphocytic leukemia and lymphoma	No data

As earlier mentioned in section 1.4.2, a body of research has reported TF expression in a variety of cancer. An association between more advanced disease and high expression of TF in malignant tumor has been established. The latter is connected with metastasis,<sup>89</sup> and is a pointer to deficient prognosis.<sup>115</sup> Intriguingly, upregulation of isoforms of alternatively spliced TF (asTF) has been reported in some tumor cells and tumor angiogenesis and cancer cell growth have been shown to be advanced by asTF.<sup>116</sup> Notably, a recent study reported that Pin1 interacts with TF through the pSer<sup>258</sup>-Pro<sup>259</sup> motif in its cytoplasmic domain resulting in increase in the protein's half-life and procoagulant activity thereby acting as a molecular switch.<sup>117</sup>

## 1.6 PIN1 AS A MOLECULAR TIMER

Under normal physiological conditions, expression of TF in vascular endothelial cells is negligible or undetectable.<sup>118</sup> However, pro-inflammatory signaling molecules for example tumor necrosis factor- $\alpha$  (TNF- $\alpha$ ) and lipopolysaccharides (LPs) can promote TF expression and activity in endothelial and smooth muscle cells consequent upon induction of TF expression through activating protein 1 (AP-1) and nuclear factor-kappa B (NF- $\kappa$ B).<sup>119</sup> The enzyme, peptidyl-prolyl *cis-trans* isomerase, NIMA-Interacting 1 (Pin1), modulates the activity of these two transcription factors. Within its substrate proteins, Pin1 catalyses the *cis-trans* isomerization of the peptide bond in pSer/Thr-Pro motif (Figure 1.8). Pin1, through its N-terminal WW binding domain, mediates the protein-protein interaction and substrate specificity while the *cis/trans* isomerization of the peptide bond is catalyzed by the C-terminal prolyl-isomerase (PPIase) domain.<sup>120,121</sup> Induced conformational transformations, mediated through Pin1 catalysed isomerization, results in regulation of protein stability, cell function, protein-protein interaction, subcellular localization and phosphorylation status. Kurakula et al.,<sup>117</sup> reported that in activated vascular cells, Pin1 enhances expression of TF gene and showed direct interaction with TF via pSer<sup>258</sup>-Pro<sup>259</sup> in its cytoplasmic domain. They further suggested that both phosphorylation of

Ser258 and *trans*-isomer of the peptide bond in the pSer<sup>258</sup>-Pro<sup>259</sup> motif are essential requirements for Pin1 interaction with TF. In addition, the group demonstrated that Pin1 increased the half-life and procoagulant activity of the protein. Compelling evidence demonstrates that TF performs instrumental functions in numerous aspects of cancer biology including tumor angiogenesis, tumor growth, metastasis and thrombosis.<sup>122</sup> Moreover, a recent study reported that the conformational-specific interaction of Pin1 with TF prolongs the half-life and procoagulant activity of TF.<sup>117</sup> Therefore the catalytic role and substrate specificity of Pin1 in pSer/Thr-Pro motif isomerization and the subsequent post-transcriptional function in cancer makes Pin1 a possible target for anticancer therapy.

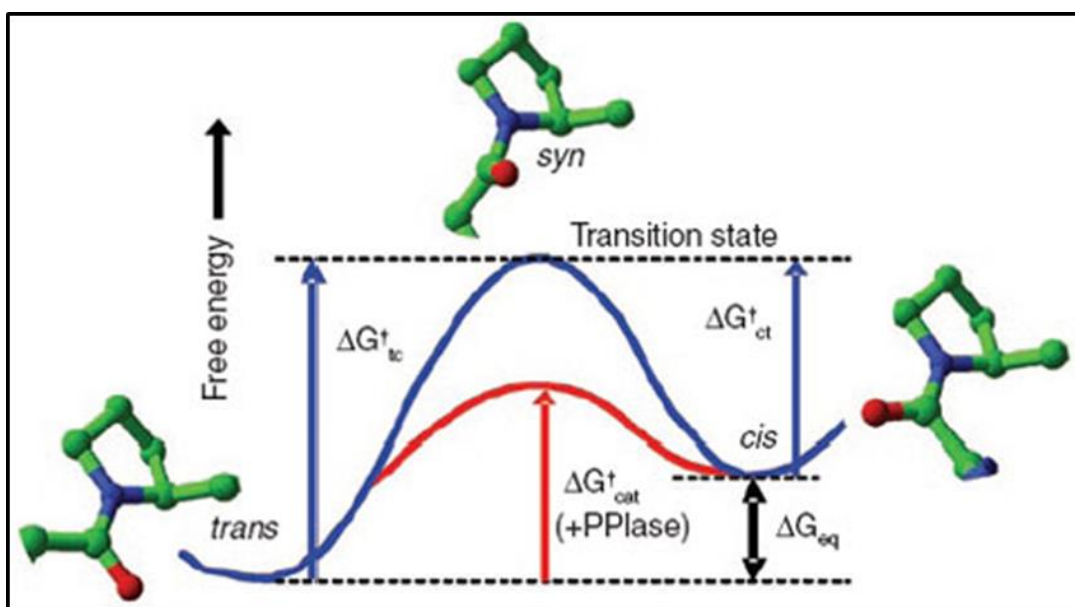


**Figure 1.8.** Energy profile for peptidyl prolyl *cis-trans* isomerases-catalysed *cis-trans* isomerization of proline. The blue curve represents the intrinsic slow process involving the high-energy barrier while the red curve represents the PPIase-catalysed pathway.<sup>123</sup>

### 1.6.1 Modular domain architecture of Pin1

The human Pin1 protein weighs approximately 18 kDa.<sup>124</sup> It is a small monomeric enzyme, which encodes a polypeptide consisting of 163 amino acids divided into two domains. A flexible linker, as shown in the barrel illustration (Figure 1.9), separates both the N-terminal WW domain and the C-

terminal PPlase domain. Equally, Figure 1.10 shows a ribbon representation of both domains of Pin1.

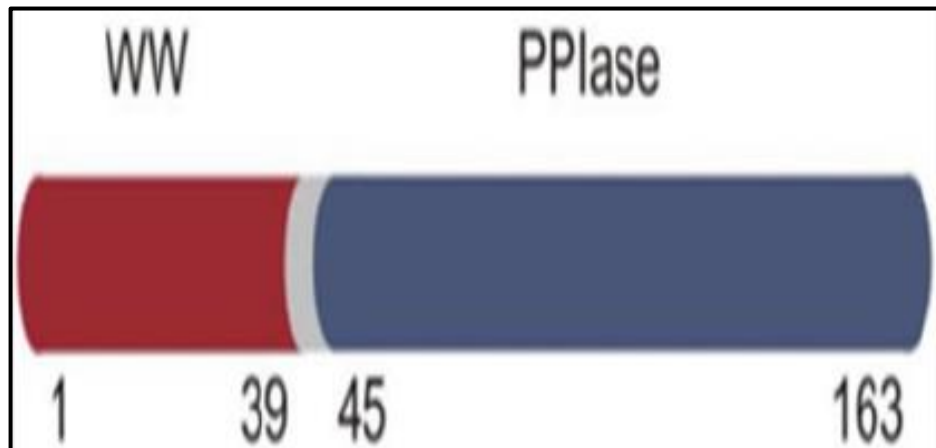


**Figure 1.9.** A barrel representation of the domains of human Pin1. The red region represents the N-terminal WW domain, the blue region represents the C-terminal PPlase domain and the grey region represents the linker.<sup>125</sup>

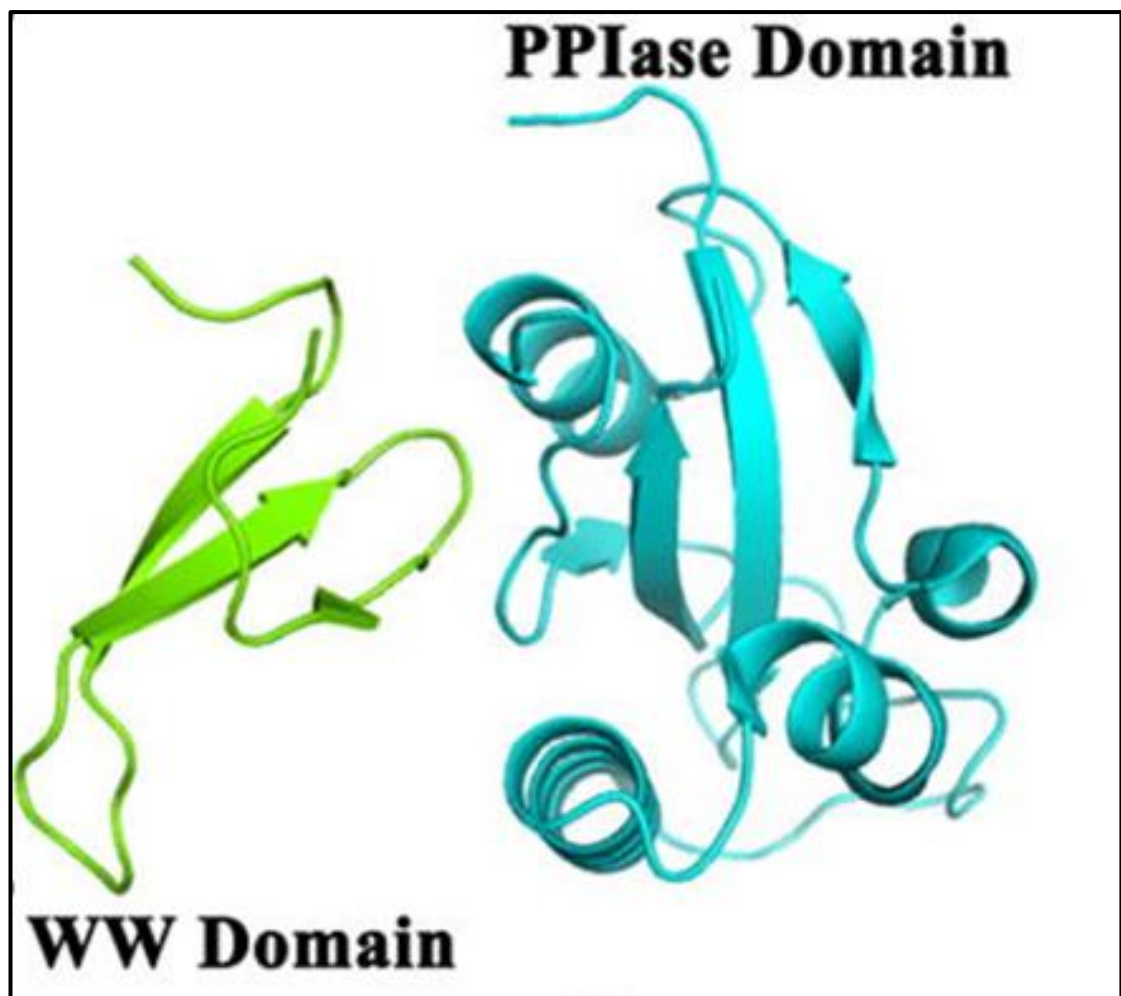


**Figure 1.10.** The ribbon representation of human Pin1 domain architecture. The green colour shows WW domain while the PPlase domain is shown in cyan colour.<sup>126</sup>

The WW domain consists of 39 amino acid residues; the linker region comprises 5 amino acids (residues 40-44) while the PPlase domain consists of 119 amino acids (residues 45-163).<sup>127</sup> Through the WW recognition domain, Pin1 binds to pSer/Thr-Pro motif within the substrate proteins.<sup>128</sup> The active site of the WW domain of human Pin1 comprises a prolyl-binding pocket, a phosphate-binding pocket, and reaction centre.<sup>127</sup> Furthermore, three basic amino acids at the entrance of the active site (Lys63, Arg68, and Arg69), form a cluster that plays a vital role in mediating binding of phosphorylated substrates by providing a selective filter for substrate recognition (Figure 1.11).

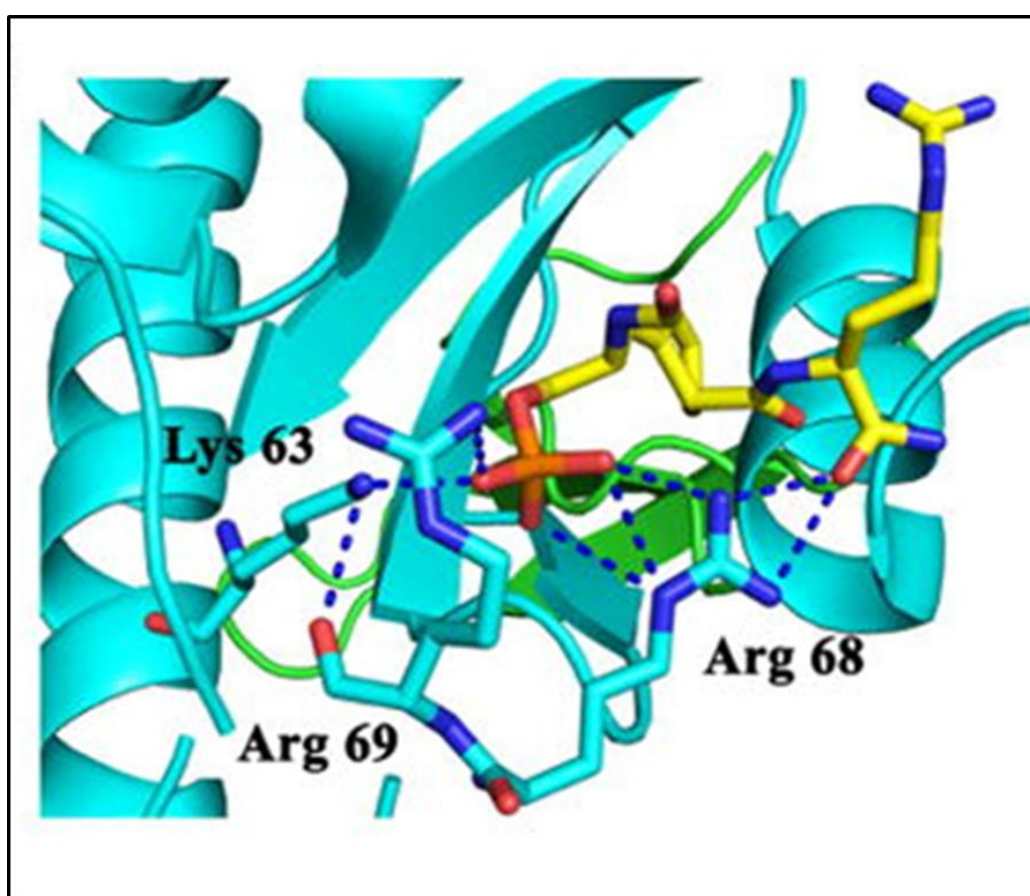


**Figure 1.11.** Pin1 PPlase domain showing the active site bound to a phosphoryl-peptide substrate. The three basic amino acids (Lysine 63, Arginine 68, and Arginine 69), constitute a selective filter for substrate recognition by forming a cluster at the entrance of the active site of the enzyme.<sup>126</sup>

Following binding of a substrate to the binding pocket, a characteristic closure of the active site sequesters the prolyl peptide to undergo the process of *cis*-

*trans* transformation.<sup>129</sup> It is supposed that the isomerization process is facilitated by the spatial arrangement of amino acid residues in the pocket around the prolyl-peptide substrate.

### **1.6.2 Expression of Pin1 in cancer**

Prevalence of overexpression of Pin1 in human cancer has been reported and analyses of a number of human tumors showed that not less than 60% of cancers overexpress Pin1.<sup>130</sup> In accordance with this result, it is found that Pin1 expression is frequently higher in numerous kinds of human cancer than that in their healthy counterparts.<sup>131</sup> Furthermore, cancer prognosis has been associated with Pin1 expression. In some studies on levels of Pin1 expression in prostate cancer, it was shown that subsequent to radical prostatectomy, overexpression of Pin1 correlates positively with a shorter time and a higher probability of tumor recurrence.<sup>132</sup> It has also been reported that in patients with non-small cell lung cancer (NSCLC), high Pin1 expression correlates with lymph node metastasis and poor survival as well as with progression of disease in patients with oral squamous cell carcinoma.<sup>130</sup> Likewise, in esophageal squamous cell carcinoma, Pin1 overexpression was shown to correlate with poor prognosis and metastatic lymph node; it represents an independent prognostic element for the disease.<sup>133</sup> Besides, overexpression of Pin1 has been identified to correlate closely with some biomarkers of tumor in human cancers. For instance, Pin1 expression in oral squamous cell carcinoma is related to accumulation of  $\beta$ -catenin and correlates closely with increased cyclin D1 expression in both oral squamous cell and esophageal squamous cell carcinomas.<sup>133,134</sup> Thus, these reports established the vital role that Pin1 plays in tumorigenesis and tumor progression.

### **1.6.3 Inhibition of Pin1 for cancer therapy**

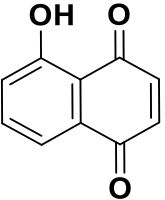
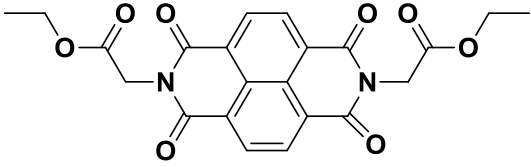
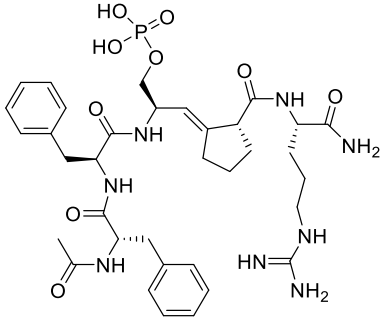
It is validated from fascinating data that Pin1 can be a target in treatment of human cancer using target-based approach. To date, there has been development of a number of effective Pin1 inhibitors that either prevent substrates from binding to Pin1 WW domain or inhibit Pin1 PPLase activity.<sup>135</sup> Some known inhibitors of the PPLase domain currently in use in cell-based enzymatic assays include dipentamethylenethiuram, juglone, PiB, and monosulfide.<sup>123,135</sup> Using structure-guided drug design, low nanomolar small

molecule Pin1 inhibitors have also been discovered, however they often show poor cell permeability.<sup>123,135</sup> Inhibitors exhibiting their activity by binding to the WW domain prevent Pin1 from binding to its substrates. For example, the cancer chemo-preventive agent epigallocatechin-3-gallate (EGCG) has been reported to exert its inhibitory effect on Pin1 by using two of its molecules. The first molecule binds to the WW domain thereby preventing Pin1 interaction with its substrates mediated by WW domain, while the second molecule binds to the PPIase domain thus hindering the isomerization reaction.<sup>136</sup> Though there is development of an array of potent Pin1 antagonists, efficient preclinical and clinical trials for thorough evaluation of safety and their effect on tumor development is required. Success in specifically inhibiting Pin1 and its regulators as key drug targets in cancers may provide a new and efficient approach for elimination of cancer.

#### **1.6.4 Structures and Biological Data of Some Known Pin1 Inhibitors**

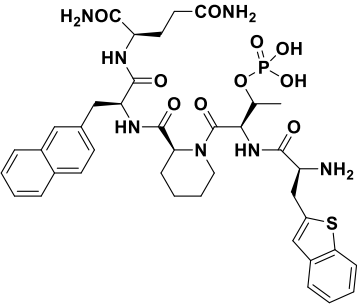
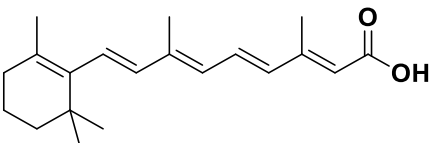
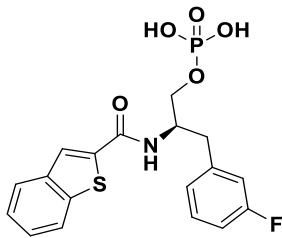
A number of Pin1 inhibitors in several categories have been identified using various means such as mechanism-associated high-throughput screening, PPIase binding assays, as well as substrate-mimicking and structure-based designs<sup>108,109</sup> (Table 1.3).

**Table 1.3.** Structures and biological data of some known Pin1 inhibitors

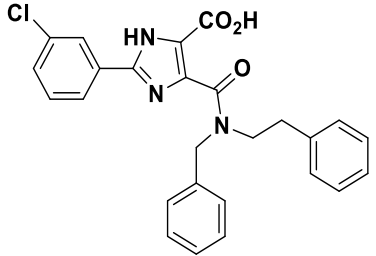
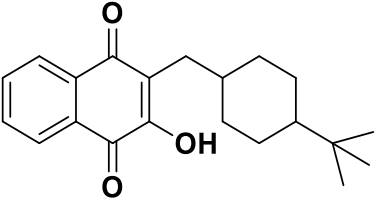
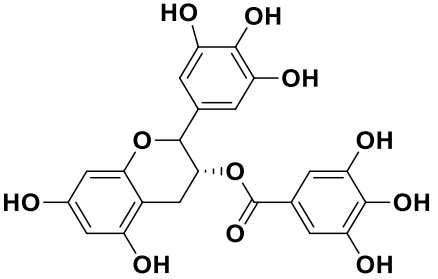
S/N	Pin1 Inhibitor	Chemical structure	IC <sub>50</sub>	Pin1 inhibitory mechanism and specificity	System where inhibition of Pin1 was detected
1	Juglone <sup>137</sup>		Not determined	Cys in the active site of Pin1 and other enzymes containing Cys modified.	<i>In vitro</i>
2	PiB <sup>138</sup>		1.5 μM	Inhibition of Pin1 and parvulin type PPLases; unknown mechanism	<i>In cell lines in vitro</i>
3	Cis-locked peptidomimetics <sup>139</sup>		1.5 μM	Binds as a mimic of a substrate to Pin1 active site.	<i>In cell lines in vitro</i>



**Table 1.3.** Structures and biological data of some known Pin1 inhibitors (Cont.)

S/N	Pin1 Inhibitor	Chemical structure	IC <sub>50</sub>	Pin1 inhibitory mechanism and specificity	System where inhibition of Pin1 was detected
4	pTide <sup>129</sup>		1 nM	Binds to Pin1 active site as a mimic of a substrate with high potency and specificity. Confirmation through study of crystal structure.	<i>In vitro</i> No activity in cell lines
5	ATRA (all trans retinoic acid) <sup>140</sup>		0.8 μM	Induces degradation by binding to Pin1 active site. Confirmation through study of crystal structure.	In human with APL In mouse model In cell lines <i>In vitro</i>
6	Benzothiophene <sup>141</sup>		6 nM	Binds to Pin1 active site as a mimic of a substrate with high potency and specificity. Confirmation through study of crystal structure.	<i>In vitro</i> Inactive in cell lines

**Table 1.3.** Structures and biological data of some known Pin1 inhibitors (Cont.)

S/N	Pin1 Inhibitor	Chemical structure	IC <sub>50</sub>	Pin1 inhibitory mechanism and specificity	System where inhibition of Pin1 was detected
7	Phenyl imidazoles <sup>142</sup>		0.8 μM	Binds to Pin1 active site. Confirmation through study of crystal structure.	In cell lines <i>In vitro</i>
8	Buparvaquone <sup>143</sup>		Not determined	Covalent modification of Cys in active site of TaPin1 secreted by intra-cellular parasites.	In zebrafish In cell lines <i>In vitro</i>
9	EGCG (epigallocatechin-3-gallate) <sup>144</sup>		22 μM	Binds to the PPLase and WW domains of Pin1 and many other targets. Confirmation through study of crystal structure	In vitro In cell lines In mouse model

Since currently available Pin1 inhibitors have shown some limitations, such as activity *in vitro* without activity in cells and non-Pin1-specific inhibition, an urgent need therefore arises for development of more effective and Pin1-specific inhibitors with thorough investigation of the efficiency, potency and side effects of this therapeutic strategy. In addition to efficacy and potency, the therapeutic agent should be able to translocate the plasma membrane and specifically target any molecular part irrespective of the location of the target within. This is a hallmark of small molecule therapeutic agents.

## 1.7 AIMS AND OBJECTIVES

This study aims to prepare and explore the ability of a synthetic metabolically stable mimic of pSer-Pro motif to inhibit Pin1. Another aim is to prepare and test a new class of small molecules for their ability to inhibit Pin1, with a view to investigating their interference with the proliferative mechanisms specific to cancer cells only and the outcome on TF activity and cellular apoptosis. The subsequent self-poisoning of the tumor cells, through the apoptotic mechanism would discriminate between normal and cancerous cells.

Our objectives therefore include:

- Synthesis of phosphorylated Serine-Proline dipeptides to serve as control for other derivatives
- Synthesis of amino analogues (N-derivatives) of the seryl-prolyl motif for probable metabolic stability.
- Preparation of the prodrug forms of the target molecule and its N-derivatives to give the products a chance of being able to cross the cell membrane.
- Preparation of non-labile phosphonate analogues of the target compound
- Synthesis of new derivatives of a non-peptide Pin1 inhibitor
- Cell based assay to investigate the effect of some of the compounds synthesised on tissue factor.

# Chapter 2: Materials and methods

---

## 2.1 GENERAL (CHEMISTRY)

All solvents were of analytical grade. Anhydrous methanol was obtained by adding oven-dried Linde-type 3Å molecular sieves to the supplied solvents and standing it in a stoppered flask until required. Petroleum ether was dried with anhydrous sodium sulphate ( $\text{Na}_2\text{SO}_4$ ) and distilled, while *tert*-butyl alcohol was stood over calcium hydride ( $\text{CaH}_2$ ) and distilled as needed. Merck 200-300 mesh silica gel was used for column chromatography while Merck 60 mesh size precoated aluminium plates were used for thin layer chromatography (TLC). Visualization of TLC bands was at 254 nm using a MINERALIGHT® UV lamp Model UVG-54. Records of NMR signals was obtained with the aid of a spectrometer (Jeol JNM ECP400). Internal standard is TMS  $\delta\text{H} = 0$ , or  $\text{CDCl}_3$   $\delta\text{H} = 7.26$ , or  $(\text{CD}_3)_2\text{SO}$   $\delta\text{H} = 2.50$ , being residual protic solvents. Designation of chemical shifts and coupling constants are in ppm ( $\delta$ ) and Hertz (Hz) respectively. The following notations have been used to denote the peak type, s, d, t, q and m for singlet, doublet, triplet, quartet and multiplet respectively. Frequency of recording  $^1\text{H}$ NMR was 400 MHz while 101 MHz was that for  $^{13}\text{C}$ . The central peak of internal reference for  $^{13}\text{C}$  at 25 °C (298 K) was  $(\text{CD}_3)_2\text{SO}$  ( $\delta\text{C} = 39.5$  ppm) or  $\text{CDCl}_3$  ( $\delta\text{C} = 77.0$  ppm). DEPT 135 sequence was on occasions used in assigning  $^{13}\text{C}$  multiplicities. ES-MS data were collected on HCT ultra ETD II and melting points were taken using a Fischer-Johns apparatus. All glassware was properly cleaned and evaporation of solvents was with a rotary evaporator (BÜCHI Rotavapor R-200).

## **2.2 MATERIALS (BIOLOGY)**

### **Active Motife, Rixensart, Belgium**

- Crystal violet solution

### **Applied Biosystem, Warrington, UK**

- Power SYBR Green RT-PCR mix

### **BD Bioscience, Oxford, UK**

- Becton Dickinson FACS Calibur flow cytometer
- CellQuest software version 3.3
- Falcon FACS tubes

### **BDH, Pool, UK**

- SDS (sodium dodecyl sulphate)
- Glycerol
- Magnesium chloride
- Sodium acetate
- Sodium hydroxide

### **Bio-rad, Hemel Hempstead, Hertfordshire, UK**

- iCycler real-time thermal cycle
- Nitrocellulose membrane

### **BMG lab Tech, Offenburg, Germany**

- POLAR star OPTIMA Plate reader

### **Carl Zeiss Ltd, Welwyn Garden City, UK**

- Zeiss LSM 710 fluorescence microscope
- ZEN software

### **Fermentas, Sankt Leon-Rot, Germany**

- Multicolour broad range protein ladder (10-260 kDa)

### **Fisher scientific, Loughborough, Leicestershire, UK**

- Glycine
- NaCl
- Tris Base
- DAPI (4',6-diamidino-2-phenylindole), NucBlue™ Fixed Cell ReadyProbes™ Reagent

**Flowgen Bioscience, Nottingham, UK**

- Proto FlowGel (acrylamide: bisacrylamide)
- Proto FlowGel, resolving buffer (1.5 M Tris-HCl (ph 8.8), 0.4% (w/v) SDS.)
- Proto FlowGel staking buffer

**Greiner Bio-One Ltd, Gloucestershire, UK**

- 12 well culture plates, 25 and 75 cm<sup>2</sup> cell culture flasks

**Hoefer, Inc, San Francisco, USA**

- TE 50X protein transfer tank

<http://imagej.nih.gov/ij/>

- ImageJ program

**LGC-ATCC, Teddington, UK**

- MDA-MB-231 breast cancer cell line

**Lonza, Basel, Switzerland**

- DMEM medium

**Promega Corporation, Southampton, UK**

- TMB stabilised substrate for horseradish peroxidase
- Western blue stabilised substrate for alkaline phosphatase

**Promocell, Heidelberg, Germany**

- Foetal calf serum (FCS)

**R & D Sytem, Abingdon, UK**

- Donkey anti-rabbit IgG-NL637 NorthernLights
- HT TiterTACS™ apoptosis assay kit

**Santa Cruz Biotechnology, Heidelberg, Germany**

- Donkey anti-goat alkaline phosphatase-conjugated antibody
- Goat-anti-GAPDH polyclonal IgG antibody
- Goat-anti-rabbit alkaline phosphatase-conjugated antibody

#### **Sigma Chemical Company, Poole, UK**

- Ammonium persulphate
- Antibiotic antimycotic solution (Penicillin - Streptomycin - Neomycin Solution) (100X)
- Bovine serum albumin (BSA)
- Laemmli electrophoresis buffer
- *N,N,N',N'*-Tetramethylethylenediamine (TMEDA)
- Phosphate buffered saline (PBS)
- Trypsin/EDTA solution (1X)
- Tween 20

#### **SPPSS Inc. Chicago, USA**

- Statistical Package for the Social Sciences

#### **TCS Cellworks, Claydon, UK**

- DMSO freeze medium

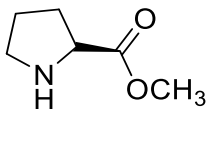
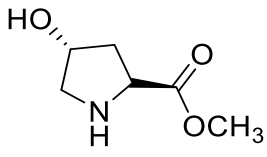
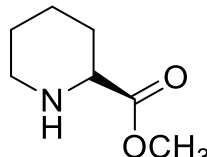
#### **WPA, Cambridge, UK**

- UV-Visible spectrophotometer

## 2.3 CHEMICAL SYNTHESIS

The *cis-trans* isomerization of pSer-Pro dipeptides by Pin1 modulated by the proline-directed phosphorylation motif, has been identified as an indispensable mechanism in tumor growth and metastasis. Since the primary goal of this study is to explore the possibility of interfering with the peculiar proliferative mechanisms of cancer cells using synthetic pSer-Pro motif organic compounds to inhibit Pin1, we started by preparing C-terminal protected proline and its analogues (Table 2.1, Section 2.3.1).

**Table 2.1.** C-terminal protected proline and its analogues

		
Methyl-L-prolinate	Methyl <i>trans</i> -4-hydroxy-L-prolinate	Methyl-L-pipecolate

This was followed by synthesis of a proline-based dipeptide, which entails coupling the protected proline with *N*-terminal protected serine (Section 2.3.2). Considering the chemical stability of phosphoamino acids in general, and the fact that all *O*-phosphates are stable under acidic conditions whereas the human cellular cytoplasmic pH is in the range 7.0 and 7.4 and normally higher for a growing cell, we decided to design and synthesize an *N*-analogue of serine ( $\beta$ -aminoalanine) starting from asparagine (Section 2.3.3). We believe that successful phosphorylation of this amino acid residue (moiety) will produce less labile, alkaline-stable *N*-phosphates (phosphoramidates). The Merrifield solid phase peptide synthesis procedure was employed to synthesize some peptides including the phosphoseryl-prolyl dipeptide (Section 2.3.4). Various phosphorylation approaches involving *O*-, *N*-, and *C*-phosphorylation (to give corresponding phosphates, phosphoramidates, and phosphonates respectively) using phosphoramidite, phosphochloridite and phosphite approaches were employed. This is described under phosphorylation reactions (Section 2.4).



It has been established that reversible protein phosphorylation is among the most significant and universal cellular regulatory mechanisms. Also, phosphorylation of protein on Ser/Thr-Pro motifs, that is, serine or threonine preceding proline plays a vital regulatory function in various cellular processes. In particular, the phosphorylation of TF at Ser253 is known to be mediated by protein kinase  $\alpha$  (a family to which our target enzyme, Pin1, belongs). It was therefore thought that modification of the scissile P-O covalent bond on serine residue (at the phosphodiester linkage) by replacing it with a non-hydrolysable P-C (phosphonate) bond may prevent the conformational changes in the target enzyme and its substrates thereby inhibiting its enzymatic activities. A trial synthesis of phosphonates starting with methionine is presented in Section 2.4.3.

From reports that the sulfamate moiety offers very attractive possibilities for the drug design of various pharmacological agents with impressive biological activity coupled with the special position the sulfamates occupied in anticancer drug armamentarium, a consideration was given to this moiety as a possible substitute for the phosphate group (phosphoramidate) on the *N*-analogue designed molecule. Trial experiments on preparation of sulfamates were carried out first with some primary amines and simple amino acids including benzylamine,  $\beta$ -aminoalanine and lysine (Section 2.5).

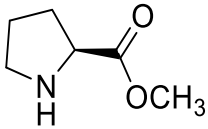
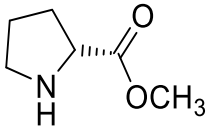
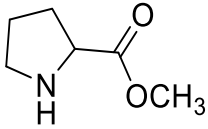
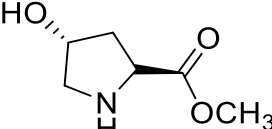
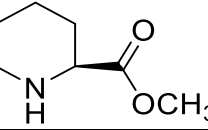
Limited success in phosphorylation experiments as a result of tedious work-up in purification of products obtained prompted our search to turn to non-peptide small molecule Pin1 inhibitors. This led to identification of 2-methyl-5-(*p*-methoxyphenyl)-3-furoryl-3-(2-naphthyl)-D-alanine from the literature. Amongst several structure-guided designed Pin1 inhibitors reported, it was one and the more active of the two compounds active in cell-based assays. Synthesis of this compound and some of its new derivatives is presented in Section 2.6.

### **2.3.1 Preparation of amino acid methyl esters**

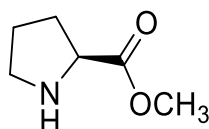
Amino acids methyl esters were synthesized using a method reported by Jones et al.<sup>145</sup> with modifications. A suspension of L-proline or its analogue (50.9 mmol) in anhydrous methanol (40.0 mL) was maintained at 0 °C with stirring. The mixture was stirred further for 30 min after dropwise addition of

thionyl chloride (5.45 mL, 75.0 mmol). The temperature of the clear colourless solution was increased by heating under reflux (24 h). On cooling, excess thionyl chloride and methanol were removed using rotary evaporator. The product was obtained as either golden yellow viscous oil or a white solid. The liquid was used as such in subsequent reactions, while the solid was recrystallized in methanol-diethyl ether (1:4). The resulting methyl ester hydrochloride was subjected to filtration, washing with diethyl ether and drying in a vacuum desiccator over fused calcium chloride. A range of yields between 80 and 98% were obtained as summarized in Table 2.2.

**Table 2.2.** Synthesized amino acid methyl esters

Compound Name	Code	Structure	Yield
Methyl-L-prolinate	<b>1</b>		7.0 g, 83%
Methyl-D-prolinate	<b>2</b>		7.4 g, 88%
Methyl-DL-prolinate	<b>3</b>		7.1 g, 84%
Methyl trans-4-hydroxy-L-prolinate	<b>4</b>		9.1 g, 98%
Methyl-L-pipecolate	<b>5</b>		8.0 g, 88%

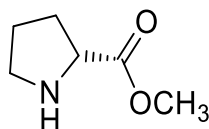
***Methyl L-prolinate (1):***



Golden yellow liquid -  $^1\text{H}$  NMR (400 MHz, DMSO- $d_6$ )  $\delta$ : 4.21 (t,  $J = 7.3$  Hz, 1H; **H-2**), 3.74 (s, 3H; **OCH<sub>3</sub>**), 3.12 - 3.25 (m, 2H; **H-5**), 2.20 - 2.29 (m, 2H; **H-3**), 1.85 - 2.03 (m, 3H; **H-4** & **NH**);  $^{13}\text{C}$  NMR (101 MHz, DMSO- $d_6$ )  $\delta$ : 169.68 (**C=O**), 58.87 (**C-2**), 53.53 (**OCH<sub>3</sub>**), 45.64 (**C-5**), 28.22(**C-3**), 23.61 (**C-4**). Anal.

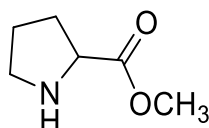
calcd. for C<sub>6</sub>H<sub>12</sub>CINO<sub>2</sub> (165.62): C, 43.51; H, 7.30; N, 8.46; Found: C, 40.20; H, 8.36; N, 7.77. *m/z* (ES-MS) for (C<sub>6</sub>H<sub>11</sub>NO<sub>2</sub>): [MH]<sup>+</sup>, 130.0; [M-CH<sub>3</sub>]<sup>+</sup>, 116.0

***Methyl D-prolinate (2):***



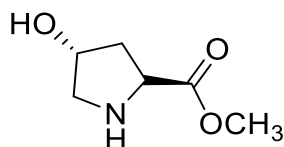
Golden yellow liquid - <sup>1</sup>H NMR (400 MHz, DMSO-d<sub>6</sub>) δ: 4.30 (t, J = 7.3 Hz, 1H; **H-2**), 3.74 (s, 3H; **OCH<sub>3</sub>**), 3.14 – 3.26 (m, 2H; **H-5**), 2.20-2.29 (m, 2H; **H-3**), 1.86-2.03 (m, 3H; **H-4 & NH**); <sup>13</sup>C NMR (101 MHz, DMSO-d<sub>6</sub>) δ: 169.67 (**C=O**), 58.86 (**C-2**), 53.52 (**OCH<sub>3</sub>**), 45.62 (**C-5**), 28.22 (**C-3**), 23.62 (**C-4**). Anal. calcd. for C<sub>6</sub>H<sub>12</sub>CINO<sub>2</sub> (165.62): C, 43.51; H, 7.30; N, 8.46; Found: C, 42.05; H, 8.15; N, 7.87. *m/z* (ES-MS) for (C<sub>6</sub>H<sub>11</sub>NO<sub>2</sub>): [MH]<sup>+</sup>, 130.0

***Methyl DL-prolinate (3):***



White hygroscopic solid - <sup>1</sup>H NMR (400 MHz, DMSO-d<sub>6</sub>) δ: 4.35 (dd, J = 11.3, 3.4 Hz, 1H; **H-2**), 3.75 (s, 3H; **OCH<sub>3</sub>**), 3.14-3.26 (m, 2H; **H-5**), 2.21-2.30 (m, 2H; **H-3**), 2.09 (s, 1H; **NH**) 1.87-2.03 (m, 2H; **H-4**); <sup>13</sup>C NMR (101 MHz, DMSO-d<sub>6</sub>) δ: 169.73 (**C=O**), 5.87 (**C-2**), 53.53 (**OCH<sub>3</sub>**), 45.67 (**C-5**), 28.25 (**C-3**), 23.63 (**C-4**) Anal. calcd. for C<sub>6</sub>H<sub>12</sub>CINO<sub>2</sub> (165.62): C, 43.51; H, 7.30; N, 8.46; Found: C, 43.03; H, 7.36; N, 8.30. *m/z* (ES-MS) [MH]<sup>+</sup> for (C<sub>6</sub>H<sub>11</sub>NO<sub>2</sub>): 130.0

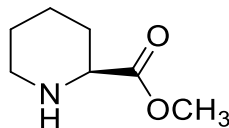
***Methyl trans-4-hydroxy-L-prolinate (4):***



White powder (mpt-158-160 °C) - <sup>1</sup>H NMR (400 MHz, DMSO-d<sub>6</sub>) δ: 4.43 (dd, J = 18.3, 10.7 Hz, 2H, **H-2&4**), 3.74 (s, 3H, **OCH<sub>3</sub>**), 3.04-3.37 (m, 2H, **H-5**), 2.03-2.21 (m, 2H, **H-3**). <sup>13</sup>C NMR (101 MHz, DMSO-d<sub>6</sub>) δ: 169.61 (**C=O**), 68.98 (**C-4**), 57.96 (**C-5**), 53.56 (**C-2**), 53.56 (**OCH<sub>3</sub>**), 37.5 (**C-3**) Anal. calcd. for C<sub>6</sub>H<sub>12</sub>CINO<sub>3</sub> (181.62): C, 39.68; H, 6.66; N, 7.71; Found: C, 39.40; H, 6.85; N,

7.61.  $m/z$  (ES-MS) for  $C_6H_{11}NO_3$   $[M+Na]^+$ , 167.9;  $[MH]^+$ , 145.9;  $[M-H_2O]^+$ , 128.0;  $[M-HCOOCH_3]^+$ , 86.1

***Methyl DL-pipecolate (5):***

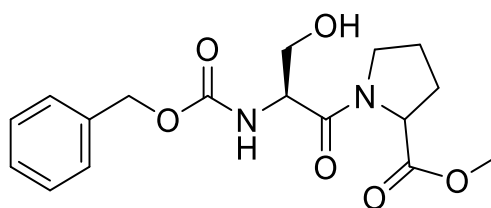


White powder (mpt-198-199 °C) -  $^1H$  NMR (400 MHz, DMSO- $d_6$ )  $\delta$ : 4.02 (dd,  $J$  = 11.3, 3.6 Hz, 1H; **H-2**), 3.71 (s, 3H; **OCH<sub>3</sub>**), 3.12 (d, 1H; **H-6**), 2.84-2.79 (m, 1H; **H-6**), 2.00-1.97 (m, 1H; **H-3**), 1.65-1.56 (m, 5H; **H-4, H-5 & H-3**);  $^{13}C$  NMR (101 MHz, DMSO- $d_6$ )  $\delta$ : 170.44 (**C=O**), 56.01 (**C-2**), 53.80 (**OCH<sub>3</sub>**), 43.83 (**C-6**), 26.09 (**C-3**), 21.73 (**C-5**), 21.60 (**C-4**). Anal. calcd. for  $C_7H_{14}ClNO_2$  (179.64): C, 46.80; H, 7.86; N, 7.80; Found: C, 46.56; H, 8.05; N, 7.65.  $m/z$  (ES-MS) for  $C_7H_{13}NO_2$ :  $[M+Na]^+$ , 165.9;  $[MH]^+$ , 143.9;  $[MH-CH_3OH]^+$ , 112.1;  $[M-HCOOCH_3]^+$ , 84.1.

**2.3.2 Synthesis of proline-based dipeptides (peptide coupling)**

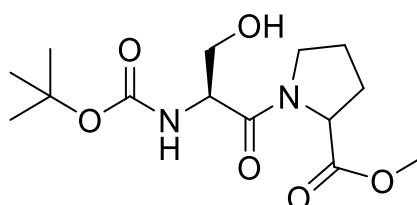
Diisopropylethylamine (24.0 mL, 137.8 mmol) was added dropwise at 0 °C to methyl L-prolinate hydrochloride or methyl L-pipecolate hydrochloride solution (52.4 mmol) in dichloromethane (40 mL) with stirring for 20 min. To the resulting mixture, N-carbamate-protected serine (52.4 mmol) in dichloromethane (20 mL) was added in portions. After 1-hydroxybenzotriazole (63.4 mmol) had been added and the solution stirred at 0 °C for 20 min, *N*-(3-dimethylaminopropyl)-*N'*-ethylcarbodiimide hydrochloride (13.8 g, 72.1 mmol) was added portionwise. Stirring continued at 0 °C for 30 min and for about 40 h at room temperature. Then, 10% solution of monosodium citrate (50 mL) was added. The separated organic layer was successively washed with (20 mL x 2) of each of saturated  $NaHCO_3$ , water and brine. Evaporation of the solvent using rotary evaporator gave the product as either sticky yellow oil or a white solid. Recrystallization of the solid product was in ethyl acetate-hexane.

### Z-Ser-Pro-OMe (6):



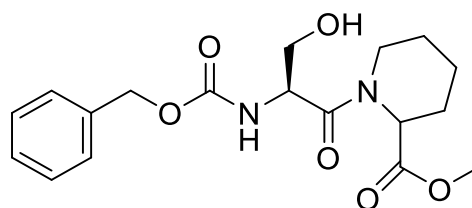
White solid (12.7 g, 69%); (mpt:108-110 °C) -  $^1\text{H}$  NMR (400 MHz,  $\text{CDCl}_3$ )  $\delta$ :7.35 (s, 5H; **ar-H**), 5.75 (d,  $J = 8.2$  Hz, 1H; **NH**), 5.11 (s, 2H; **z-CH<sub>2</sub>**), 4.70-4.68 (m, 1H; **Ser-H $\alpha$** ), 4.62-4.59 (m, 1H; **Pro-H-2**), 3.95-3.85 (m, 2H; **Ser-H $\beta$** ), 3.76 (s, 3H; **OCH<sub>3</sub>**), 3.75-3.65 (m, 2H; **Pro-C-5**), 3.23 (m, 1H;), 2.35-2.00 (m, 4H; **Pro-H-3 & H-4**)  $^{13}\text{C}$  NMR  $\delta$ : 173.03 (**Ser-C=O**), 169.93 (**Pro-C=O**), 156.17(**z-C=O**), 136.26 (**Ar-C<sub>i</sub>**), 128.83 (**Ar-C<sub>m</sub>**), 128.28 (**Ar-C<sub>p</sub>**), 128.12 (**Ar-C<sub>o</sub>**), 67.15 (**z-CH<sub>2</sub>**), 64.22 (**Ser-C $\beta$** ), 59.01 (**Ser-C $\alpha$** ), 53.78 (**Pro-C-2**), 52.79 (**OCH<sub>3</sub>**), 47.36 (**Pro-C-5**), 28.96 (**Pro-C-3**), 24.93 (**Pro-C-4**). Anal. calcd. for  $\text{C}_{17}\text{H}_{22}\text{N}_2\text{O}_6$  (350.37): C, 58.28; H, 6.33; N, 8.00; Found: C, 58.20; H, 6.39; N, 8.00.  $m/z$  (ES-MS):  $[\text{M}_2+\text{Na}]^+$ , 723.2;  $[\text{MH}]^+$ , 351.1;  $[\text{C}_6\text{H}_{11}\text{NO}_2]^+$ , 129.9;  $[\text{PhCH}_2]^+$ , 91.1.

### Boc-Ser-Pro-OMe (7):



White solid (10.4 g, 63%) -  $^1\text{H}$ -NMR (400 MHz,  $\text{CDCl}_3$ )  $\delta$  5.47 (s, 1H, **OH**), 4.58-4.62 (m, 2H, **Pro-H-2 & Ser-H $\alpha$** ), 4.01-3.78 (2H, **Ser-H- $\beta$** ), 3.76 (s, 3H, **OCH<sub>3</sub>**), 3.67-3.79 (m, 2H, **Pro-H-5**), 1.99-2.06 (m, 3H, **Pro-H-3 & H-4**), 1.68-1.56 (m, 1H, **Pro-H-4**), 1.44 (s, 9H, **t-Bu**).  $^{13}\text{C}$  NMR  $\delta$ :173.08 (**Pro-C=O**), 170.28 (**Ser-C=O**), 155.69 (**Boc-C=O**), 80.15 (**t-Bu-C**), 64.44 (**Ser-C $\beta$** ), 58.99 (**Pro-C-2**), 53.34 (**Ser-C $\alpha$** ), 52.78 (**OCH<sub>3</sub>**), 47.32 (**Pro-C-5**), 28.98 (**Pro-C-3**), 28.41(**t-Bu-CH<sub>3</sub>**), 24.95 (**Pro-C-4**). Anal. calcd. for  $\text{C}_{14}\text{H}_{24}\text{N}_2\text{O}_6$  (316.35): C, 53.15; H, 7.65; N, 8.86; Found: C, 52.76; H, 8.00; N, 8.69.  $m/z$  (ES-MS)  $[\text{M}_2+\text{Na}]^+$ , 655.2;  $[\text{M}+\text{Na}]^+$ , 339.2;  $[\text{M}-t\text{-Bu}]^+$ , 260.9;  $[\text{M}-\text{Boc}]^+$ , 216.9;  $[\text{C}_6\text{H}_{11}\text{NO}_2]^+$ , 130;  $[\text{Boc}]^+$ , 102.1

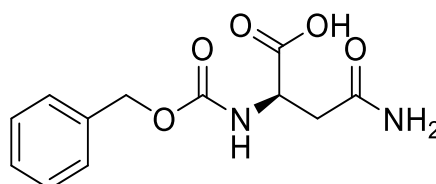
### **Z-Ser-DL-Pip-OMe (8):**



Golden yellow viscous liquid (10.3 g, 54%):  $^1\text{H}$  NMR (400 MHz,  $\text{CDCl}_3$ )  $\delta$ : 7.34 (s, 5H; **Ar-H**), 5.09 (s, 2H; **z-CH<sub>2</sub>**), 4.87 (t,  $J = 3.9$  Hz, 1H; **Ser-H $\alpha$** ), 3.73 (s, 3H; **OCH<sub>3</sub>**), 1.40-1.71 (m, 9H; **Pip-H**).  $^{13}\text{C}$  NMR  $\delta$ : 172.30 (**Ser-C=O**), 169.13 (**Pip-C=O**), 156.00 (**z-C=O**), 143.95 (**Ar-C<sub>i</sub>**), 141.36, 137.90, 128.50 (**Ar-C<sub>m</sub>**), 127.79 (**ar-C<sub>p</sub>**), 127.17 (**Ar-C<sub>o</sub>**), 125.29, 120.07, 73.47 (**z-CH<sub>2</sub>**), 70.32 (**Ser-C $\beta$** ), 67.27 (**Ser-C $\alpha$** ), 59.18 (**Pip-C-<sub>2</sub>**), 52.37 (**OCH<sub>3</sub>**), 47.17 (**Pip-C-<sub>6</sub>**), 31.69 (**Pip-C-<sub>3</sub>**), 29.13 (**Pip-C-<sub>5</sub>**), 25.01 (**Pip-C-<sub>4</sub>**). Anal. calcd. for  $\text{C}_{18}\text{H}_{24}\text{N}_2\text{O}_6$  (364.40): C, 59.33; H, 6.64; N, 7.69; Found: C, 59.16; H, 6.58; N, 8.69.  $m/z$  (ES-MS)  $[\text{M}_2+\text{Na}]^+$ , 751.1;  $[\text{MH}]^+$ , 365.1;  $[\text{C}_6\text{H}_{11}\text{NO}_2]^+$ , 130.1

### **2.3.3 Synthesis of amino ( $\beta$ -aminoalanine) derivatives of serylprolyl motif**

#### **Z-L-asparagine (9):**

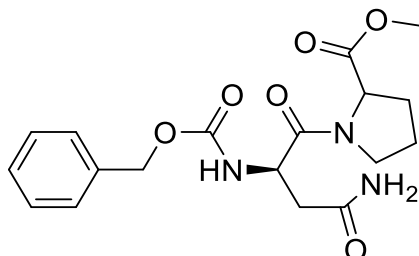


To a solution of *L*-asparagine (6.05 g, 40 mmol) in 10%  $\text{Na}_2\text{CO}_3$  (100 mL) was added 1,4-dioxane (56 mL) and benzyl chloroformate (6.9 mL, 48 mmol) at 0 °C. The reaction mixture was stirred overnight at room temperature and was poured into  $\text{H}_2\text{O}$  (300 mL). The mixture was washed three times with diethyl ether. The aqueous layer was acidified with 2M HCl in water and a white precipitate fell out. The precipitate was filtered off and washed extensively with diethyl ether to afford the  $\text{N}^\alpha$ -benzyloxycarbonyl-*L*-asparagine as a white solid.

White solid (7.7 g, 72%); (mpt-158-160 °C)  $^1\text{H}$  NMR (400 MHz,  $\text{DMSO-d}_6$ )  $\delta$ : 7.45 (d, 1H,  **$\alpha$ -NH**), 7.34 (m, 7H, **Ar-H**), 6.92 (s, 2H, **CONH<sub>2</sub>**), 5.02 (s, 2H, **z-CH<sub>2</sub>**), 4.33 (q, 1H, **H $\alpha$** ), 2.50 (m, 2H, **H $\beta$** ).  $^{13}\text{C}$  NMR (101 MHz,  $\text{DMSO-d}_6$ )  $\delta$ : 173.19 (**COOH**), 171.17 (**CONH<sub>2</sub>**), 155.82 (**z-C=O**), 136.95 (**Ar-C<sub>i</sub>**), 128.36

(**Ar-C<sub>m</sub>**), 127.81 (**Ar-C<sub>p</sub>**), 127.72 (**Ar-C<sub>o</sub>**), 65.42 (**z-CH<sub>2</sub>**), 50.60 (**C<sub>α</sub>**), 36.44 (**C<sub>β</sub>**), Anal. Calcd. For C<sub>12</sub>H<sub>14</sub>N<sub>2</sub>O<sub>5</sub> (266.25): C, 54.13; H, 5.30; N, 10.52; found C, 54.00; H, 5.30; N, 10.34. *m/z* (ES-MS): [M<sub>2</sub>+Na]<sup>+</sup>, 555.1; [M+Na]<sup>+</sup>, 289.0; [PhCH<sub>2</sub>]<sup>+</sup>, 91.1.

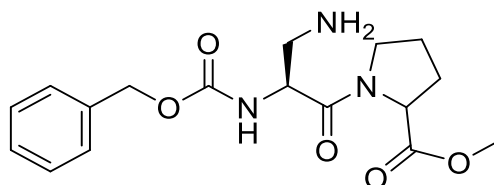
**Z-Asn-Pro-OMe (10):**



Following the procedure for preparation of (**6-8**) Section 2.3.2, using methyl L-prolinate (**1**) (28.13 mmol) and Z-L-asparagine (**9**) (28.13 mmol), the crude Z-Asp-Pro-OMe (grey solid) was obtained. This was recrystallized in dichloromethane-hexane to give the pure product.

White solid (8.2 g, 77%): <sup>1</sup>H NMR (400 MHz, DMSO-d<sub>6</sub>) δ: 7.42 (d, 1H; **NH**), 7.33 (s, 5H; **Ar-H**), 6.69 (t, 1H), 5.03-4.92 (m, 2H; **H-α Asn & H-α Pro**), 2.48-1.87 (m, 4H; **Pro-H-3 & H-4**). <sup>13</sup>C NMR (101 MHz, DMSO-d<sub>6</sub>) δ: 172.24 (**Asn-CONH<sub>2</sub>**), 171.14 (**Asn-C=O**), 169.68 (**Pro-C=O**), 155.51 (**z-C=O**), 137.02 (**Ar-C<sub>i</sub>**), 128.32 (**Ar-C<sub>m</sub>**), 127.76 (**Ar-C<sub>p</sub>**), 127.63 (**Ar-C<sub>o</sub>**), 65.42 (**z-CH<sub>2</sub>**), 58.57 (**Pro-C-2**), 51.65 (**OCH<sub>3</sub>**), 48.98 (**Asn-C<sub>α</sub>**), 46.44 (**Pro-C-5**), 39.29 (**Asn-C<sub>β</sub>**), 28.62 (**Pro-C-3**), 24.42 (**Pro-C-4**). Anal. calcd. for C<sub>18</sub>H<sub>23</sub>N<sub>3</sub>O<sub>6</sub> (377.39): C, 57.29; H, 6.14; N, 11.13; Found C, 57.39; H, 6.33; N, 10.80; *m/z* (ES-MS): [M<sub>2</sub>+Na]<sup>+</sup>, 777.2; [MH]<sup>+</sup> 378.1;

**Z-(β-amino)Ala-Pro-OMe (11):**

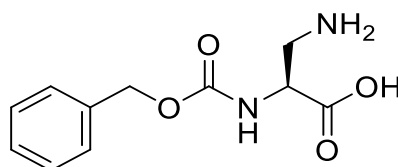


A slurry of Z-Asn-Pro-OMe (**10**), (2.5 g, 6.62 mmol) and iodosobenzene diacetate (2.56 g, 7.95 mmol) in a mixture of acetonitrile, ethyl acetate and water (2:2:1 v/v respectively, 30 mL) was stirred at 15 °C for 30 min. The temperature was then allowed to rise to ambient temperature and the reaction

mixture was stirred until completion (24 h). The reaction mixture was concentrated under reduced pressure to give the product as golden yellow viscous liquid.

(Yield 2.9 g)  $^1\text{H}$  NMR (400 MHz, DMSO- $d_6$ )  $\delta$ : 7.39 (s, 1H, **NH $\alpha$** ), 7.38 (s, 5H, **ArH**), 5.2 (s, 2H, **PhCH $_2$** ), 4.31-4.26 (m, 1H, **H $\alpha$ -ala**).  $^{13}\text{C}$  NMR (101 MHz, DMSO- $d_6$ )  $\delta$ : 172.20 (**Ala-C=O**), 172.08 (**Pro-C=O**), 157.72 (**z-C=O**), 137.10 (**Ar-C $_i$** ), 127.80 (**Ar-C $_m$** ), 127.74 (**Ar-C $_p$** ), 127.71 (**Ar-C $_o$** ), 65.48 (**z-CH $_2$** ), 58.63 (**Pro-C-2/Ala-C $\alpha$** ), 51.69 (**OCH $_3$** ), 46.54 (**Pro-C-5**), 39.70 (**Ala-C $\beta$** ), 28.57 (**Pro-C-3**), 24.41 (**Pro-C-4**). Anal. calcd. for  $\text{C}_{17}\text{H}_{23}\text{N}_3\text{O}_5$  (377.39): C, 58.44; H, 6.64; N, 12.03; Found C, 49.23; H, 6.57; N, 8.48;  $m/z$  (ES-MS):  $[\text{MH}]^+$  350.1;  $[\text{MH} - \text{PhCH}_2\text{OH}]^+$ , 241.9;  $[\text{C}_6\text{H}_{11}\text{NO}_2]^+$ , 130.1

### **Z-( $\beta$ -aminoalanine) (12):**

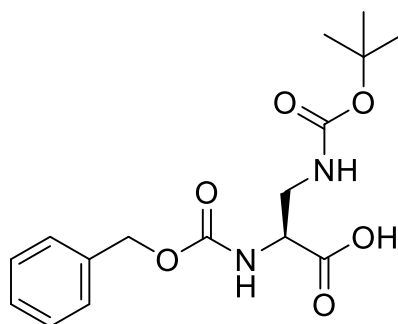


A slurry of iodosobenzene diacetate (2.9 g, 9.00 mmol) and Z-L-asparagine (**9**) (2.0 g, 15.14 mmol), in a mixture of acetonitrile, ethyl acetate and water (2:2:1, v/v respectively, 30 mL) was stirred at 15 °C for 30 min. Allowing the temperature to rise to room temperature, the reaction mixture was stirred for 6 h whereupon the product, a white solid, separated out. The temperature of the resultant mixture was then maintained at 5 °C and the product collected by suction filtration, washed with 20 mL ethyl acetate and dried *in vacuo* to yield the product.

White solid (3.14 g, 87%); (mpt: 219-220 °C)-  $^1\text{H}$  NMR (400 MHz, DMSO- $d_6$ /TFA)  $\delta$ : 8.07 (br, s, 3H, **NH $_3^+$** ), 7.75 (d, 1H, **NH $\alpha$** ), 7.38 (m, 5H, **H-Ar**), 5.08 (s, 2H, **z-CH $_2$** ), 4.31 (m, 1H, **H- $\alpha$** ), 3.25 (br, s, 1H, **H- $\beta$** ), 3.04 (br, s, 1H, **H- $\beta$** ).  $^{13}\text{C}$  NMR (101 MHz, DMSO- $d_6$ /TFA)  $\delta$ : 171.39 (**COOH**), 156.79 (**z-C=O**), 137.22 (**Ar-C- $_i$** ), 128.93 (**Ar-C- $_m$** ), 128.49 (**Ar-C- $_p$** ), 128.37 (**Ar-C- $_o$** ), 66.40 (**z-CH $_2$** ), 52.37 (**C $\alpha$** ), 39.88 (**C $\beta$** ). Anal. calcd. for  $\text{C}_{11}\text{H}_{14}\text{N}_2\text{O}_4$  (238.24): C, 55.46; H, 5.92; N, 11.76; Found C, 55.31; H, 5.81; N, 11.57;  $m/z$  (ES-MS):  $[\text{M}_2\text{H}]^+$ , 477.1;  $[\text{MH}]^+$ , 238.9;  $[\text{M}-\text{CO}_2]^+$ , 194.9;  $[\text{PhCH}_2]^+$ , 91.1.



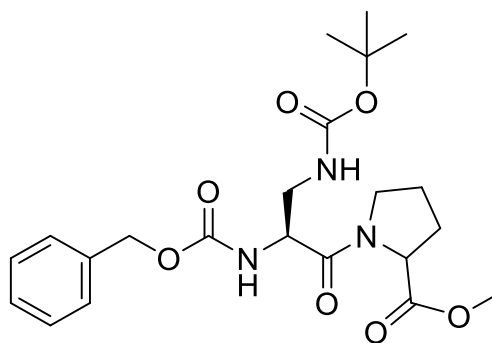
### Z-(β-Boc-amino)alanine (13):



To a solution of Z-β-aminoalanine (**12**) (4.5 g, 19 mmol) in 10% Na<sub>2</sub>CO<sub>3</sub> (47 mL) were added 1,4-dioxane (28 mL) and di-*tert*-butyl dicarbonate (6.18 g, 28.4 mmol) at 0 °C. The reaction mixture was stirred overnight at room temperature and was poured into H<sub>2</sub>O (100 mL) after which the mixture was washed with diethyl ether (30 mL x 3). The aqueous layer was acidified with 2N HCl in water and the white suspension was extracted three times with ethyl acetate. The combined ethyl acetate layer was dried on anhydrous MgSO<sub>4</sub>, filtered and evaporated to dryness. The crude product was crystallized from diethyl ether to afford the title compound.

White solid (5.5 g, 86%) <sup>1</sup>H NMR (400 MHz, DMSO-d<sub>6</sub>) δ: 7.43 (d, J=8 1H; NH<sub>α</sub>), 7.34 (s, 5H; Ar-H), 6.85 (br. s, 1H; NH<sub>β</sub>), 5.04 (d, J=1.6, 2H; z-CH<sub>2</sub>), 4.08 (d, J=5.7 1H; Ala-H<sub>α</sub>), 3.27 (m, 2H, Ala-H<sub>β</sub>), 1.37 (s, 9H; t-Bu-CH<sub>3</sub>). <sup>13</sup>C NMR (101 MHz, DMSO-d<sub>6</sub>) δ: 172.61 (COOH), 156.50 (z-C=O), 156.21 (Boc-C=O), 137.48 (Ar-C<sub>i</sub>), 128.92 (Ar-C<sub>m</sub>), 128.41 (Ar-C<sub>p</sub>), 128.31 (Ar-C<sub>o</sub>), 78.58 (t-Bu-C), 66.07 (z-CH<sub>2</sub>), 54.67 (Ala-C<sub>α</sub>), 41.70 (Ala-C<sub>β</sub>), 28.74 (t-Bu-CH<sub>3</sub>). *m/z* (ES-MS) [M+Na]<sup>+</sup> 361.1; [M<sub>2</sub> + Na]<sup>+</sup>, 699.2; [M - Boc]<sup>+</sup>, 238.9; [PhCH<sub>2</sub>]<sup>+</sup>, 91.1

### Z-(β-Boc-amino)Ala-Pro-OMe (14):



The procedure for synthesis of (**6-8**) above was followed using methyl L-prolinate (**1**) (1.22 g, 7.39 mmol) and Z-(β-Boc-amino)alanine (**13**) (2.5 g, 7.39

mmol). After the removal of the solvent using a rotavapor, a greenish yellow solid (2.72 g) was obtained. Recrystallization in dichloromethane yielded the pure product as a white solid.

White solid (2.5 g, 72%): <sup>1</sup>H NMR (400 MHz, DMSO-d<sub>6</sub>) δ: 7.42 (d, 1H; α-NH), 7.33 (s, 5H; H-Ar), 6.69 (t, 1H; β-NH), 5.03-4.92 (m, 2H; z-CH<sub>2</sub>), 2.48-1.87 (m, 4H; Pro-H-3 & H-4), 1.36 (s, 9H; t-Bu-CH<sub>3</sub>). <sup>13</sup>C NMR (101 MHz, DMSO-d<sub>6</sub>) δ: 172.21 (Ala-C=O), 168.88 (Pro-C=O), 155.91 (z-C=O), 155.73 (Boc-C=O), 136.89 (Ar-C-*i*), 128.35 (Ar-C-*m*), 127.84 (Ar-C-*p*), 127.77 (Ar-C-*o*), 78.07 (C-t-Bu), 65.54 (z-CH<sub>2</sub>), 58.43 (Pro-C-<sub>2</sub>), 52.27 (Ala-C<sub>α</sub>), 51.86 (OCH<sub>3</sub>), 46.50 (Pro-C-<sub>5</sub>), 39.92 (Ala-C-β), 28.52 (Pro-C-<sub>3</sub>), 28.14 (t-Bu-CH<sub>3</sub>), 24.48 (Pro-C-<sub>4</sub>). *m/z* (ES-MS): [M+Na]<sup>+</sup>, 472.2; [MH - Boc]<sup>+</sup>, 350.1; [M<sub>2</sub> + Na]<sup>+</sup>, 921.3; [C<sub>6</sub>H<sub>11</sub>NO<sub>2</sub>]<sup>+</sup>, 130.0

### 2.3.4 The Merrifield procedure for peptide synthesis

The synthesis of a pentapeptide residue consisting of amino acid sequence, Glu-Asn-Ser-Pro-Leu (ENSPL) in the cytoplasmic domain of tissue factor (residue 256-260) was carried out using Fmoc-protected amino acids. The side chain in glutamic acid was protected with *tert*-butyl ester while the side chain in serine was protected with *tert*-butyl ether. The Wang resin was placed on top of a glass filter and washed with dimethyl formamide (DMF) under vacuum. It was deprotected with 20% piperidine (using approximately 5 mL) and gently agitating the resin beads with nitrogen gas in the piperidine for approximately 10 min. The piperidine was cleared under vacuum and the deprotected resin washed three times with DMF, each time allowing resin to agitate for 30 s and then cleared under vacuum.

The amount of each of the component amino acids used with 200 mg of Wang resin having a loading capacity of 0.20 mmol/g was calculated according to the equation:

$$\text{Amount of amino acid required} = \text{loading capacity} \times \text{molecular weight}$$

$$\text{Amount of amino acid required} = 0.20 \times \text{molecular weight}$$

The various quantities are shown in Table 2.3 below.

**Table 2.3.** Amount of component amino acids required for 200 mg resin

<b>Fmoc amino acid</b>	<b>One, letter symbol</b>	<b>Molecular weight (g/mol)</b>	<b>Mass needed (mg)</b>
Glutamic acid	E	425	85
asparagine	N	354	71
Serine	S	383	77
Proline	P	337	67
Leucine	L	353	71

The coupling mixture containing the first Fmoc amino acid (Glutamic acid) was prepared by adding an appropriate volume of diisopropylethylamine (DIPEA) (2-5 mL depending on the amount of HBTU and the solubility of the Fmoc amino acid) and dissolving by shaking. The coupling mixture was added to the resin and gently agitated with nitrogen gas for 40 min. Up to 2 mL more DMF was added. The mixture was cleared under vacuum and washed three times with DMF, each time allowing the resin to agitate for 0.5 min and then cleared under vacuum. After coupling the first amino acid to the resin, the peptide chain was extended by repeating the steps from deprotection of the resin to washing after adding the first amino acid for successive amino acid until the desired sequence was achieved.

Finally, the last Fmoc was removed as in deprotecting the resin and the peptide washed three times with DMF. Traces of DMF were removed by washing the resin with diethyl ether and clearing under vacuum as before. The resin was manually transferred into a centrifuge tube, trifluoroacetic acid (TFA) mixture (2-5 mL) was added and left to deprotect overnight on a rolling table. An excess of cold ether was added to the tube and a cream colour precipitate was formed almost immediately. The mixture was centrifuged and the supernatant was carefully discarded. It was washed three times with ether repeating the centrifugation each time. The precipitate was then dried under vacuum. The peptide was thereafter dissolved in a minimum amount of water, centrifuged and the supernatant was kept.

The theoretical yield of the synthesized peptide was calculated using the equation:

*Peptide yield*

= resin loading capacity x mass of resin used x molecular weight of peptide

$$\text{Peptide yield} = 0.20 \frac{\text{mmol}}{\text{g}} \times 0.20 \text{ g} \times 1852 \frac{\text{g}}{\text{mol}} \times \frac{1 \text{ mol}}{1000 \text{ mmol}}$$

$$\text{Peptide yield} = 0.074 \text{ g}$$

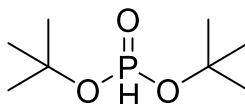
$$= 74 \text{ mg}$$

The yield obtained was, however, deemed too low therefore no analytical data was obtained.

## 2.4 ATTEMPTED PHOSPHORYLATION REACTIONS

### 2.4.1 Attempted synthesis of O-phosphorylserylproline motif

#### *Di-tert-butyl phosphonate (15)*



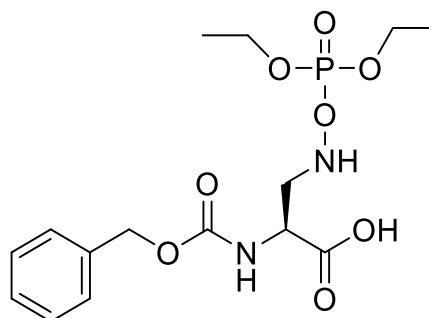
A solution of phosphorus trichloride (5.24 mL, 60 mmol) in 50 cm<sup>3</sup> of petroleum ether was cautiously dropped over a period of 30 min into ice-methanol chilled solution of *t*-butyl alcohol (34.45 mL, 360 mmol) and trimethylamine (12.56 mL, 180 mmol) in petroleum ether (300 mL). Stirring was continued for 1 h without external cooling, after which time the suspension was filtered, the cake being washed well with additional petroleum ether (100 mL). The solvent was removed under reduced pressure on a rotary evaporator. The resultant yellow residue was used as such in the following reaction.

(Yield: 8.9 g, 76%) <sup>1</sup>H-NMR (400 MHz, CDCl<sub>3</sub>) δ 1.46 (s, 18H; **t-Bu-H**). <sup>13</sup>C-NMR (101 MHz, CDCl<sub>3</sub>) δ 83.44 (**C-t-Bu**), 30.35 (**t-Bu-CH<sub>3</sub>**). <sup>31</sup>P-NMR (162 MHz, DMSO-d<sub>6</sub>) δ 2.58,

#### 2.4.2 Attempted synthesis of *N*-phosphoryl amino derivatives of the serylprolyl motif

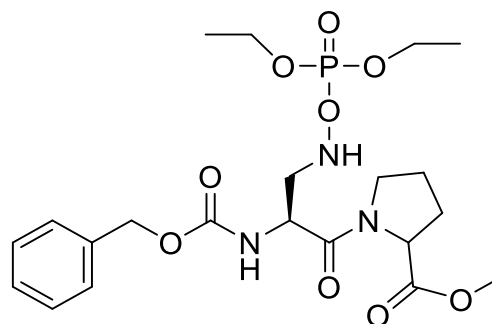
A solution (suspension) of amino acid (10.00 mmol) in triethylamine (Et<sub>3</sub>N) 5 mL, water (3 mL) and ethanol (2 mL) was cooled to 0 °C. A mixture of diethylphosphite (10.00 mmol) and carbon tetrachloride (4 mL) was added dropwise and the mixture was stirred at 20 °C overnight. The reaction was quenched by acidifying the mixture to pH2 with dilute HCl. The resulting mixture was then extracted with ethyl acetate (3 x 20 mL), the solution was dried with MgSO<sub>4</sub>. After filtration, the solvent was evaporated and the colourless oily residue was purified by crystallization from ethyl acetate-petroleum ether.

##### *N*<sup>β</sup>-(Diethoxyphosphoryl)-*z*-β-aminoalanine (16)



(Yield: 2.8 g, 75%) <sup>31</sup>P NMR (162 MHz, DMSO-d<sub>6</sub>) δ: 10.20. m/z(ES-MS): [M<sub>3</sub>]<sup>+</sup>, 1122.16; [M<sub>2</sub>]<sup>+</sup>, 748.42; [M]<sup>+</sup>, 374.84; [M-OC<sub>2</sub>H<sub>5</sub>]<sup>+</sup>, 331.02; [M-PhCH<sub>3</sub>]<sup>+</sup>, 285.01; [M-PO(OC<sub>2</sub>H<sub>5</sub>)<sub>2</sub>]<sup>+</sup>, 238.92. Anal. Calcd. For C<sub>15</sub>H<sub>23</sub>N<sub>2</sub>O<sub>7</sub>P (374.33) C, 48.13; H, 6.19; N, 7.48; Found C, 46.68; H, 6.62; N, 6.72.

##### *Methyl N*<sup>β</sup>-(diethoxyphosphorylamino)-*N*<sup>α</sup>-(*Z*)-β-aminoalaninyl – prolinatate (17)



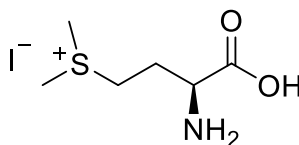
A solution of the methyl *Z*-β-aminoalaninylprolinatate (2.5 g, 6.6 mmol) in trimethylamine (5 mL), water (3 mL) and ethanol (2 mL) was cooled to 0 °C. A

mixture of diethylphosphite (1.3 mL, 10.00 mmol) and carbon tetrachloride (4 mL) was added dropwise and the mixture was stirred at 20 °C overnight. The reaction was quenched by acidifying the mixture to pH2 with dilute HCl. The resulting mixture was then extracted with ethyl acetate (3 x 20 mL), the extract was dried with MgSO<sub>4</sub>. The solvent was evaporated and the product [methyl N<sup>β</sup>-(diethoxyphosphorylamino)-N<sup>α</sup>-(Z)-β-aminoalaninylprolinate] was obtained as a golden yellow oil residue (2.71 g, 85%).

<sup>1</sup>H-NMR (400 MHz, DMSO-d<sub>6</sub>) δ 7.26 (s, 6H, **Ar-H & NH**), 3.53 (s, 3H, **OCH<sub>3</sub>**), 1.98-2.13 (m, 2H, **H<sub>α</sub> Ala**), 1.65-1.91 (m, 4H, **H<sub>3</sub> & H<sub>4</sub> pro**), 1.06-1.17 (m, 6H, **CH<sub>3</sub> Et**). <sup>13</sup>C-NMR (101 MHz, DMSO-d<sub>6</sub>) δ 172.80, 137.69 (**Ar-C<sub>i</sub>**), 131.26 (**Ar-C<sub>m</sub>**), 128.93 (**Ar-C<sub>p</sub>**), 128.43 (**Ar-C<sub>o</sub>**), 66.32 (**Z-CH<sub>2</sub>**), 63.34 (**C<sub>2</sub> Pro**), 62.00 (**CH<sub>2</sub> Et**), 60.39 (**C<sub>α</sub> Ala**), 52.36 (**OCH<sub>3</sub>**), 45.97 (**C<sub>5</sub> Pro**), 29.29 (**C<sub>β</sub> Ala**), 24.84 (**C<sub>3</sub> Pro**), 21.49 (**C<sub>4</sub> Pro**), 16.57(**CH<sub>3</sub> Et**),

### 2.4.3 Attempted preparation of non-hydrolysable phosphonates

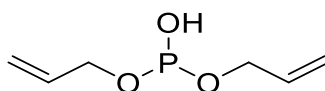
#### *(2S)-Methionine Methylsulfonium Iodide (18)*



Methyl iodide (5.2 mL, 83.9 mmol) was added to a solution of L- methionine (5.0 g, 33.6 mmol) in water (50 mL) and the reaction mixture was stirred at 40 °C for 20 h. The mixture was then concentrated on a rotary evaporator and the resulting white solid was dissolved in a minimum volume of water (10 mL) with gentle heating and treated with ethanol (70 mL) to give a white precipitate. The suspension was allowed to stand for 12 h for maximum precipitation. The precipitate was collected by filtration to give (2S)-methionine methylsulfonium iodide as a white solid.

White solid (8.7 g, 89%) <sup>1</sup>H-NMR (400 MHz, D<sub>2</sub>O) δ 3.77 (t, J = 6.4 Hz, 1H, **H<sub>α</sub>**), 3.28-3.45 (m, 2H, **H<sub>γ</sub>**), 2.84 (s, 6H, **S(CH<sub>3</sub>)<sub>2</sub>**), 2.26 (q, J = 7.5 Hz, 2H, **H<sub>β</sub>**). <sup>13</sup>C-NMR (101 MHz, D<sub>2</sub>O) δ 172.78 (**C=O**), 53.05 (**C<sub>γ</sub>**), 39.53 (**C<sub>α</sub>**), 25.09 (**CH<sub>3</sub>**), 24.83 (**C<sub>β</sub>**). Calcd. For C<sub>6</sub>H<sub>14</sub>INO<sub>2</sub>S (291.15) C, 24.75; H, 4.85; N, 4.81; S, 11.01; Found C, 24.76; H, 4.72; N, 4.76; S, 10.22.

#### 2.4.4 Attempted preparation of diallyl phosphite (19)



A solution of anhydrous *tert*-butyl alcohol (50 mmol) in dry dichloromethane (10 mL) was added dropwise to a stirred solution of phosphorus trichloride (50 mmol) in dichloromethane (10 mL) over a period of 5 min. The mixture was maintained at 0-5 °C under a nitrogen atmosphere. Stirring continued for an additional 30 min at 0 °C. A solution of anhydrous allyl alcohol (100 mmol) in dichloromethane (10 mL) was added to the mixture at 0-5 °C over a period of 5 minutes. Stirring continued under a stream of nitrogen at 25 °C for 16 h. Dichloromethane was removed under reduced pressure to obtain product as a colourless liquid.

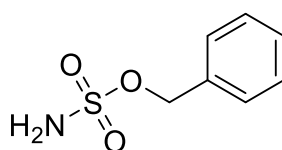
(Yield: 5.7 g, 71%) <sup>1</sup>H-NMR (400 MHz, CDCl<sub>3</sub>) δ: 5.86-5.97 (m, 2H, **H-2** Allyl), 5.23-5.39 (m, 4H, **H-3** Allyl), 4.50-4.59 (m, 4H, **H-1** Allyl)

#### 2.5 SYNTHESIS OF N-SUBSTITUTED SULPHAMIC ACIDS

The compounds were prepared using a procedure described by Audrieth and Sveda.<sup>146</sup>

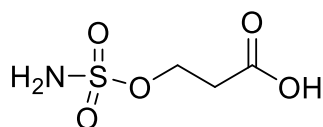
A solution of three equivalents of amino acid (60 mmol) in dry chloroform (50 mL) was cooled to 0 °C in a three-neck flask fitted with a dropping funnel, a thermometer and an efficient magnetic stirrer. One equivalent of chlorosulfonic acid (2.37 g, 1.35 mL, 20 mmol) was added in drops over a period of 30 min at such a rate as not to cause the temperature of the mixture to rise above 0 °C. The resulting [white] precipitate was stirred for another 30 min and then filtered. The solid was suspended in 30 mL of water to produce an emulsion. Upon addition of 7 mL of concentrated 37% HCl, a precipitate was produced which was filtered and dried *in vacuo* as a white solid.

#### ***Benzyl sulfamate (20)***



(Yield: 2.5 g, 67%)  $^1\text{H-NMR}$  (400 MHz, DMSO- $d_6$ /TFA)  $\delta$  7.27-7.39 (m, 5H, **ArH**), 4.13 (s, 2H, **CH<sub>2</sub>**).  $^{13}\text{C-NMR}$  (101 MHz, DMSO- $d_6$ /TFA)  $\delta$  132.42 (**C<sub>Ar-i</sub>**), 129.70(**C<sub>Ar-m</sub>**), 128.90(**C<sub>Ar-p</sub>**), 128.63 (**C<sub>Ar-o</sub>**), 47.80 (**CH<sub>2</sub>**). Calcd. For  $\text{C}_7\text{H}_9\text{NO}_3\text{S}$  (187.21) C, 44.91; H, 4.85; N, 7.48; S, 17.12; Found C, 45.45; H, 4.99; N, 7.76; S, 16.10.

### ***$\beta$ -alanine sulfamate (21)***



(Yield: 1.4 g, 41%)  $^1\text{H-NMR}$  (400 MHz, DMSO- $d_6$ )  $\delta$  2.94 (t,  $J = 6.9$  Hz, 2H), 2.53 (t,  $J = 6.9$  Hz, 2H).  $^{13}\text{C-NMR}$  (101 MHz, DMSO- $d_6$ )  $\delta$  172.61 (**C=O**), 35.43 (**C $\beta$** ), 31.94 (**C $\alpha$** )

## **2.6 SYNTHESIS OF NEW DERIVATIVES OF A NON-PEPTIDE PIN1 INHIBITOR**

The furan-containing moiety of this set of compounds was synthesized using two methods. One was a modified form of a procedure described by Wild and Johnson.<sup>147</sup> The second based on a procedure described by Poretta *et al.*<sup>148</sup> with modifications.

### **2.6.1 Preparation of ethyl phenacylacetate (22)**

#### **Method 1:**

A mixture of sodium chips (1.34 g, 58.3 mmol) and ethyl acetoacetate (7.5 mL) in dry toluene (75 mL) was stirred in a 250 mL three-neck round-bottom flask. To the resulting sodium derivative was added *p*-methoxyphenacyl bromide (2-bromo-4'-methoxyacetophenone) or phenacyl bromide (2-bromoacetophenone) (29.0 mmol). The mixture was heated under reflux for 6 h. After cooling, the solvent was evaporated to obtain the corresponding crude ethyl phenacylacetate as dark brown oily liquid (18 - 27%).

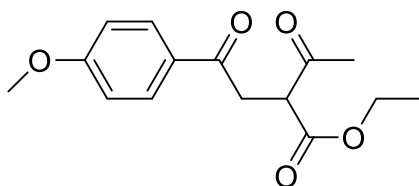
#### **Method 2:**

To a suspension of sodium pellets (0.09 mol) in toluene (120 mL) was added ethyl acetoacetate (0.132 mol) in drops with stirring. The mixture was stirred at room temperature for 3 days. After cooling at 0 °C a solution of 2-bromo-4'-



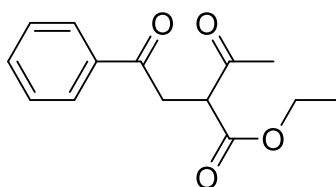
methoxyacetophenone or 2-bromoacetophenone (0.09 mol) in toluene (210 mL) was also added dropwise. The resulting suspension was stirred at 0 °C for 1 h then it was kept stirring at room temperature for 3 days. After filtration, the solution was evaporated under reduced pressure at bath temperature of 30 °C. The crude product obtained (a reddish-brown, oily liquid, 88%) was used in subsequent reactions without further purification.

***Ethyl 2-(*p*-methoxyphenacyl)acetoacetate (22a) – method 2***



(21.9 g, 88%) <sup>1</sup>H-NMR (400 MHz, CDCl<sub>3</sub>) δ 7.93 (d, J = 9.2 Hz, 2H, **Ar-H<sub>o</sub>**), 6.90 (d, J = 8.7 Hz, 2H, **Ar-H<sub>m</sub>**), 4.20 (q, 3H, **H<sub>α</sub> & CH<sub>2</sub> Et**), 3.85 (s, 3H, ***p*-OMe**), 3.55 (ABX-q, J = 18.3, 8.3, 6.0 Hz, 2H, **-CH<sub>2</sub>COAr**), 2.42 (s, 3H, **CH<sub>3</sub>C=O**), 1.26 (t, 3H, **CH<sub>3</sub> Et**). <sup>13</sup>C-NMR (101 MHz, CDCl<sub>3</sub>) δ 203.60 (**C<sub>3</sub>**), 195.80 (**ArC=O**), 169.60 (**C<sub>1</sub>**), 164.00 (**Ar-C<sub>p</sub>**), 130.86 (**Ar-C<sub>o</sub>**), 129.41 (**Ar-C<sub>i</sub>**), 111.82 (**Ar-C<sub>m</sub>**), 61.00 (**CH<sub>2</sub> Et**), 56.00 (***p*-OCH<sub>3</sub>**), 54.50 (**C<sub>2</sub>**), 37.49 (**-CH<sub>2</sub>COAr**), 27.78(**C<sub>4</sub>**), 14.19 (**CH<sub>3</sub> Et**).

***Ethyl 2-phenacylacetoacetate (22b) – method 2***



(19.0 g, 85%) <sup>1</sup>H-NMR (400 MHz, CDCl<sub>3</sub>) δ 7.96 (d, J = 6.9 Hz, 2H, **Ar-H<sub>o</sub>**), 7.56 (t, J = 7.3 Hz, 1H, **Ar-H<sub>p</sub>**), 7.45 (t, J = 7.8 Hz, 2H **Ar-H<sub>m</sub>**) 4.18-4.24 (m, 3H, **H<sub>α</sub> & CH<sub>2</sub> Et**) 3.48-3.74 (m, 2H, **CH<sub>2</sub>COPh**), 2.43 (s, 3H, **CH<sub>3</sub>C=O**), 1.28 (t, J = 7.1 Hz, 3H,**CH<sub>3</sub> Et**) <sup>13</sup>C-NMR (101 MHz, CDCl<sub>3</sub>) δ: 202.51 (**C<sub>3</sub>**), 197.14 (**ArC=O**), 169.13 (**C<sub>1</sub>**), 136.14 (**Ar-C<sub>i</sub>**), 133.59 (**Ar-C<sub>p</sub>**), 128.74 (**Ar-C<sub>o</sub>**), 128.23 (**Ar-C<sub>m</sub>**), 61.49 (**CH<sub>2</sub> Et**), 53.96 (**C<sub>2</sub>**), 37.48 (**CH<sub>2</sub>COAr**), 30.23 (**C<sub>4</sub>**), 14.13 (**CH<sub>3</sub> Et**).

## 2.6.2 Preparation of Ethyl 2-methyl-5-aryl-3-furoate (23)

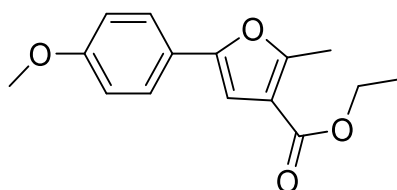
### Method 1

A mixture of the appropriate crude ethyl phenacylacetate (0.02 mol) and concentrated hydrochloric acid (30 mL) was heated under reflux (20 h) protected from air by means of nitrogen trap. After cooling, the mixture was extracted with toluene and washed with water. The dark crude material was allowed to stand overnight to allow for crystallization of the furan ester. The granular crystals formed were washed from the mother liquor with ethanol to obtain grey crystals (20 - 23%).

### Method 2

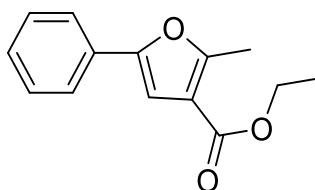
Concentrated hydrochloric acid (20 mL) was added to a solution of suitable ethyl phenacylacetate (0.020 mol) in ethanol (200 mL) and the resulting solution was heated at reflux with stirring for 24 h. The solution was evaporated under reduced pressure to a small volume and transferred into water (200 mL) then extracted with diethyl ether. The organic layer was separated, washed with water, dried over anhydrous sodium sulphate and the solvent removed using a rotary evaporator. The residue was dissolved in toluene and passed through an aluminium oxide column. The central eluates were collected and evaporated to give a residue which was crystallized from ethanol in 76-78% yield.

### *Ethyl 2-methyl-5-(p-methoxyphenyl)-3-furoate (23a) – method 2*



(4.06 g, 78%)  $^1\text{H-NMR}$  (400 MHz,  $\text{CDCl}_3$ )  $\delta$  7.54 (d,  $J = 8.7$  Hz, 2H, **Ar-H<sub>o</sub>**), 6.89 (d,  $J = 8.7$  Hz, 2H, **Ar-H<sub>m</sub>**), 6.93 (s, 1H, **H<sub>4</sub> furan**), 4.27 (q, 2H, **CH<sub>2</sub> Et**), 3.82 (s, 3H, **OCH<sub>3</sub>**), 2.62 (s, 3H, **CH<sub>3</sub> furan**), 1.36 (s, 3H, **CH<sub>3</sub> Et**).  $^{13}\text{C-NMR}$  (101 MHz,  $\text{CDCl}_3$ )  $\delta$  164.37 (**Ar-C<sub>p</sub>**), 159.32 (**C=O**), 158.05 (**C<sub>5</sub> furan**), 151.86 (**C<sub>2</sub> furan**), 125.35 (**Ar-C<sub>o</sub>**), 123.23 (**Ar-C<sub>i</sub>**), 115.27 (**C<sub>3</sub> furan**), 114.50 (**Ar-C<sub>m</sub>**), 103.93 (**C<sub>4</sub> furan**), 60.53 (**CH<sub>2</sub> Et**), 55.59 (**OCH<sub>3</sub>**), 14.55 (**CH<sub>3</sub> Et**), 13.58 (**CH<sub>3</sub> furan**).  
 $m/z$  (ES-MS) :  $[\text{M}_2+\text{Na}]^+$ , 543.12,  $[\text{MH}]^+$ , 261.07,  $[\text{M}-\text{C}_3\text{H}_5\text{O}_2]$ , 188.03

### **Ethyl 2-methyl-5-phenyl-3-furoate (23b) – method 2**



(3.5 g, 76%)  $^1\text{H-NMR}$  (400 MHz,  $\text{CDCl}_3$ )  $\delta$  7.63 (d,  $J = 8.3$  Hz, 2H, **Ph-H<sub>o</sub>**), 7.37 (t,  $J = 7.6$  Hz, 2H, **Ph-H<sub>m</sub>**), 7.25 (t,  $J = 3.7$  Hz, 1H, **Ph-H<sub>p</sub>**), 6.88 (s, 1H, **H-4 furan**), 4.30 (q,  $J = 7.1$  Hz, 2H, **CH<sub>2</sub> Et**), 2.64 (s, 3H, **CH<sub>3</sub> furan**), 1.36 (t,  $J = 7.1$  Hz, 3H, **CH<sub>3</sub> Et**).  $^{13}\text{C-NMR}$  (101 MHz,  $\text{CDCl}_3$ )  $\delta$  164.43 (**C<sub>5</sub> furan**), 159.08 (**C=O furan**), 151.97 (**C<sub>2</sub> furan**), 131.04 (**Ph-C<sub>i</sub>**), 129.14 (**Ph-C<sub>m</sub>**), 125.19 (**Ph-C<sub>p</sub>**), 123.20 (**Ph-C<sub>o</sub>**), 114.24 (**C<sub>3</sub> furan**), 103.90 (**C<sub>4</sub>**), 60.26 (**CH<sub>2</sub> Et**), 14.48 (**CH<sub>3</sub> Et**), 13.98 (**CH<sub>3</sub> furan**).

### **2.6.3 Preparation of 2-Methyl-5-aryl-3-furoic acids (24)**

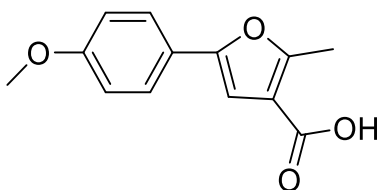
#### **Method 1**

The furan ester [ethyl 2-methyl-5-aryl-3-furoate (0.02 mol)] was hydrolysed by heating at reflux with 5% aqueous potassium hydroxide solution (250 mL) for 3 h. After cooling, some neutral materials were extracted with toluene (50 mL x 2), the aqueous layer was then acidified with 2M HCl until a white precipitate is formed. The precipitate was filtered and dried *in vacuo*. This gave the corresponding furan acid (2-methyl-5-aryl-3-furoic acid) as a white solid.

#### **Method 2**

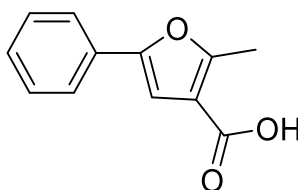
To a stirred solution of ethanol (300 mL) small pieces of sodium (0.15 mol) were added slowly at room temperature. After the reaction was stopped a solution of suitable ethyl ester of 2-methyl-5-aryl-3-furoic acid (0.03 mol) in ethanol (50 mL) was added and the solution was refluxed overnight. The solution was reduced to a small volume, poured into water (200 mL) and extracted with diethyl ether (200 mL x 2). The aqueous layer was separated and acidified by hydrochloric acid (2M). The precipitate formed on cooling was filtered off and recrystallized from ethanol as a white solid.

### 2-Methyl-5-(*p*-methoxyphenyl)-3-furoic acid (24a) – method 2



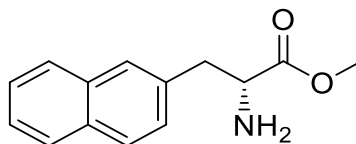
(5.1 g, 73%)  $^1\text{H-NMR}$  (400 MHz,  $\text{DMSO-d}_6$ )  $\delta$  7.59 (d,  $J = 8.7$  Hz, 2H **Ar-H<sub>o</sub>**), 6.94 (d,  $J = 9.2$  Hz, 2H **Ar-H<sub>m</sub>**), 6.88 (s, 1H, **H-4 furan**), 3.74 (s, 3H, ***p*-OCH<sub>3</sub>**), 2.54 (s, 3H, **CH<sub>3</sub> furan**).  $^{13}\text{C-NMR}$  (101 MHz,  $\text{d}_6\text{-DMSO}$ )  $\delta$  165.12 (**C<sub>5</sub> furan**), 159.65 (**Ar-C<sub>p</sub>**), 157.60 (**C=O**), 151.59 (**C<sub>2</sub> furan**), 125.48 (**Ar-C<sub>o</sub>**), 122.91 (**Ar-C<sub>i</sub>**), 116.17 (**C<sub>3</sub> furan**), 114.88 (**Ar-C<sub>m</sub>**), 104.99 (**C<sub>4</sub> furan**), 55.71 (**OCH<sub>3</sub>**), 14.01 (**CH<sub>3</sub> furan**). Anal. Calcd. For  $\text{C}_{13}\text{H}_{12}\text{O}_4$  (232.23): C, 67.23; H, 5.21; O, 27.56; found C, 67.09; H, 5.33; O, 27.58  $m/z$  (ES-MS):  $[\text{M}_2+\text{Na}]^+$ , 487.30;  $[\text{MH}]^+$ , 233.06

### 2-Methyl-5-phenyl-3-furoic acid (24b) – method 2



(4.8 g, 79%)  $^1\text{H-NMR}$  (400 MHz,  $\text{DMSO-d}_6$ )  $\delta$  7.66 (d,  $J = 6.9$  Hz, 2H, **Ph-H<sub>o</sub>**), 7.38 (t,  $J = 7.8$  Hz, 2H, **Ph-H<sub>m</sub>**), 7.26 (t,  $J = 7.3$  Hz, 1H, **Ph-H<sub>p</sub>**), 7.06 (s, 1H, **H-4 furan**), 2.56 (s, 3H, **CH<sub>3</sub> furan**)  $^{13}\text{C-NMR}$  (101 MHz,  $\text{d}_6\text{-DMSO}$ )  $\delta$  165.16 (**C<sub>5</sub> furan**), 158.53 (**C=O**), 151.60 (**C<sub>2</sub> furan**), 130.02 (**Ph-C<sub>i</sub>**), 129.44 (**Ph-C<sub>m</sub>**), 128.47 (**Ph-C<sub>p</sub>**), 123.89 (**Ph-C<sub>o</sub>**), 116.47 (**C<sub>3</sub> furan**), 106.64 (**C<sub>4</sub> furan**), 14.06 (**CH<sub>3</sub>**)

### 2.6.4 Preparation of methyl ester of 3-(2-naphthyl)-D-alanine (25)



Methyl ester of 3-(2-naphthyl)-D-alanine was prepared from 3-(2-naphthyl)-D-alanine (2.3 g, 10.69 mmol), anhydrous methanol (40 mL) and thionyl chloride (1.4 mL, 18.6 mmol) as described in section 2.3.1. The product was recrystallized from methanol to obtain a white solid.

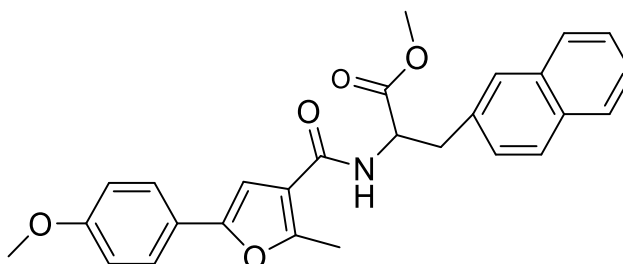
(2.17 g, 89%) <sup>1</sup>H-NMR (400 MHz, DMSO-d<sub>6</sub>) δ 8.76 (s, 2H, **NH**<sub>2</sub>), 7.82-7.88 (m, 3H, **H**<sub>1,4</sub> & 5 **Naph**), 7.35-7.50 (m, 4H, **H**<sub>2,3,6</sub> & 8 **Naph**), 4.33 (s, 1H, **H**<sub>α</sub> **Naph-ala**), 3.63 (s, 3H, **OCH**<sub>3</sub>), 3.30 (ddd, J = 33.0, 13.8, 6.5 Hz, 2H, **H**<sub>β</sub> **Naph-ala**).

### 2.6.5 Coupling of 2-methyl-5-aryl-3-furoic acid with amino acid esters

The coupling of the amino acids (D-tryptophan methyl ester, D-tyrosine methyl ester, D-phenylalanine methyl ester, or 3-(2-naphthyl)-D-alanine methyl ester) with 5-(*p*-methoxyphenyl)-2-methylfuran-3-carboxylic acid followed the procedure described under section 2.3.2 as described below.

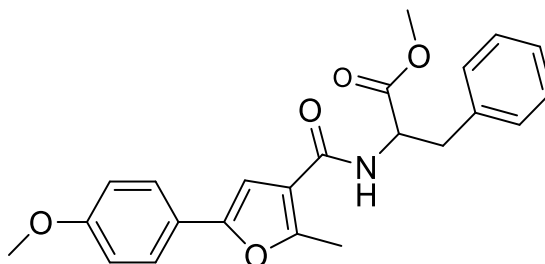
Diisopropylethylamine (DIPEA) (3.9 mL, 22.6 mmol) was added dropwise (using a dropping funnel) to a solution of D-tryptophan methyl ester hydrochloride or D-tyrosine methyl ester hydrochloride or D-phenylalanine methyl ester hydrochloride or 3-(2-naphthyl)-D-alanine (8.6 mmol) in dichloromethane (40 mL) at 0 °C and the clear colourless solution was stirred for 20 min. Then, 5-(*p*-methoxyphenyl)-2-methylfuran-3-carboxylic acid or 5-phenyl-2-methylfuran-3-carboxylic acid (8.6 mmol) in dichloromethane (20 mL) was added in portions to the reaction mixture. After the addition of 1-hydroxybenzotriazole, HOBt (1.6 g, 10.4 mmol), the solution was stirred for 20 min at 0 °C and *N*-(3-dimethylaminopropyl)-*N'*-ethylcarbodiimide (EDC) hydrochloride (2.3 g, 11.8 mmol) was added in portions. The resulting mixture was stirred at 0 °C for 30 min and stirred at room temperature for 24 h. Then, 10% monosodium citrate solution (30 mL) was added. The organic layer was separated, washed with saturated NaHCO<sub>3</sub> solution (20 mL x 2), H<sub>2</sub>O (20 mL x 2), and saturated brine (20 mL x 2), dried over anhydrous Na<sub>2</sub>SO<sub>4</sub>, and filtered. The solvent was evaporated under reduced pressure to obtain the corresponding crude furoate ester as yellow 'oily solid'. The recrystallization was in ethyl acetate to provide the corresponding amide.

#### ***Methyl (2-methyl-5-(*p*-methoxyphenyl)-3-furoyl)-3-(2-naphthyl)-alaninate (26)***



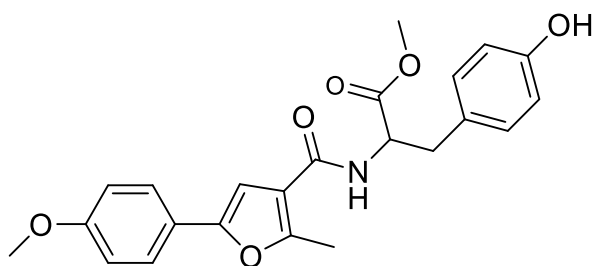
(2.6 g, 72%)  $^1\text{H-NMR}$  (400 MHz,  $\text{CDCl}_3$ )  $\delta$  8.09 (d,  $J = 8.2$  Hz, 1H), 7.78 (d,  $J = 8.7$  Hz, 3H), 7.63 (d,  $J = 9.1$  Hz, 2H), 7.48 (q,  $J = 9.3$  Hz, 4H), 7.26 (d,  $J = 6.4$  Hz, 2H), 6.96 (d,  $J = 5.9$  Hz, 1H), 6.89 (d,  $J = 8.7$  Hz, 2H,  $\text{H}_m$  Ar-furan), 6.42 (s, 1H,  $\text{H}_4$  furan), 6.20 (d,  $J = 9.1$  Hz, 1H, **NH**), 5.13 (s, 1H,  $\text{H}_\alpha$  Naph), 3.81 (s, 3H, **OCH<sub>3</sub>** Ar-furan), 3.76 (s, 3H, **OCH<sub>3</sub>** Naph), 3.39 (m, 2H,  $\text{H}_\beta$  Naph), 2.58 (s, 3H, **CH<sub>3</sub>** furan).  $^{13}\text{C-NMR}$  (101 MHz,  $\text{CDCl}_3$ )  $\delta$  172.32 (**C=O** Naph), 163.29 (**C<sub>5</sub>** furan), 159.35 (**C=O** furan), 155.94 (**C<sub>p</sub>** Ar-furan), 151.87 (**C<sub>2</sub>** furan), 133.52 (**C<sub>i</sub>** naphthyl), 132.59 (**C<sub>8a</sub>** naphthyl), 128.41, 128.26, 127.80, 127.65, 127.49 (**C<sub>3,3a,4,5,&7a</sub>** naphthyl), 126.34 (**C<sub>2</sub>** naphthyl), 125.91 (**C<sub>8</sub>** naphthyl), 125.23 (**C<sub>o</sub>** Ar-furan & **C<sub>7</sub>** naphthyl), 123.02 (**C<sub>i</sub>** Ar-furan), 117.01 (**C<sub>3</sub>** furan), 114.24 (**C<sub>m</sub>** Ar-furan), 101.66 (**C<sub>4</sub>** furan), 55.26 (**C<sub>\alpha</sub>** Naph), 53.13 (**p-OCH<sub>3</sub>**), 52.59 (**OCH<sub>3</sub>** Naph), 38.10 (**C<sub>\beta</sub>** Naph), 13.70 (**CH<sub>3</sub>** furan). Anal. calcd. for  $\text{C}_{27}\text{H}_{25}\text{NO}_5$  (443.50): C, 73.12; H, 5.68; N, 3.16; Found: C; 71.34; H, 5.68; N, 3.62.  $m/z$  (ES-MS) :  $[\text{MH}]^+$ , 444.13.

***Methyl (2-methyl-5-(p-methoxyphenyl)-3-furoyl)phenylalaninate***  
(27)



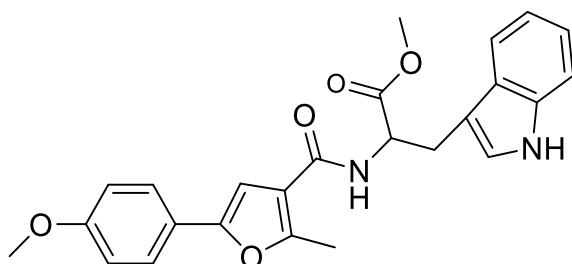
(2.4 g, 75%)  $^1\text{H-NMR}$  (400 MHz,  $\text{CDCl}_3$ )  $\delta$  7.53 (d,  $J = 11.9$  Hz, 2H,  $\text{H}_o$  Ar-furan), 7.24-7.29 (m, 3H,  $\text{H}_m$  &  $\text{H}_p$  Phe), 7.12 (d,  $J = 6.4$  Hz, 2H,  $\text{H}_o$  Phe), 6.90 (d,  $J = 2.3$  Hz, 2H,  $\text{H}_m$  Ar-furan), 6.45 (s, 1H,  $\text{H}_4$  furan), 6.16 (d,  $J = 7.8$  Hz, 1H, **NH**), 5.04 (q, 1H,  $\text{H}_\alpha$  Phe), 3.82 (s, 3H, **p-OCH<sub>3</sub>**), 3.75 (s, 3H, **OCH<sub>3</sub>** Phe), 3.22 (ABX q,  $J = 23.0, 13.8, 5.6$  Hz, 2H,  $\text{H}_\beta$  Phe), 2.58 (s, 3H, **CH<sub>3</sub>** furan).  $^{13}\text{C-NMR}$  (101 MHz,  $\text{CDCl}_3$ )  $\delta$  172.29 (**C=O** Phe), 163.35 (**C<sub>5</sub>** furan), 159.37 (**C=O** furan), 155.90 (**C<sub>p</sub>** Ar-furan), 151.97 (**C<sub>2</sub>** furan), 135.94 (**C<sub>i</sub>** Phe), 129.45 (**C<sub>m</sub>** Phe), 128.72 (**C<sub>o</sub>** Phe), 127.30 (**C<sub>o</sub>** Ar-furan), 125.25 (**C<sub>p</sub>** Phe), 123.04 (**C<sub>i</sub>** Ar-furan), 117.01 (**C<sub>m</sub>** Ar-furan), 114.26 (**C<sub>3</sub>** furan), 101.55 (**C<sub>4</sub>** furan), 55.43 (**C<sub>\alpha</sub>** Phe), 53.08 (**p-OCH<sub>3</sub>**), 52.54 (**OCH<sub>3</sub>** Phe), 38.06 (**C<sub>\beta</sub>** Phe), 13.77 (**CH<sub>3</sub>** furan). Anal. calcd. for  $\text{C}_{23}\text{H}_{23}\text{NO}_5$  (393.44): C, 70.21; H, 5.89; N, 3.56; Found: C; 69.90; H, 5.97; N, 3.72.  $m/z$  (ES-MS) :  $[\text{M}_2]^+$ , 786.78;  $[\text{MH}]^+$ , 394.19;  $[\text{M}-\text{C}_{10}\text{H}_{11}\text{NO}_2]$ , 214;

**Methyl (2-methyl-5-(*p*-methoxyphenyl)-3-furoyl)tyrosinate (28)**



(2.7 g, 81%)  $^1\text{H-NMR}$  (400 MHz,  $\text{CDCl}_3/\text{TFA}$ )  $\delta$  7.52 (d,  $J = 8.7$  Hz, 2H,  $\text{H}_o$  Ar-furan), 6.98 (d,  $J = 8.7$  Hz, 2H,  $\text{H}_m$  Ar-furan), 6.92 (d,  $J = 8.7$  Hz, 2H,  $\text{H}_o$  Tyr), 6.76 (d,  $J = 8.7$  Hz, 2H,  $\text{H}_m$  Tyr), 6.62 (d,  $J = 8.2$  Hz, 1H, **NH**), 6.49 (s, 1H,  $\text{H}_4$  furan), 5.02 (q, 1H,  $\text{H}_\alpha$  Tyr), 3.84 (s, 3H, ***p*-OCH<sub>3</sub>**), 3.81 (s, 3H, **OCH<sub>3</sub>** Tyr), 3.14 (ABX q,  $J = 13.8, 5.8$  Hz, 2H,  $\text{H}_\beta$  Tyr), 2.52 (s, 3H, **CH<sub>3</sub>** furan).  $^{13}\text{C-NMR}$  (101 MHz,  $\text{CDCl}_3/\text{TFA}$ )  $\delta$  173.00 (**C=O** Tyr), 165.50 (**C<sub>5</sub>** furan), 159.54 (**C=O** furan), 156.61 (**C<sub>p</sub>** Ar-furan), 154.78 (**C<sub>2</sub>** furan), 152.66 (**C<sub>p</sub>** Tyr), 130.58 (**C<sub>o</sub>** Tyr), 127.31 (**C<sub>i</sub>** Tyr), 125.40 (**C<sub>o</sub>** Ar-furan), 122.56 (**C<sub>i</sub>** Ar-furan), 115.66 (**C<sub>m</sub>** Tyr), 114.35 (**C<sub>m</sub>** Ar-furan), 113.25 (**C<sub>3</sub>** furan), 101.44 (**C<sub>4</sub>** furan), 55.51 (**C<sub>\alpha</sub>** Tyr), 53.66 (***p*-OCH<sub>3</sub>**), 52.85 (**OCH<sub>3</sub>** Tyr), 37.03 (**C<sub>\beta</sub>** Tyr), 13.84 (**CH<sub>3</sub>** furan). Anal. calcd. for  $\text{C}_{23}\text{H}_{23}\text{NO}_6$  (409.44): C, 67.47; H, 5.66; N, 3.42; Found: C, 66.79; H, 5.69; N, 3.50.  $m/z$  (ES-MS) :  $[\text{M}_2]^+$ , 818.82;  $[\text{MH}]^+$ , 410.18;  $[\text{M}-\text{C}_{10}\text{H}_{12}\text{NO}_3]^+$ , 215.03.

**Methyl (2-methyl-5-(*p*-methoxyphenyl)-3-furoyl)tryptophanate (29)**



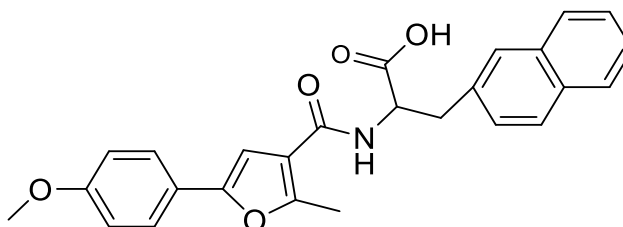
(2.8 g, 76%)  $^1\text{H-NMR}$  (400 MHz,  $\text{CDCl}_3$ )  $\delta$  8.24 (s, 1H, **NH** indole), 7.57 (d,  $J = 7.8$  Hz, 1H,  $\text{H}_4$  indole), 7.47 (d,  $J = 9.1$  Hz, 2H,  $\text{H}_o$  Ar-furan), 7.37 (d,  $J = 7.8$  Hz, 1H,  $\text{H}_7$  indole), 7.20 (t, 1H,  $\text{H}_6$  indole), 7.11 (t, 1H,  $\text{H}_5$  indole), 7.00 (s, 1H,  $\text{H}_2$  indole), 6.89 (d,  $J = 8.7$  Hz, 2H,  $\text{H}_m$  Ar-furan), 6.28 (s, 1H,  $\text{H}_4$  furan), 6.25 (d,  $J = 7.8$  Hz, 1H, **NH** Trp), 5.08 (q, 1H,  $\text{H}_\alpha$  Trp), 3.82 (s, 3H, ***p*-OCH<sub>3</sub>**), 3.71 (s, 3H, **OCH<sub>3</sub>** Trp), 3.41 (d,  $J = 5.0$  Hz, 2H,  $\text{H}_\beta$  Trp), 2.57 (s, 3H, **CH<sub>3</sub>** furan).  $^{13}\text{C-NMR}$  (101 MHz,  $\text{CDCl}_3$ )  $\delta$  172.59 (**C=O** Trp), 163.46 (**C<sub>5</sub>** furan), 159.41 (**C=O** furan), 155.80 (**C<sub>p</sub>** Ar-furan), 152.00 (**C<sub>2</sub>** furan), 136.23 (**C<sub>7a</sub>** indole), 127.80 (**C<sub>i</sub>** Ar-furan), 125.16 (**C<sub>o</sub>** Ar-furan),

123.07 (**C**<sub>3a</sub> indole), 122.97(**C**<sub>2</sub> indole), 122.41(**C**<sub>6</sub> indole), 119.87 (**C**<sub>5</sub> indole), 118.80 (**C**<sub>4</sub> indole), 116.98 (**C**<sub>3</sub> furan), 114.23 (**C**<sub>m</sub> Ar-furan), 111.48 (**C**<sub>7</sub> indole), 110.00 (**C**<sub>3</sub> indole), 101.79 (**C**<sub>4</sub> furan), 55.42 (**C**<sub>α</sub> Trp), 53.16 (**p-OCH**<sub>3</sub>), 52.63 (**OCH**<sub>3</sub> Trp), 27.72 (**C**<sub>β</sub> Trp), 13.73 (**CH**<sub>3</sub> furan). Anal. calcd. for C<sub>25</sub>H<sub>24</sub>N<sub>2</sub>O<sub>5</sub> (432.48): C, 69.43; H, 5.59; N, 6.48; Found: C, 69.29; H, 5.53; N, 6.52. *m/z* (ES-MS) : [M<sub>2</sub>H]<sup>+</sup>, 865.00; [MH]<sup>+</sup>, 433.19.

### 2.6.6 Hydrolysis of methyl ester of the coupled amide

Methanol (30 mL) was added to the white powder of the coupled amide (3.4 mmol) in a 100 mL three-neck flask equipped with a magnetic stirrer and a condenser. The mixture was then stirred for 20 min. Aqueous 5% KOH solution (10 mL) was added to the mixture and the resulting mixture was allowed to stir at room temperature overnight. The resulting solution was concentrated on a rotary evaporator to a smaller volume (10 mL). A solution of 1M hydrochloric acid was added to the concentrated solution in drops until a precipitate was formed. The precipitate was filtered and washed with more 1M HCl. The solid was dried *in vacuo* to obtain a cream colour solid.

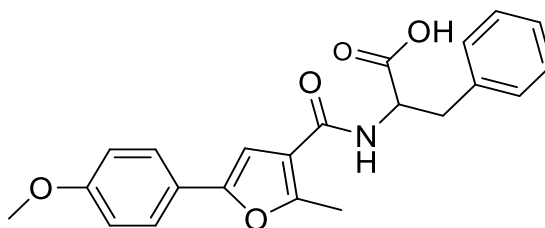
#### (2-Methyl-5-(*p*-methoxyphenyl)-3-furoyl)-3-(2-naphthyl)alanine (30)



(0.80 g, 55%) <sup>1</sup>H-NMR (400 MHz, DMSO-*d*<sub>6</sub>) δ 7.44-7.79 (m, 9H, **Ar-H**), 6.88-6.97 (m, 3H, **Ar-H**), 6.42 (s, 1H, H<sub>4</sub> furan), 6.20 (d, J = 7.8 Hz, 1H, **NH**), 5.12 (dd, J = 13.0, 5.7 Hz, 1H, **H**<sub>α</sub> Naph), 3.39 (t, J = 5.7 Hz, 2H, **H**<sub>β</sub> Naph), 2.58 (s, 3H, **CH**<sub>3</sub> furan). <sup>13</sup>C-NMR (101 MHz, *d*<sub>6</sub>-DMSO) δ 172.10 (**C=O** Naph), 171.24(**C**<sub>5</sub> furan), 163.64 (**C=O** furan), 159.37 (**C**<sub>2</sub> furan), 133.59(**C**<sub>7</sub> Naph), 133.53(**C**<sub>9</sub> Naph), 132.60(**C**<sub>10</sub> Naph), 128.39(**C**<sub>m</sub> Ar-furan), 128.21(**C**<sub>p</sub> Ar-furan), 127.77(**C**<sub>6</sub> & 8 Naph), 127.64 (**C**<sub>4</sub> Naph), 127.47(**C**<sub>1</sub> Naph), 126.31(**C**<sub>5</sub> Naph), 125.88(**C**<sub>2</sub> Naph), 125.21(**C**<sub>o</sub> Ar-furan & **C**<sub>7</sub> Naph), 123.03, 117.04, 114.23(**C**<sub>2</sub> furan), 101.70(**C**<sub>4</sub> furan), 60.47 (**C**<sub>α</sub> Naph), 38.22(**C**<sub>β</sub> Naph), 13.70 (**CH**<sub>3</sub> furan). Anal. calcd. for C<sub>26</sub>H<sub>23</sub>NO<sub>5</sub> (429.47): C, 72.71; H, 5.40; N, 3.26; Found: C, 71.89; H, 5.35; N, 3.15. *m/z* (ES-MS): [MH]<sup>+</sup>, 430.14.

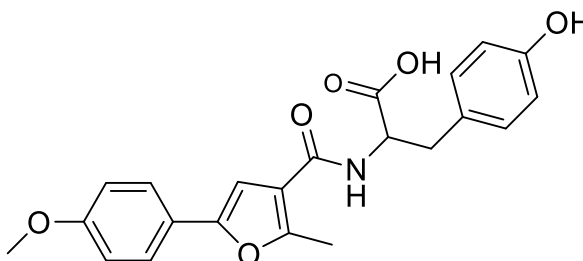


**(2-Methyl-5-(*p*-methoxyphenyl)-3-furoyl)phenylalanine (31)**



(0.86 g, 67%)  $^1\text{H-NMR}$  (400 MHz,  $\text{DMSO-d}_6$ )  $\delta$  8.24 (d,  $J = 8.2$  Hz, 1H, **NH**), 7.50 (d,  $J = 9.1$  Hz, 2H, **H<sub>o</sub> Ar-furan**), 7.21-7.28 (m, 4H, **H<sub>o</sub> & H<sub>m</sub> Phe**), 7.14 (t,  $J = 7.1$  Hz, 2H, **H<sub>p</sub> Phe & H<sub>4</sub> furan**), 6.97 (d,  $J = 8.7$  Hz, 2H, **H<sub>m</sub> Ar-furan**), 4.50-4.56 (m, 1H, **H<sub>α</sub> Phe**), 3.74 (s, 3H, ***p*-OCH<sub>3</sub>**), 2.96-3.15 (m, 2H, **H<sub>β</sub> Phe**), 2.43 (s, 3H, **CH<sub>3</sub> furan**)  $^{13}\text{C-NMR}$  (101 MHz,  $\text{d}_6\text{-DMSO}$ )  $\delta$  173.79 (**C=O Phe**), 163.36 (**C<sub>5</sub> furan**), 159.36 (**C=O furan**), 155.56 (**C<sub>p</sub> Ar-furan**), 150.99 (**C<sub>2</sub> furan**), 138.66 (**C<sub>i</sub> Phe**), 129.59 (**C<sub>m</sub> Phe**), 128.74 (**C<sub>o</sub> Phe**), 126.89 (**C<sub>o</sub> Ar-furan**), 125.19 (**C<sub>p</sub> Phe**), 123.07 (**C<sub>i</sub> Ar-furan**), 117.77 (**C<sub>3</sub> furan**), 115.02 (**C<sub>m</sub> Ar-furan**), 103.56 (**C<sub>4</sub> furan**), 55.73 (**C<sub>α</sub> Phe**), 54.20 (***p*-OCH<sub>3</sub>**), 36.78 (**C<sub>β</sub> Phe**), 13.79 (**CH<sub>3</sub> furan**). Anal. calcd. for  $\text{C}_{22}\text{H}_{21}\text{NO}_5$  (379.14): C, 69.65; H, 5.58; N, 3.69; Found: C, 67.59; H, 5.53; N, 3.87.  $m/z$  (ES-MS) :  $[\text{MH}]^+$ , 380.13.

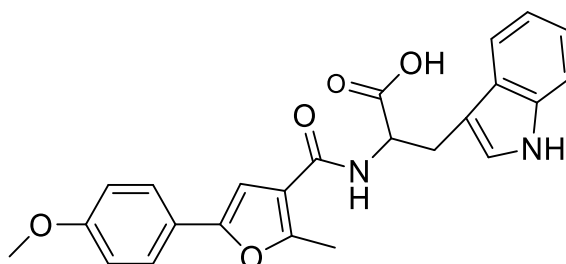
**(2-Methyl-5-(*p*-methoxyphenyl)-3-furoyl)tyrosine (32)**



(0.82 g, 61%)  $^1\text{H-NMR}$  (400 MHz,  $\text{DMSO-d}_6$ )  $\delta$  8.06 (d,  $J = 7.8$  Hz, 1H, **NH**), 7.51 (d,  $J = 8.7$  Hz, 2H, **H<sub>o</sub> Ar-furan**), 7.10 (s, 1H, **C<sub>4</sub> furan**), 7.04 (d,  $J = 8.7$  Hz, 2H, **H<sub>m</sub> Ar-furan**), 6.97 (d,  $J = 9.1$  Hz, 2H, **H<sub>o</sub> Tyr**), 6.60 (d,  $J = 8.7$  Hz, 2H, **H<sub>m</sub>Tyr**), 4.42 (t,  $J = 5.0$  Hz, 1H, **H<sub>α</sub> Tyr**), 3.74 (s, 3H, ***p*-OCH<sub>3</sub>**), 2.82-3.03 (m, 2H, **H<sub>β</sub> Tyr**), 2.52 (s, 3H, **CH<sub>3</sub> furan**).  $^{13}\text{C-NMR}$  (101 MHz,  $\text{DMSO-d}_6$ )  $\delta$  174.00 (**C=O Tyr**), 163.22 (**C<sub>5</sub> furan**), 159.35 (**C=O furan**), 156.32 (**C<sub>p</sub> Ar-furan**), 155.41 (**C<sub>2</sub> furan**), 150.99 (**C<sub>p</sub> Tyr**), 130.53 (**C<sub>o</sub> Tyr**), 128.74 (**C<sub>i</sub> Tyr**), 125.21 (**C<sub>o</sub> Ar-furan**), 123.10 (**C<sub>i</sub> Ar-furan**), 117.91 (**C<sub>3</sub> furan**), 115.48 (**C<sub>m</sub> Tyr**), 115.01 (**C<sub>m</sub> Ar-furan**), 103.54 (**C<sub>4</sub> furan**), 55.72 (**C<sub>α</sub> Tyr**), 54.73 (***p*-OCH<sub>3</sub>**), 36.20 (**C<sub>β</sub> Tyr**), 13.79 (**CH<sub>3</sub> furan**). Anal. calcd.

for C<sub>22</sub>H<sub>21</sub>NO<sub>6</sub> (395.41): C, 66.83; H, 5.35; N, 3.54; Found: C, 66.51; H, 5.44; N, 3.37. *m/z* (ES-MS) : [M<sub>2</sub>H]<sup>+</sup>, 791.03; [MH]<sup>+</sup>, 396.13.

**(2-Methyl-5-(*p*-methoxyphenyl)-3-furoyl)tryptophan (33)**



(1.05 g, 74%) <sup>1</sup>H-NMR (400 MHz, DMSO-d<sub>6</sub>) δ 10.85 (s, 1H, **OH**), 8.11 (d, J = 7.8 Hz, 1H, **NH** indole), 7.55 (d, J = 7.8 Hz, 1H, **NH** Trp), 7.50 (d, J = 9.2 Hz, 2H, **H<sub>o</sub>** Ar-furan), 7.29 (d, J = 7.8 Hz, 1H, **H<sub>7</sub>** indole), 7.16 (s, 1H, **H<sub>2</sub>** indole), 7.13 (s, 1H, **H<sub>4</sub>** furan), 6.93-7.04 (m, 4H, **H<sub>m</sub>** Ar-furan, **H<sub>5&6</sub>** indole), 4.58 (t, J = 12.8, 4.9 Hz, 1H, **H<sub>α</sub>** Trp), 3.74 (s, 3H, ***p*-OCH<sub>3</sub>**), 3.09-3.27 (m, 2H, **H<sub>β</sub>** Trp), 2.44 (s, 3H, **CH<sub>3</sub>** furan). <sup>13</sup>C-NMR (101 MHz, DMSO-d<sub>6</sub>) δ 174.14 (**C=O** Trp), 163.35 (**C<sub>5</sub>** furan), 159.38 (**C=O** furan), 155.59 (**C<sub>p</sub>** Ar-furan), 150.99 (**C<sub>2</sub>** furan), 136.63 (**C<sub>7a</sub>** indole), 127.65 (**C<sub>3a</sub>** indole), 125.18 (**C<sub>o</sub>** Ar-furan), 124.14 (**C<sub>2</sub>** indole), 123.10 (**C<sub>i</sub>** Ar-furan), 121.46 (**C<sub>6</sub>** indole), 118.89 (**C<sub>5</sub>** indole), 118.64 (**C<sub>4</sub>** indole), 117.78 (**C<sub>3</sub>** furan), 115.02 (**C<sub>m</sub>** Ar-furan), 111.97 (**C<sub>7</sub>** indole), 110.80 (**C<sub>3</sub>** indole), 103.55 (**C<sub>4</sub>** furan), 55.73 (**C<sub>α</sub>** Trp), 53.56 (***p*-OCH<sub>3</sub>**), 27.25 (**C<sub>β</sub>** Trp), 13.79 (**CH<sub>3</sub>** furan). Anal. calcd. for C<sub>24</sub>H<sub>22</sub>N<sub>2</sub>O<sub>5</sub> (418.45): C, 68.89; H, 5.30; N, 6.69; Found: C, 66.63; H, 5.62; N, 7.74. *m/z* (ES-MS) : [M<sub>2</sub>]<sup>+</sup>, 836.32; [MH]<sup>+</sup>, 419.16

## 2.7 BIOLOGICAL PROTOCOLS

### 2.7.1 Cell culture

The cell culture was carried out in aseptic conditions in a class II biological safety cabinet. Prior to culturing, every surface was cleaned using ethanol (75% v/v). All the media and reagents were pre-warmed for about 30 min before use in a 37 °C water bath. Only sterile plastic was used. MDA-MB-231, human breast cancer cell line, was used in this experiment. The MDA-MB-231 cell line was cultured in 75 cm<sup>2</sup> flasks in 10 mL of DMEM medium supplemented with 10% FCS (v/v). The cells were incubated at 37 °C under 5% (v/v) CO<sub>2</sub>. Every 2 to 3 days, 2-3 mL of the media were replaced with fresh medium while maintaining the total volume at 10 mL.

### 2.7.2 Subculturing, harvesting and counting the cells

When cells attained 80% confluence, they were washed with sterile phosphate buffered saline (PBS; pH 7.2; 5 mL) following removal of the spent medium from the flask. The washing is for removal of traces of serum and maintenance of the correct pH. The MDA-MB-231 cells were incubated with trypsin/EDTA solution (2-3 mL) for 3-4 min at 37 °C for detachment of the cells. To release the cells, the flask was tapped firmly. Then, the activity of trypsin was blocked by adding pre-warmed complete growth medium (2-3 mL). For cell density determination, the cell suspension (20 µL) was loaded into a haemocytometer and the number of cells in 1 mm<sup>2</sup> area counted. The total number of cells in flask was then calculated as:

$$\text{Total number of cells} = \text{number of cells per mm}^2 \times \text{volume} \times 10,000$$

After transferring to a sterile tube, the cell suspension was centrifuged at 2,400 g at room temperature for 5 min. Following decantation of the supernatant aseptically without disturbing the cell pellet, the cells were re-suspended in fresh medium (2 mL). Aliquots of the cells were then placed in flasks or plates, as required.

### **2.7.3 Cryopreservation of cells**

For cryopreservation of the cells as stocks, the cell pellet was re-suspended in DMSO freezing medium (1 mL) and  $2 \times 10^5$  cells/mL aliquots were dispensed into labelled cryogenic storage vials. The cryovials containing the cells were frozen at  $-70$  °C overnight after placing in a freezing chamber that contained isopropanol. This step ensures a controlled rate decrease in temperature ( $-1$  °C/min) to maintain the optimal viability of the cells. For long-term storage, the cryovials were transferred to liquid nitrogen container the following day. To start a new culture from frozen cells, cryovials containing the cells were defrosted in a  $37$  °C water bath for 1-2 min. The thawed cells were then immediately transferred to flasks that contained pre-warmed complete growth medium.

### **2.7.4 Estimation of protein concentration using the Bradford assay**

For determination of the concentration of protein in the cell lysates, a serial dilution of lipid-free bovine serum albumin (BSA) (0, 10, 20, 50, 100 and 200 µg/mL) was prepared to generate a standard curve. The cell lysates and standards (10 µL) were placed individually into 96-well plates and 200 µL of Bradford reagent (Bradford reagent stock diluted in dH<sub>2</sub>O 3:2 v/v) was added per well. After incubating both the standards and samples in a dark place for 15 min at room temperature, the absorbance of the samples and the standards was measured at 584 nm using a POLARstar OPTIMA plate reader. Based on the absorbance data, a standard curve was generated from a plot of the absorbance reading of the standards against protein concentrations (Figure 2.1). Using the equation from the standard curve, the concentrations of the protein samples were then estimated.

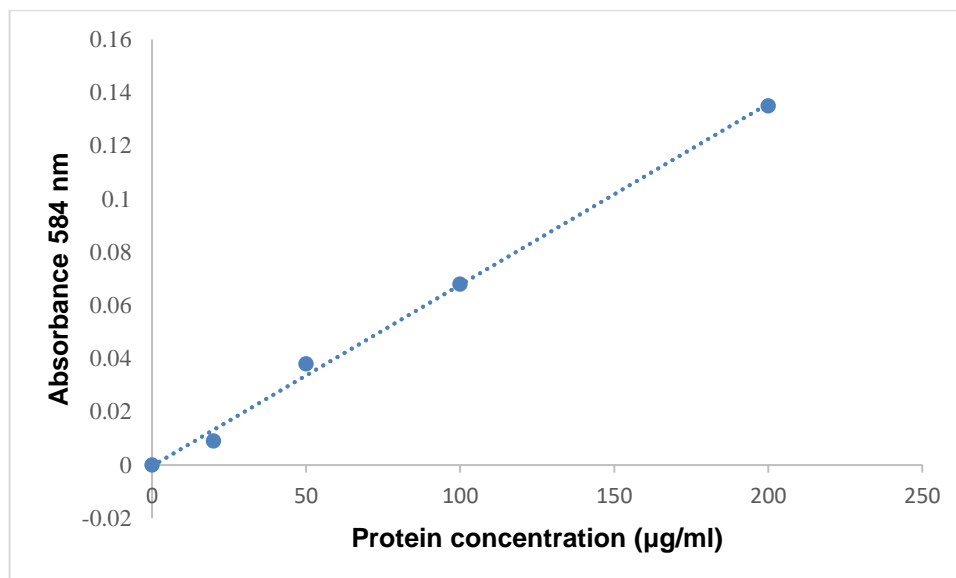


**Figure 2.1.** Standard curve for the Bradford assay. The standard curve was constructed using serially diluted lipid-free BSA solutions prepared with a range of concentration between 0 and 200 µg/mL. The standards (10 µL) were mixed with 200 µL of diluted Bradford reagent in a 96-well plate. Subsequently, the samples were incubated at room temperature in the dark for 15 min. The absorbance of the samples was then measured at 584 nm using a plate reader.

### 2.7.5 SDS-polyacrylamide gel electrophoresis (SDS-PAGE)

To prepare the separating gel 12% (w/v), de-ionised water (3.3 mL), 4 mL acrylamide solution (30% (w/v) acrylamide, 0.8% (w/v) bisacrylamide), 2.6 mL resolving buffer (1.5 M Tris-HCl pH 8.8, 0.4% (w/v) SDS) and 100 µL ammonium persulphate (10% w/v) were mixed. The solution was then gently swirled before adding *N,N,N',N'*-tetramethylethylenediamine (TEMED) (10 µL) to start polymerisation. The gel mixture was then pipetted into the gap between the glass electrophoresis plates in a gel caster. After covering the gel mixture with a layer of butanol (100%), it was left to set at room temperature for 1 h. The butanol was poured from the gel once it was set and a 4% (w/v) stacking gel was prepared by mixing 3 mL de-ionised water, 0.65 mL of the acrylamide solution, 1.3 mL stacking buffer (0.5 M Tris-HCl pH 6.8, 0.4% (w/v) SDS), and 100 µL ammonium persulphate (10% w/v). The solution was then gently mixed and 10 µL of *N,N,N',N'*-tetramethylethylenediamine (TEMED) was added. The solution was pipetted on top of the separating gel and an appropriate comb was inserted and allowed to set for about 1.5 h. The gel and glass plates were

placed in the electrophoresis tank followed by the removal of the comb. The tank was filled with electrophoresis buffer (25 mM Tris-HCl pH 8.3, 192 mM glycine, 0.035% (w/v) SDS) until it covered the gel. 5  $\mu$ L of the molecular-weight protein markers (10-260 kDa) was loaded into the first well, while 20  $\mu$ L of the pre-heated protein samples were loaded into the subsequent wells. Approximately 20  $\mu$ g of protein lysate was loaded on the western blot. Electrophoresis was carried out at 100 V for protein separation until the line of blue dye reach the bottom.

### **2.7.6 Western blot analysis**

Using a transfer system, the proteins were transferred onto a nitrocellulose membrane subsequent to electrophoresis. Prior to positioning of the gel in between the nitrocellulose membrane and blotting paper, the blotting paper and nitrocellulose membrane were prepared and soaked for 2 min in the transfer buffer (150 mM glycine, 20 mM Tris-HCl pH 8.3, 20 % (v/v) methanol). The holder containing the gel-membrane sandwich was placed in a transfer tank containing transfer buffer. The protein bands were transferred at 300 mA for 60 min at 4 °C. Before antibody probing, the nitrocellulose membrane was then blocked with TBST (20 mM Tris-HCl pH 8.0, 150 mM NaCl, 0.05 % (v/v) Tween 20) for 1 h at room temperature on a bench rocker. The membrane was then incubated overnight at 4 °C in primary antibody diluted in TBST. After washing the membrane with TBST three times (5 min each time), it was incubated with an appropriate secondary antibody diluted in TBST for 2 h at room temperature on a bench rocker. At the end of the incubation, the membrane was washed again three times with TBST and finally washed with dH<sub>2</sub>O. The bands were developed with Western Blue-stabilised substrate for alkaline phosphatase, the images were recorded using a digital camera and the visualised bands analysed using the ImageJ program.

### **2.7.7 Determination of optimum concentration for assay**

The optimum concentration was determined by running preliminary experiments whereby MDA-MB-231 cells ( $10^5$ /well) were cultured in 96-well plate; it was afterward incubated for adherence for 4 h. The plates were then incubated for 24 h with 50, 100, 150, 200 or 250  $\mu$ M of the test agents in

triplicate. The cell number was determined using crystal violet staining protocol. The cell number was quantified using the standard curve previously constructed for MDA-MB-231 cells. The concentration that caused 50% reduction in cell number was estimated to be 100  $\mu$ M. This optimum concentration was employed in subsequent experiments.

### **2.7.8 Crystal Violet Staining (CVS) Assay**

The adherent cells were detached and counted as described in section 2.7.2. The resultant mixture was centrifuged at 1000 rpm for 5 minutes. The supernatant medium was carefully decanted into the waste flask and a fresh growth medium was added to give a concentration ( $1 \times 10^6$  cells/mL). In a 96-well plate,  $10^4$  cells per well were seeded by dispensing 10  $\mu$ L of the cell suspension into each well and adding 500  $\mu$ L of culture medium. To three wells were added medium without cells (to serve as controls for nonspecific binding of the crystal violet dye) and the cells were incubated for 4 h at 37 °C to allow for cell adhesion to wells. The medium was aspirated from the wells, and 500  $\mu$ L of fresh medium supplemented with individual test agents (100  $\mu$ M) was added per well. The cells were treated in triplicate wells for each condition while three of the wells were not treated to serve as control. The cells were incubated for 24 h at 37 °C. The medium was aspirated and the cells washed twice in a gentle stream of PBS added down the side of each well. After washing, the plate was inverted on filter paper and tapped gently to remove any liquid remaining.

Following the addition of 0.5% crystal violet staining solution (100  $\mu$ L) to each well, the cells were incubated at room temperature for 20 min on a bench rocker. The crystal violet was removed and kept for further use. Each well was then gently washed three times with distilled water (dH<sub>2</sub>O). After washing, the plate was drained and air-dried. The cells in each well were lysed by adding 100  $\mu$ L of 1% SDS (sodium dodecyl sulphate) solution and incubating for 20 minutes on a bench rocker at room temperature. The absorption of each well was measured with a plate reader at 570 nm (OD<sub>570</sub>). The average OD<sub>570</sub> of the wells without cells was subtracted from the OD<sub>570</sub> of each well on the plate. The average absorption of non-stimulated cells was set to 100% and the average absorption values of stimulated cells compared with the set value to

determine the percentage of stimulated cells that are viable. The mean and the standard error of the mean for at least three independent experiments were calculated.

### **2.7.9 Determination of cell number by crystal violet assay**

MDA-MB-231 breast cancer cells ( $10^5$  cells/well) were seeded in 96-well plate plus a further three wells without cells (as controls for nonspecific binding of the crystal violet dye). The cells were incubated for 4 h at 37 °C to allow for cells to adhere to wells. The medium was then aspirated from the wells; it was replaced with 500  $\mu$ L of fresh medium containing the test agents (100  $\mu$ M) in triplicate. An additional set of untreated cells was used as negative control. The cells were then incubated for 24 h at 37 °C. Cell numbers were determined using the crystal violet staining assay (section 2.7.8) and quantified from a previously constructed standard curve (section 2.7.11).

### **2.7.10 Measurement of cellular apoptosis using the TiterTACS™ chromogenic TUNEL assay.**

During apoptosis, endonucleases are activated resulting in the fragmentation of chromosomal DNA. In this study, a quantitative assay based on fluorescent end-labelling of DNA fragments (TUNEL assay) was employed to detect cellular apoptosis. MDA-MB-231 cells ( $10^5$ /well) were seeded out in 12-well plate and treated with the test reagents (100  $\mu$ M) and the level of cellular apoptosis measured. A set of untrated cells was used as control. Following incubation of cells for 24 h at 37 °C, the cells were washed three times with PBS at room temperature. The cells were then fixed with formaldehyde solution 4% (v/v) (200  $\mu$ L) and incubated at room temperature for 10 min. The cell were washed twice with PBS. Pure methanol (200  $\mu$ L) was added to each well and allowed to stand at room temperature for 20 min to further fix the cells. The methanol was then discarded and cells washed twice with PBS (200  $\mu$ L) per well. The cells were then incubated with cytonin solution (50  $\mu$ L/well) for 15 min at room temperature in order to permeabilise the cells and then washed twice with 800  $\mu$ L of distilled water. H<sub>2</sub>O<sub>2</sub> solution 2.5% (v/v) in methanol (50  $\mu$ L/well) was then added to the cells and incubated for 5 min at room temperature. The cells were washed once with 600  $\mu$ L/well of distilled water after which TdT labelling buffer (600  $\mu$ L/well) was added and incubated for 5



min at room temperature. The labelling buffer was removed and replaced with 200  $\mu\text{L}$ /well of labelling reaction mix (1X TdT labelling buffer containing TdT dNTP Mix (1.4  $\mu\text{L}$ ), TdT Enzyme (1.4  $\mu\text{L}$ ), and 50X  $\text{Mn}^{2+}$  (4  $\mu\text{L}$ )) and incubated for 1 h at 37 °C. The labelling reaction was stopped by adding TdT Stop Buffer (600  $\mu\text{L}$ /well) and incubated for 5 min. Samples were then washed twice with PBS (200  $\mu\text{L}$ /well). Subsequently, Streptavidin-HRP solution (200  $\mu\text{L}$ /well) was added to sample and incubated for 10 min at room temperature. At the end of the incubation, samples were washed four times with Tween 20, 0.1% (v/v) in PBS (200  $\mu\text{L}$ /well). TACS-sapphire (colorimetric substrate) (400  $\mu\text{L}$ ) was then added and incubated in the dark for 30 min. The reaction was stopped with 5% (v/v) phosphoric acid solution (200  $\mu\text{L}$ /well). The content of each well was then transferred into 96-well plate and the absorption measured at 450 nm using a plate reader (POLARstar OPTIMA plate reader). The level of cellular apoptosis was determined in the treated samples based on the amount of the DNA fragments.

#### **2.7.11 Standard Curve for MDA-MB-231 cell count measurement**

MDA-MB-231 cells were seeded in 48-well plate with varying concentrations (0, 5, 10, 25, 50 and 100)  $\times 10^3$  in triplicate by dispensing (0, 5, 10, 25, 50 and 100)  $\mu\text{L}$  respectively of cell suspension with a concentration of ( $10^6$  cells/mL). Each well was then made up to 1 mL with fresh DMEM medium. The cells were incubated at 37 °C in a humidified incubator with 5%  $\text{CO}_2$  for 4 h to attach to the wells. The medium was removed and 3% glutaraldehyde (100  $\mu\text{L}$ ) was added to each well. The plate was incubated at room temperature for 20 mins for the cells to fix. After the incubation the glutaraldehyde was aspirated and the wells were gently washed with  $\text{dH}_2\text{O}$ . A solution of 0.5% crystal violet (200  $\mu\text{L}$ ) was added to each well followed by incubation on a bench rocker for 15 minutes with 20 oscillations per minute. The crystal violet solution was removed to be reused later. The cells were washed gently with  $\text{dH}_2\text{O}$  and the plate inverted on a filter paper with gentle tapping to remove any liquid remaining. A solution of 1% SDS (200  $\mu\text{L}$ ) was added to each well and incubated on a bench rocker for 15 min to lyse the cells. Subsequently, the solution from each well (100  $\mu\text{L}$ ) was appropriately transferred into a 96-well microplate and each well diluted with  $\text{dH}_2\text{O}$  (100  $\mu\text{L}$ ). The absorption of each

well was measured with a plate reader at 570 nm. A standard curve for measuring cell numbers was constructed as shown in Figure 2.2.

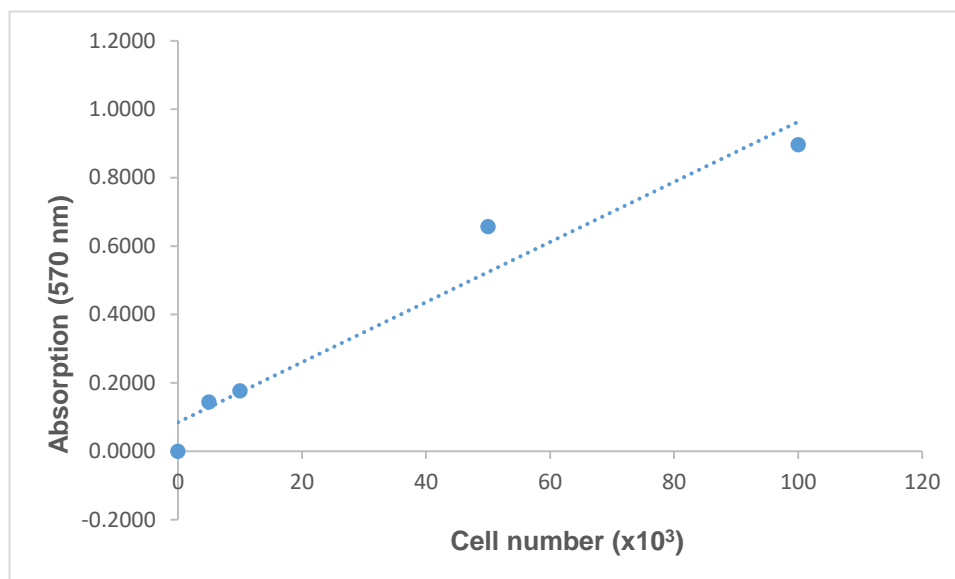


**Figure 2.2.** Standard curve for determination of cell number. MDA-MB-231 (5-100 x10<sup>3</sup> cells) were seeded out into 48-well plates in complete DMEM medium (1 mL). The cells were incubated for 4 h, fixed with 3 % (w/v) glutaraldehyde (100  $\mu$ l) for 20 min and then incubated with 0.5 % (v/v) crystal violet solution (200  $\mu$ L) for a further 30 min. After washing three times with dH<sub>2</sub>O, the cells were lysed with a solution of 1% SDS (200  $\mu$ L) and the samples transferred to 96-well plate. The absorption was measured at 570 nm using a plate reader. (The data is the average of two independent experiments carried out in triplicate).

### 2.7.12 Measurement of p53 expression mediated by the synthesized molecules

To measure the level of p53 protein expression, MDA-MB-231 cells (10<sup>5</sup>/well) were cultured in 12-well plates, then treated with the synthetic small-molecule Pin1 inhibitor for 18 h. Sets of untreated cells were used as control. In Laemmli's buffer (100  $\mu$ l), the cells were lysed and the concentration of protein concentration in individual sample was determined using Bradford assay as earlier described in the general method section 2.7.4. SDS-PAGE and western blot analysis were used to assess the quantity of p53 protein as described in sections 2.7.5 and 2.7.6. Using rabbit anti-p53 and mouse anti-GAPDH antibodies diluted in tris-buffered saline with Tween (TBST), the membranes were probed for p53 and GAPDH respectively. A digital camera was used to

record the images while imageJ program was used to compare the p53 bands to GAPDH.

### **2.7.13 Examination of the effect of the synthetic molecules on nuclear localisation of p53 by fluorescence microscopy**

A fluorescence microscope (Zeiss Axio Vert.A1 fluorescence microscope) was used to carry out investigation of effect of the synthesized agents on nuclear localisation of p53. MDA-MB-231 cells ( $10^3$ ) were placed in 35 mm glass-bottom with 14 mm micro well dishes. The dishes were incubated in a humidified incubator at 37 °C for 4 h to permit adhesion. The medium was then replaced with 100  $\mu$ L of fresh medium supplemented with test agents (100  $\mu$ M). A set of untreated cells was used as negative control and another set was treated with tumor necrosis factor- $\alpha$  (10 ng/mL) as positive control. The medium was removed after 18 h of incubation and cells were washed twice with PBS (200  $\mu$ L) and fixed using 3% (v/v) glutaraldehyde for 30 min. After washing the cells twice with PBS, they were then incubated in 0.2% (v/v) Triton X-100/PBS at room temperature for 10 min to permeabilise the cells. The samples were blocked with 1% (w/v) bovine serum albumin (BSA) for 1 h. The cells were incubated overnight with rabbit polyclonal anti-human p53 antibody diluted 1:250 (v/v) in BSA solution (1% w/v) at 4 °C. After washing twice with PBS, the cells were probed with a donkey anti-rabbit IgG-NL637 diluted 1:100 (v/v) in BSA solution (1% w/v) and incubated in the dark for 1 h. The cells were then washed twice with PBS and labelled with DAPI (5  $\mu$ g/mL) to stain the nuclei. Analysis of cell samples was carried out using a Zeiss Axio Vert.A1 inverted microscope with X40 objective and images captured using the ZEN software. Subsequently, the nuclear co-localisation of p53 was determined using ImagePro Plus software.

### **2.7.14 Investigation of the effect of the synthesized molecules on expression of Bax protein by western blot**

MDA-MB-231 cells ( $10^5$ /well) were cultured in 12-well plates then treated with the test reagents for 18 h. Sets of untreated cells were used as control for comparison. The proteins were separated by 12 % (w/v) SDS-PAGE following lysis of the cells in Laemmli's buffer. Subsequent to the transfer of the proteins onto nitrocellulose membranes, the amount of Bax in the proteins was

estimated by probing the membranes with a mouse anti-human Bax antibody 1:1000 (v/v) in TBST followed by anti-mouse HRP-conjugated antibody 1:5000 (v/v) in TBST. The membranes were also probed for GAPDH using a goat anti-human GAPDH antibody 1:5000 (v/v) in TBST followed by a donkey anti-goat alkaline phosphatase-conjugated antibody 1:5000 (v/v) in TBST. The images were recorded using a digital camera and the visualised bands analysed using the ImageJ program. The amount of Bax protein was quantified against GAPDH.

### **2.7.15 Total RNA isolation**

MDA-MB-231 cells ( $10^5$ /well) were seeded out in 12-well plates then treated with the test reagents for 6 h. Sets of untreated cells were used as negative control. In 1.5 mL tubes, the MDA-MB-231 cells were lysed in total RNA isolation (TRI) reagent (200  $\mu$ L) (manufacturer did not disclose concentrations). Prior to RNA extraction, the lysed cells were incubated for 5 min at room temperature. Following addition of Chloroform (40  $\mu$ L) to each tube to separate sample solution into organic and aqueous layers, the samples were homogenised by vortexing the tubes for 15 s and allowing them to stand at room temperature for 10 min. After centrifuging the samples in a microcentrifuge at 12,000 rpm for 15 min to form aqueous and organic layers, the aqueous phase containing the RNA was transferred carefully into a sterile RNase-free 1.5 mL tube. Isopropanol (100  $\mu$ L) was added to each sample to precipitate the RNA after mixing by vortexing and then incubating for 1 h at -20°C. Again, the samples were centrifuged in a microcentrifuge at 12,000 rpm for 10 min. Following removal of the supernatant, 75 % (v/v) ethanol (200  $\mu$ L) was added to wash the RNA pellet. The RNA pellet was re-suspended in RNase-free water (60  $\mu$ L) and stored at -70°C until required. The absorption of individual sample was measured at 260 nm on a spectrophotometer to quantify the RNA concentration in the samples. The RNA concentration was calculated from the following equation:

$$\text{RNA concentration } (\mu\text{g/mL}) = \text{Absorption}(260 \text{ nm}) \times 40 \times \text{dilution factor}$$

Similarly, the following equation was used to calculate each sample volume that contains 0.1  $\mu$ g RNA for real time RT-PCR.

$$\text{Volume of RNA required } (\mu\text{L}) = \frac{0.1}{\text{RNA concentration} \times 1000}$$

### 2.7.16 Measurement of mRNA expression by Real-time RT-PCR

Subsequent to total RNA isolation from MDA-MB-231 cells ( $10^5$ /well) by TRI reagent system (see section 2.7.15), the mRNA expression was analysed. Using *bax* primer, the RNA sample was amplified while  $\beta$ -actin primer was used to amplify the reference sample. Each primer was reconstituted in RNase-free water to obtain 100 nM solution. The volume of individual RNA solution containing 0.1  $\mu\text{g}$  RNA was calculated as shown in section 2.7.15. Further dilution of the solution of each primed sample with RNase-free water was carried out to obtain a final volume (8.6  $\mu\text{L}$ ). The samples were prepared in duplicates and transferred separately into 20 wells of a 96-well PCR plate. The reconstituted forward and reverse *bax* mRNA or  $\beta$ -actin primers (100 nM each) were mixed together. The mixed forward and reverse *bax* mRNA primers (1  $\mu\text{L}$ ) was added to each sample in duplicate while the mixed  $\beta$ -actin primers (1  $\mu\text{L}$ ) was added to each of the reference samples also in duplicate. The RNA was converted to cDNA followed by the cDNA amplification using the GoTaq® 1-Step RT-qPCR System. The 20  $\mu\text{L}$  reaction-volume per well for each RNA sample was constituted by adding RT-PCR mix (10  $\mu\text{L}$ ), reverse transcriptase enzyme mix (0.4  $\mu\text{L}$ ) (supplied in the assay kit) and RNase free water to make up the volume. Following the RT-PCR using an iCycler thermal cycler RT-PCR, the data obtained were analysed by automatic determination of number of threshold cycle (Ct), using the iQ software. Calculation of mRNA expressed in each sample was carried out using the  $2^{-\Delta\Delta\text{CT}}$  method.<sup>149</sup> For the calculation, the Ct value for each sample mRNA was normalised first against the corresponding  $\beta$ -actin to obtain  $\Delta\text{Ct}$  while the difference between  $\Delta\text{Ct}$  for each of the treated samples and that for the control gave the respective  $\Delta\Delta\text{Ct}$ .

# Chapter 3: Discussion – synthetic mimics of Pin1 substrate

## 3.1 SYNTHETIC MIMICS OF SERINE-PROLINE MOTIF

The development of the idea behind this study came from a previous report which revealed that the last eighteen amino acid residue of the cytoplasmic domain of TF (RKAGVGQSKENWSPLNVS) prevented cellular release of TF when cancer cells were transfected by the peptide.<sup>80</sup> Consequently, the prevention of TF release caused TF to accumulate within the cell with subsequent initiation of mechanisms that induce cell death. It was established from a repeat study in eight cancer cell lines including MDA-MB-231, ASPC-1 and SKOV-3 that the peptide was capable of reducing proliferation of cancer cells.<sup>150</sup> Importantly, it was reported that TF release is modulated by phosphorylation of Ser253 and Ser258 in the TF cytoplasmic domain. A recent study, however, confirmed that Pin1 is the modulator of the phosphorylation in the TF cytoplasmic domain.<sup>81</sup> In view of these reports, it was thought reasonable to investigate inhibition of Pin1 with a synthetic mimic of its specific substrate, pSer-Pro (**A**), and determine the effect on tumour cells. Similarly, another projection was the development of synthetic pathways to analogues of **A** such as **B** wherein the O- in the serine residue has been replaced by N- (Figure 3.1), to provide metabolically more stable analogues.

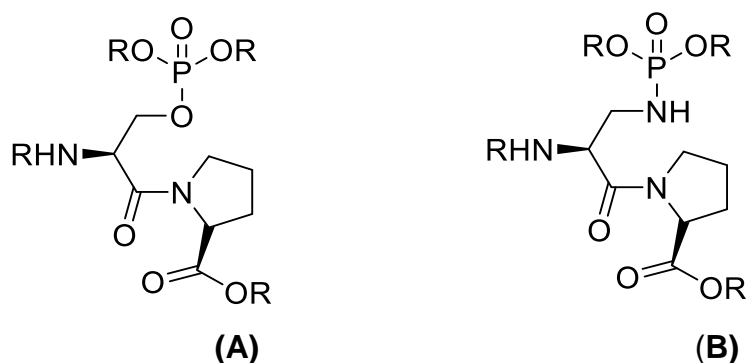
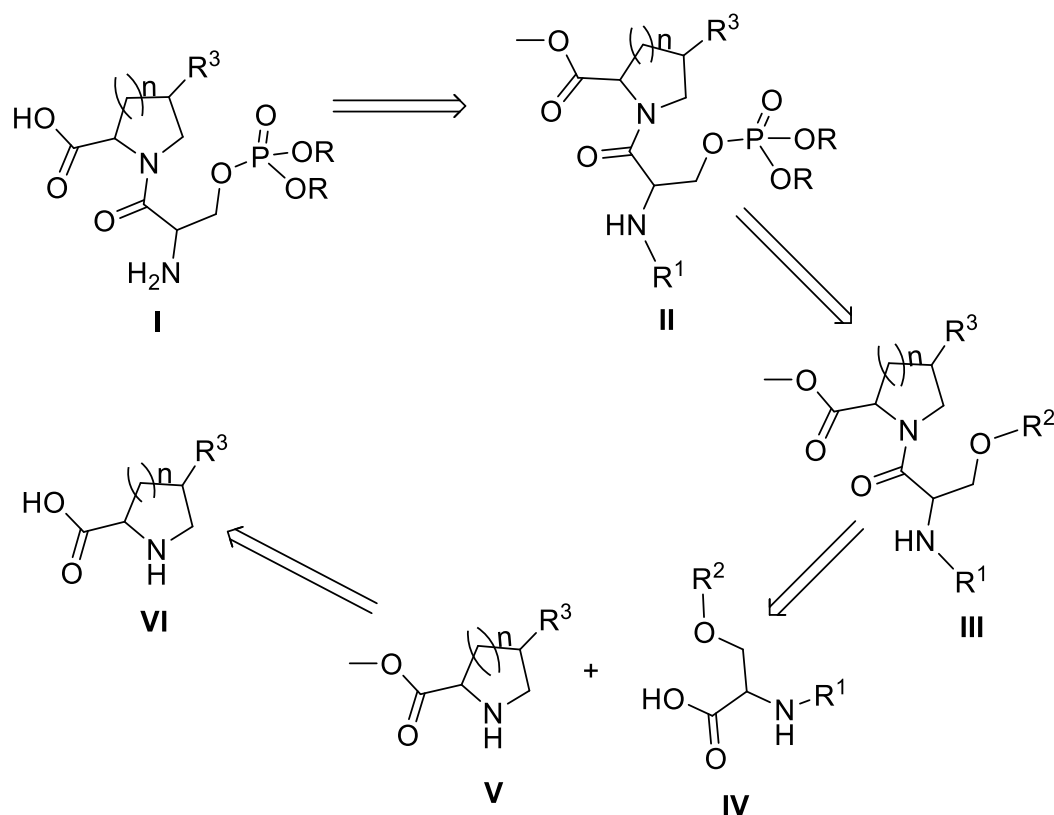


**Figure 3.1.** Basic structural skeleton of proposed Pin1 substrate. **A** is the O-phosphorylated moiety of Pin1 specific substrate while **B** is the proposed N-phosphorylated derivative.

Thus, in this chapter, we discuss experiments focussed on preparation of synthetic mimics of Pin1 substrates in the prodrug form shown in Scheme 3.1



**Scheme 3.1.** Retrosynthetic pathway of phosphoserine-proline molecule. The retrosynthetic route to the phosphoserine-proline motif (I) is outlined as follows. In the pathway, the carboxyl group of VI is esterified to give the methyl ester V. Amide coupling of the ester V with a protected serine (or its N-derivative) IV gives III. Phosphorylation of the atom on the  $\beta$ -carbon of serine moiety of III (O- or N atom) results in the protected phosphodipeptide II which can be deprotected to give I.

### 3.1.1 Aims

The objectives of the chapter include discussions of:

- Masking of the carboxyl group of amino acids;
- Peptide coupling of amino acids;
- Derivatization of the serine moiety;
- Proposed prodrug forms of the synthesized molecules.
- Proposed and attempted phosphorylation of the serine moiety and its analogues.

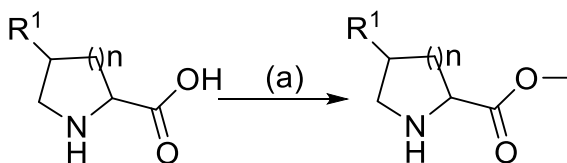
## 3.2 PREPARATION OF SERYL-PROLINE DIPEPTIDE DERIVATIVES

In this section, the following topics are discussed:

- Protection of the carboxyl group of proline and its analogues and
- Amide coupling of the masked proline and its analogues with N-protected serine molecules.

### 3.2.1 Amino acid methyl ester synthesis

The first experiment in the synthetic plan was the masking of the carboxyl group of proline and its analogues according to Scheme 3.2.



**Scheme 3.2.** Preparation of methyl ester of proline analogues. Reagents and conditions: (a) MeOH, SOCl<sub>2</sub>, reflux (24 h); n = 0, 1; R<sup>1</sup> = H, OH.

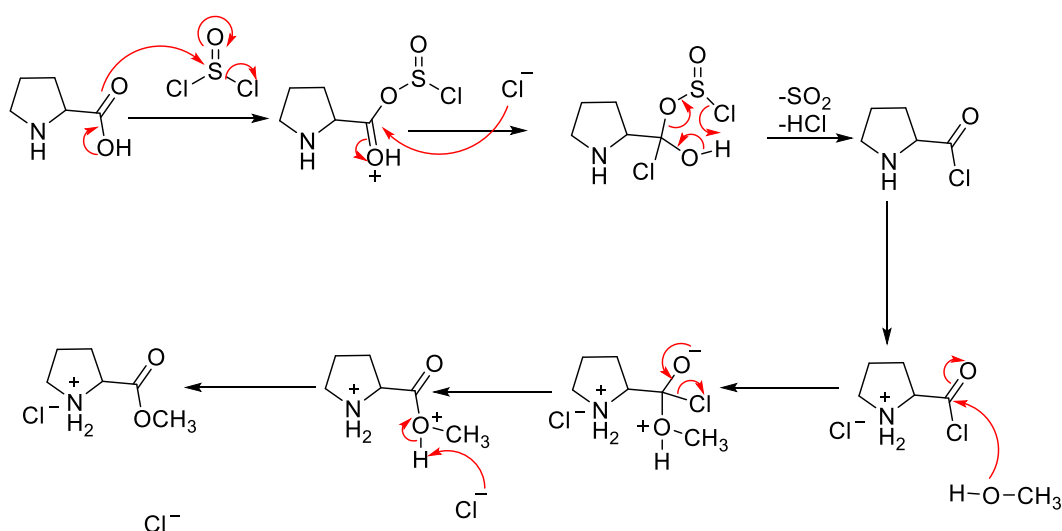
In peptide synthesis, the formation of a peptide (amide) bond between two amino acids is achieved by reacting one amino acid with another. In order to avoid amide bond formation of individual amino acids with same species and formation of a mixture of products, the N-terminus (amino group) in one amino acid and the C-terminus (carboxyl group) in the other must be protected prior to the peptide synthesis. One such procedure for protecting the C-terminus in amino acids before formation of peptide is their transformation into the corresponding ester.

The transformation of amino acids into the corresponding methyl esters has been carried out using a variety of reagents such as protic acids (HCl<sub>(g)</sub>, H<sub>2</sub>SO<sub>4</sub> and CH<sub>3</sub>C<sub>6</sub>H<sub>4</sub>SO<sub>3</sub>H),<sup>147</sup> thionyl chloride,<sup>151</sup> and 2,2-dimethoxypropane.<sup>152</sup> Other methods involving multistep reactions abound for obtaining the products but with several drawbacks, including tedious workup procedures, safety issues, waste disposal problems or harsh reaction conditions. In this project, preparation of the methyl ester of proline and its derivatives was achieved by known chemistry based on use of thionyl chloride and methanol. Thionyl



chloride ( $\text{SOCl}_2$ ) was chosen because it is efficient and racemization free. Also, the reaction is fast as the acyl chloride is first formed and then ester while the volatile by-products  $\text{HCl}$  and  $\text{SO}_2$  are easily removed from the reaction mixture.<sup>153</sup>

The formation of the acyl chloride proceeds via [1,2]-addition of a chloride ion to the carbonyl carbon followed by [1,2]-elimination of a second chloride ion to give the prolinoyl chloride,  $\text{SO}_2$  and  $\text{HCl}$  (Scheme 3.3). The prolinoyl chloride then reacts rapidly with methanol first through an addition reaction involving attack on the electrophilic acyl carbon atom by one of the lone pairs on the oxygen of the methanol. Subsequent to this is the elimination stage involving the reformation of the double bond between carbon and oxygen atoms with an initial elimination of a chloride ion and the proton abstraction by the same chloride ion to give the methyl prolinolate as the hydrochloride salt.

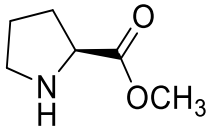
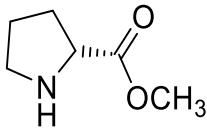
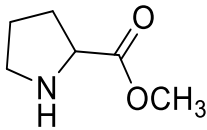
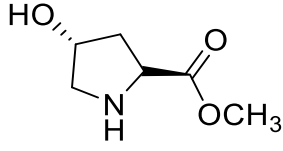
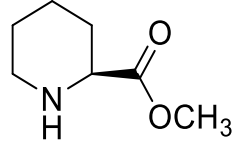


**Scheme 3.3.** A proposed mechanism for preparation of methyl prolinolate.

The methyl prolinolate hydrochloride (**1**) was prepared by heating proline, thionyl chloride and methanol under reflux for 24 h. The product was obtained in excellent yield (up to 98% yield) when appropriate amounts of the reactants were used; the summary of the product yield is presented in Table 3.1. Use of more than two equivalents of thionyl chloride resulted in a gummy solid with cumbersome workup. Similarly, a sludge was obtained when non-anhydrous methanol was used. The hygroscopic nature of the product made

determination of its melting point difficult. The spectroscopic data obtained for the products were in agreement with data from the literature.<sup>154</sup>

**Table 3.1.** Summary of some important peaks for the methyl ester hydrochlorides.

Code	Structure	Yield (%)	OCH <sub>3</sub> (ppm)	H-2 (ppm)	m/z for [MH] <sup>+</sup>
1		83	3.74	4.21	130.0
2		88	3.74	4.30	130.0
3		84	3.75	4.35	130.0
4		98	3.74	4.43	145.9
5		88	3.71	4.02	143.9

The <sup>1</sup>H NMR spectrum for the proline methyl ester (**1**) showed the absence of the signal for OH in the starting material (proline). The triplet signal at  $\delta$  4.21 that integrated for one proton is consistent with the presence of the single H-2 proton of proline, the singlet peak at  $\delta$  3.74 corresponded to the methyl protons of OCH<sub>3</sub>, the multiplets at approximately  $\delta$  3.19, 2.25 and 1.94 confirmed the protons H-5, H-3 and H-4 respectively. The <sup>13</sup>C NMR spectrum included a carbon that resonated at  $\delta$  53.53 which corresponded to the methoxy carbon. The elemental analysis also confirmed the structural assignment; the ES-MS showing an ion with m/z = 130.0 consistent with [MH]<sup>+</sup> ion further corroborated the structure. The isomers of **1**, (**2** and **3**), were similarly assigned and a summary of their characteristic peaks was given in Table 3.1.

The structure of the methyl *trans*-4-hydroxy-L-prolinate (**4**) obtained was established by the  $^1\text{H}$  NMR. The spectrum showed a multiplet peak at  $\delta$  4.43 integrating for two protons because of an overlap of the peaks for H-2 and H-4, the singlet peak at  $\delta$  3.74 is consistent with the methoxy protons. Similarly, the two doublet signals at  $\delta$ : 3.35 and 3.05 corresponded to the two H-5 protons; the multiplet at  $\delta$  2.21-2.02 corresponded to H-3 (Figure 3.2). The elemental analysis and the  $m/z = 145.9$  corresponding to  $[\text{MH}]^+$  gave further confirmation to the structure of the product. The melting point of (**4**) obtained (158-160  $^\circ\text{C}$ ), is within the range of values (149-172  $^\circ\text{C}$ ) obtained from the literature.

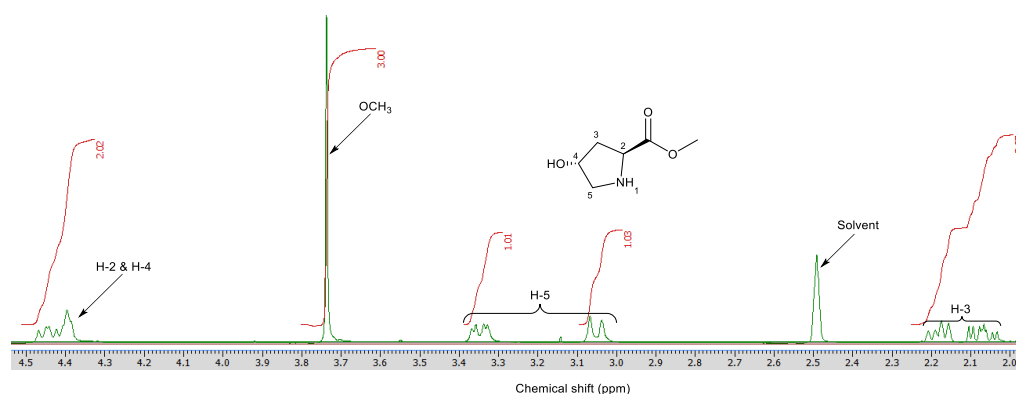


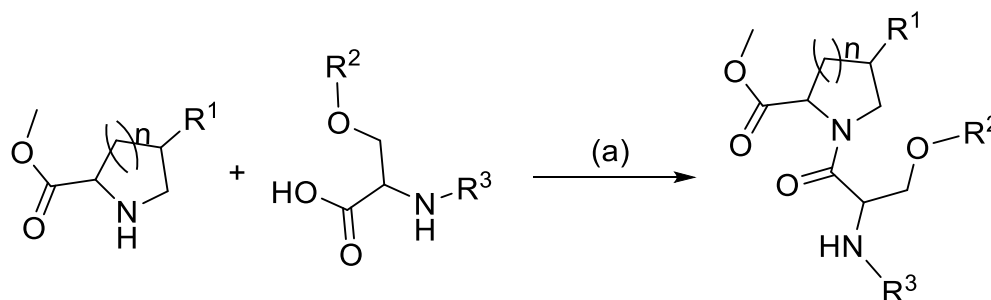
**Figure 3.2.**  $^1\text{H}$  NMR spectrum of **4** in  $\text{DMSO-}d_6$ .

The methyl DL-pipecolinate (**5**) was obtained in 88% yield. The structure was similarly established from the  $^1\text{H}$  NMR spectrum analysis that showed the absence of the signal for the OH in the precursor (pipecolic acid) and appearance of a singlet at 3.74 ppm that integrated for three protons corresponding to the methoxy protons among other peaks. In the  $^{13}\text{C}$  NMR spectrum, the methoxy carbon resonated at 53.80 ppm. The elemental analysis and the  $m/z = 143.9$  corresponding to  $[\text{MH}]^+$  supported the structure further.

Subsequent to successful preparation of the methyl esters, they were therefore available for peptide coupling with various N-carbamate-protected serine.

### 3.2.2 Preparation of seryl-proline derivatives

The objective of this subsection is to discuss experiments focussed on amide coupling of some of the amino acid esters discussed in the previous subsection with serine analogues (Scheme 3.4).

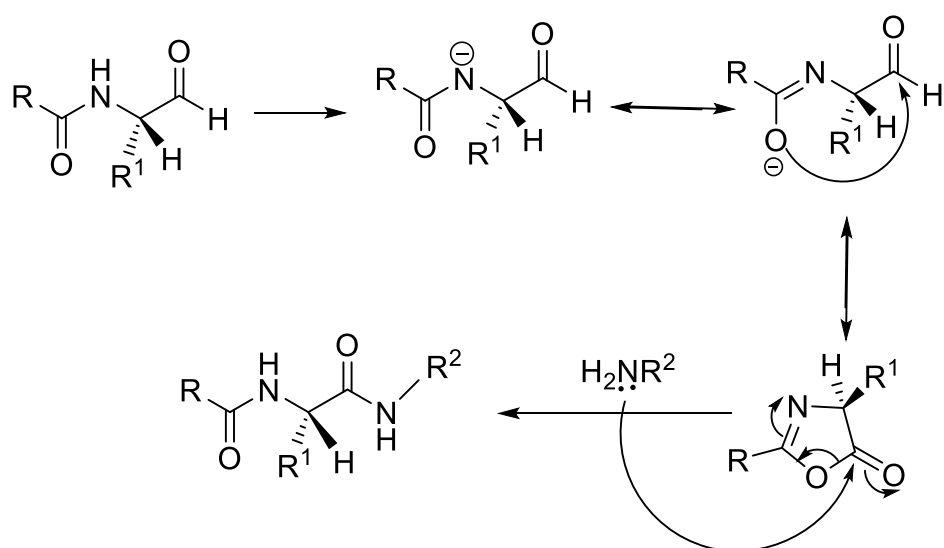


$n = 0$  or  $1$ ,  $R^1 = H$  or  $OH$ ,  $R^2 = H$ ,  $R^3 = Z-$ , Boc- or Fmoc group

**Scheme 3.4.** Amide coupling of serine and proline derivatives. Reagents and reaction conditions: (a) DIPEA, HOBT, EDC.HCl, DCM, rt, 40 h.

As mentioned in section 3.2.1 above, to avoid complex mixtures in peptide synthesis some kinds of selectivity must be introduced prior to amide bond formation by esterification of the carboxyl group of one amino acid and acylation of the amino function in the other to get rid of zwitterionic species and produce specific amino and carboxyl reactants respectively. The formation of an amide bond between the designated substrates, however, is not a spontaneous reaction at ambient temperature. The elimination of a water molecule from the reacting species takes place only at high temperatures, a typically detrimental condition to the integrity of the substrates. Therefore, relatively mild conditions are often required to first activate the carboxylic acid by converting the -OH of the acyl carbon into a good (an electron withdrawing) leaving group before treating it with the amine. Several important conventional methods for activation of the carboxyl group are known, including activation as acyl halides, acid azides, acylimidazoles, anhydrides, and active esters. The activation process is, however, prone to racemization because of the occurrence of formation of oxazolones (Scheme 3.5).

A more convenient method is the single step *in situ* activation and coupling using carbodiimides. This process involves direct addition of the coupling reagents to a mixture of the designated carboxylic acid and amine in a one-pot reaction to effect the dehydration. However, the use of these reagents is not without its own drawbacks including possible loss of optical purity and formation of unreactive by-products such as the *N*-acylurea. The reaction between the acid and the carbodiimide produces an *O*-acylisourea, the main intermediate. The *O*-acylisourea then reacts with the amine to produce the desired amide and urea. Both desired and undesired products are produced by the side reaction of the *O*-acylisourea.



**Scheme 3.5.** Formation of oxazolone and racemisation reaction.

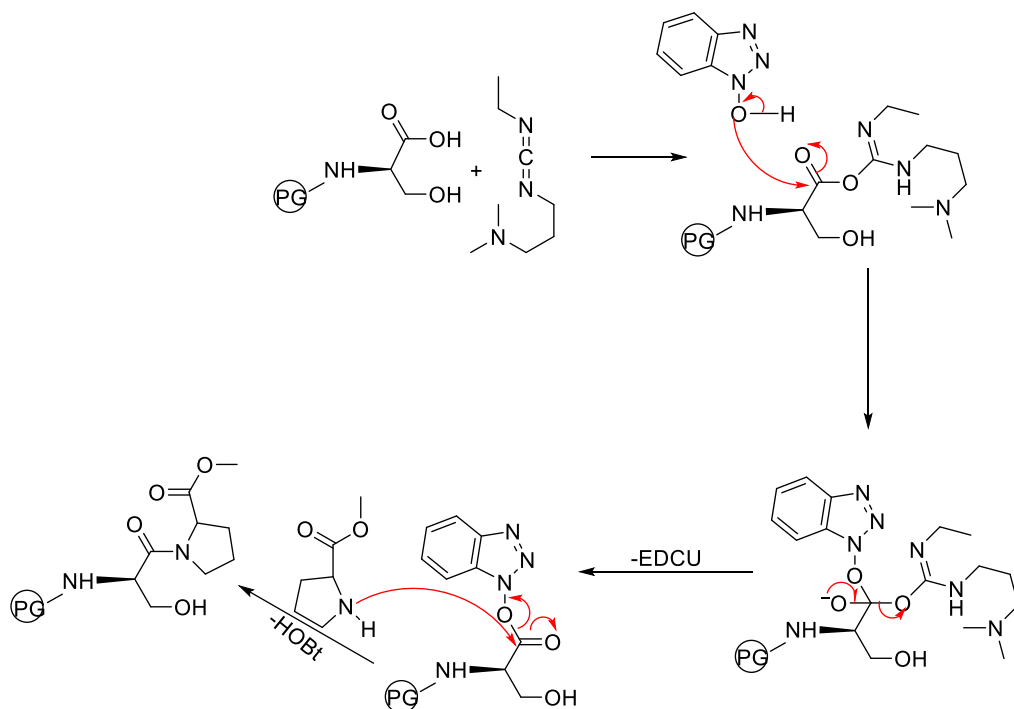
On one hand, it reacts with an additional carboxylic acid to give an acid anhydride, which undergoes further reaction to give the desired amide. On the other hand, it could rearrange to give the undesired unreactive *N*-acylurea. To overcome both of the aforementioned challenges, auxiliary nucleophilic additives e.g. *N*-hydroxysuccinimide or 1-hydroxybenzotriazole are introduced. Another way of minimizing this side reaction is to use low-dielectric constant solvents such as dichloromethane or chloroform.

Although an array of coupling reagents (carbodiimide) exists including *N,N'*-dicyclohexylcarbodiimide (DCC), diisopropylcarbodiimide (DIC) and *N*-ethyl-*N'*-dimethylaminopropylcarbodiimide (EDC) hydrochloride,<sup>155</sup> the ease of removal of the urea formed is an important factor to be considered in the choice

of a carbodiimide. The choice of EDC hydrochloride in this study was predicated upon its advantages over the popular DCC. DCC produces sparingly soluble dicyclohexylurea, which may precipitate incompletely from the reaction mixture thereby making separation from the product difficult, whereas EDC is water soluble, and forms a soluble urea, which can be separated easily from the protected peptide product in aqueous work-up.

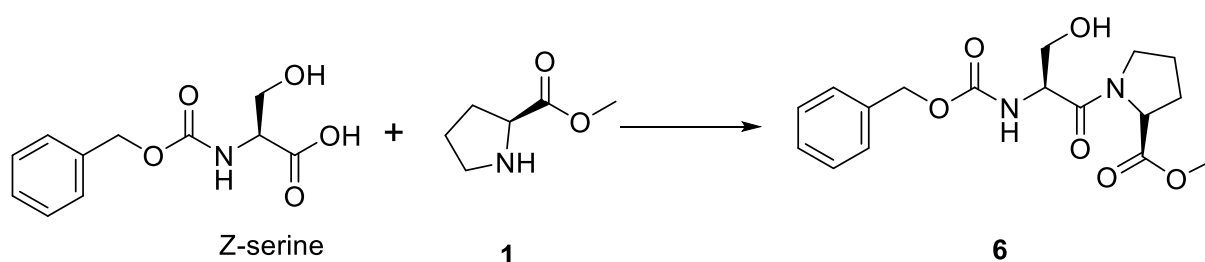
Introduction of additives such as 1-hydroxybenzotriazole (HOBt), 1-hydroxy-7-azabenzotriazole (HOAt) or ethyl 2-cyano-2-(hydroxyimino)acetate (Oxyma pure<sup>®</sup>) when working with carbodiimides is essential for reduction of racemization in the case of amino acids or epimerization in the case of peptides to satisfactory levels. Additives also reduce formation of *N*-acylureas. We chose HOBt in this study because it is one of the most efficient and the most classical benzotriazole additive when using carbodiimides. Although HOAt and Oxyma pure<sup>®</sup> showed superiority in their capacity to remarkably suppress racemization and display of impressive coupling efficiency, they are less cost-effective reagents than HOBt. It is believed that HOBt functions by firstly reacting with the *O*-acylurea to generate the HOBt-active ester, with consequent enhancement of the reactivity of the “activated *O*-acylurea” by coupling with the amine and undergoing aminolysis thereby preventing the side reactions (Scheme 3.6). The use of the tertiary amine base, DIPEA, in this coupling reaction (Section 2.3.2) is to isolate the free amino acid methyl ester of proline from the methyl proline hydrochloride salt used, otherwise there is no need for the base.

The products were obtained in high purity as shown by the analyses but the yield was relatively low. A possible explanation for the comparatively low yield may be the loss of product resulting from the idiosyncratic undesirable side reactions of carbodiimides. Perhaps, another reason that may be adduced is the solvent in which the reaction was performed.



**Scheme 3.6.** Mechanism of peptide coupling mediated by EDC and HOBt. PG = Protecting group

The first in the series of the serine-proline-based dipeptides was prepared by peptide coupling of methyl ester **1** to commercially available Z-serine using EDC.HCl to give product **6** in 69% yield (Scheme 3.7).



**Scheme 3.7.** Preparation of serine-proline-based dipeptide **6**. Reagents and conditions: (a) DIPEA, HOBt, EDC.HCl, DCM, rt, 40 h.

The structure of **6** was established from the  $^1\text{H}$  NMR spectrum showing among other peaks the appearance of two multiplet signals that each integrated for one proton at  $\delta$  4.70-4.68 and 4.62-4.59 assignable to  $\alpha$ -H of serine and H-2 of proline respectively. The  $^1\text{H}$  NMR spectrum also displayed two singlet peaks at  $\delta$  7.35 and 3.76 consistent with the aromatic and methoxy protons

respectively. The  $^{13}\text{C}$  NMR showed the presence of three carbonyl carbons at  $\delta$  173.03, 169.93, and 156.17, assignable to the carbonyl groups on serine, proline and the Z-group respectively. In the ES-MS data, the display of  $m/z = 351.1$  which is consistent with  $[\text{MH}]^+$  and the elemental analysis showing values (C, 58.20; H, 6.39; N, 8.00) which are consistent with the calculated for the compound gave further confirmation to the structure.

The second derivative was similarly obtained from a reaction between **1** and Boc-L-serine to give compound **7** in 63% yield. The structure of **7** was confirmed from its  $^1\text{H}$  NMR showing *inter alia* a multiplet at  $\delta$  4.62-4.58 assignable to H-2 in the proline moiety and H- $\alpha$  of serine moiety which is slightly more downfield than the corresponding signal in the spectrum of the precursors. This can be accounted for by the de-shielding effect of the amide and carboxyl groups flanking both protons. The  $^{13}\text{C}$  NMR spectrum supported the structure by displaying three signals for the carbonyl carbons at  $\delta$  173.08, 170.28 and 155.69. In addition, the ES-MS displayed a peak at  $m/z = 339.2$  that corresponded to  $[\text{M}+\text{Na}]^+$  to support the structural assignment.

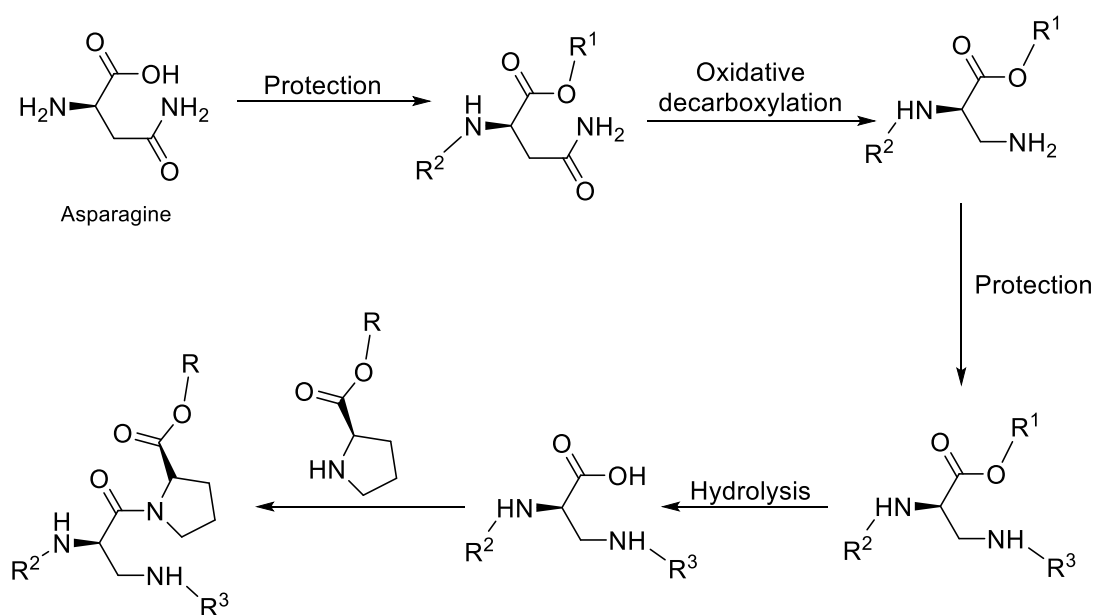
A third derivative of the dipeptide was prepared by coupling methyl DL-pipecolate (**5**) with Z-Ser-OH to obtain **8** in 54% yield. The proton NMR of **8** displayed a triplet at  $\delta$  4.87 ( $J = 3.9$  Hz) that integrated for one proton corresponding to H- $\alpha$  of serine moiety and slightly downfield because of the electron withdrawing effect of the two neighbouring amide bonds. The  $^{13}\text{C}$  NMR also supported the structure of the compound by displaying three signals at  $\delta$  172.30, 169.13 and 156.00 corresponding to the three carbonyl groups in the molecule. In addition, the  $m/z = 365.1$  displayed in the ES-MS is consistent with  $[\text{MH}]^+$ .

Attempts to prepare other derivatives with highly functionalised serine such as Boc-O-benzyl-L-serine, Fmoc-O-benzyl-L-serine, *N*-Z-O-*tert*-butyl-L-serine and Z-O-benzyl-L-serine failed to produce the desired products over 40 h and elongated time of reaction only led to a sticky mass. The more the number of the protecting groups, the more lipophilic the compound meaning that column chromatography would have been needed to purify the compounds, this could probably explain the failure to obtain the product of the coupling reaction by direct crystallization.



### 3.3 PREPARATION OF AMINO ANALOGUES OF THE SERYL-PROLYL MOTIF

Keeping in line with the general aim of this study to prepare metabolically stable mimics of Pin1 substrates, we already discussed preparation of seryl-proline dipeptides in section 3.2. From the perspective of exploration of the structure-activity relationship of the Pin1 substrate, it was of interest to attempt to prepare phosphoryl derivative of the substrate with electronegative atoms other than oxygen, such as nitrogen and sulphur. In this section, we discussed preparation of *N*-analogues of the serylproline dipeptide with an intention to produce less alkali labile *N*-phosphoamino acids. In contrast to phosphoserine which is alkali labile, phosphoramidates are comparatively base stable<sup>156</sup> thereby enhancing the stability of the molecule under physiological pH of the human body. The approach used for the synthesis is shown in a reaction pathway as illustrated in Scheme 3.8.

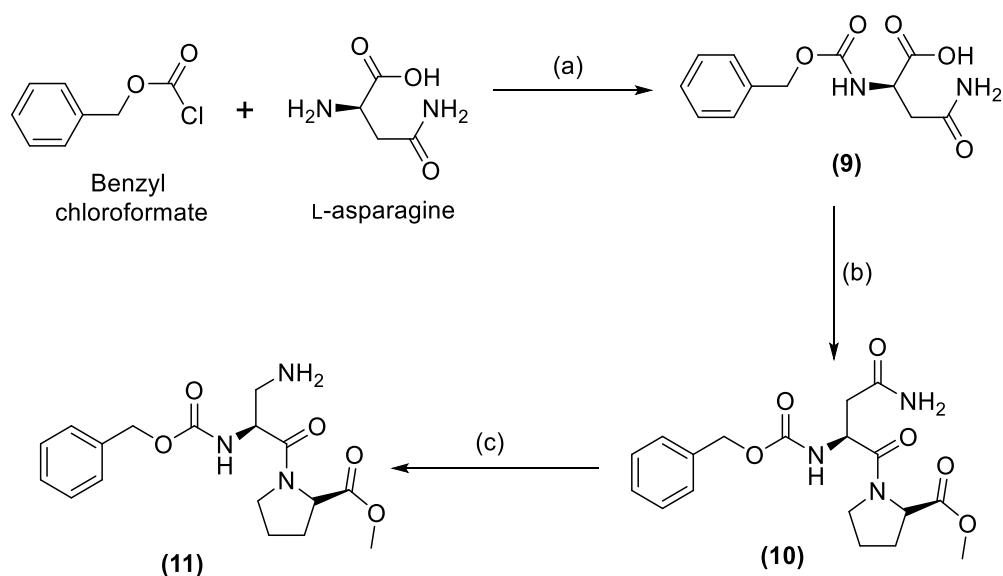


**Scheme 3.8.** Proposed pathway for synthesis of the amino analogue of serine-proline dipeptide. *R*, *R*<sup>1</sup>, *R*<sup>2</sup>, *R*<sup>3</sup> = protecting groups.

Thus, our objectives include discussion of experiments focussed on:

- *N*-terminal protection of L-asparagine;
- Oxidative decarboxylation of asparagine; and
- Amide coupling of  $\beta$ -aminoalanine with proline derivatives.

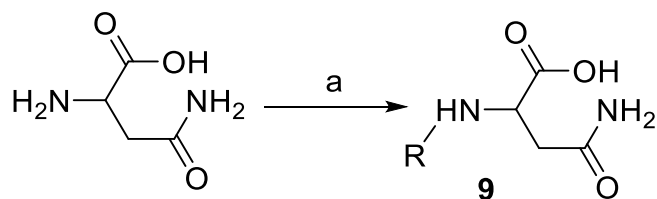
Consequent to these objectives, the product was produced according to the reaction pathway illustrated in Scheme 3.9.



**Scheme 3.9.** Preparation of amino derivative of serine-proline motif. Reagents and reaction conditions: (a) 10%  $\text{NaCO}_{3(\text{aq})}$ , 1,4-dioxane, rt, stir overnight, (b)  $\text{C}_6\text{H}_{12}\text{ClNO}_2$ , HOBT, EDC.HCl, stir (RT), 24 h, (c) PIDA,  $\text{CH}_3\text{CN}$ , EtOAc,  $\text{H}_2\text{O}$  (2:2:1), rt, stir 6 h.

### 3.3.1 N-protection of L-asparagine

The main objective of this section is to discuss the procedure for protection of the N-terminus of asparagine. The protection reaction followed Scheme 3.10.



**Scheme 3.10.** N-protection of asparagine. Reagents and conditions: (a) Benzyl- or 9-fluorenylmethyl chloroformate 10%  $\text{Na}_2\text{CO}_{3(\text{aq})}$ , 0 °C to RT, 1,4-dioxane; R = Z-group.

Synthesis of an N-analogue of serine ( $\beta$ -aminoalanine) starting from asparagine was undertaken following an approach described by Zhang et al.<sup>157</sup> The N-terminus of asparagine was protected using Z group. In this one-pot

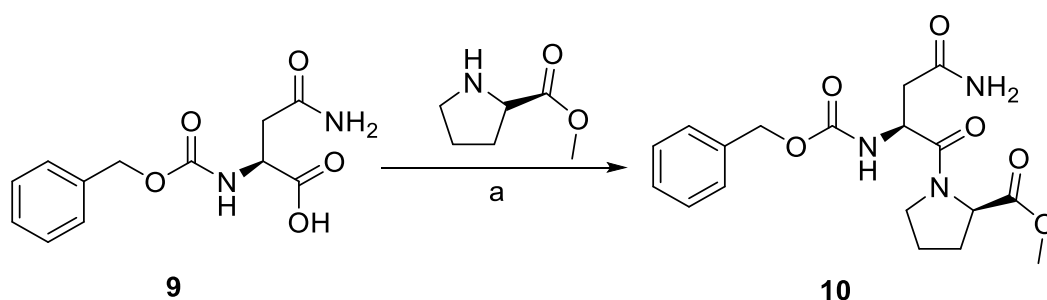
reaction, benzylchloroformate was added to a stirring mixture of asparagine, 10% Na<sub>2</sub>CO<sub>3(aq)</sub> and 1,4-dioxane at 0 °C. The mixture was stirred at room temperature overnight. It was then poured into water and washed with diethyl ether. Acidification of the aqueous layer with 2 M HCl yielded a white precipitate, which after filtration and washing extensively with diethyl ether gave the pure product as a white solid. The product yield for the Z-asparagine was 72%.

The NMR data confirmed the structure; the <sup>1</sup>H NMR spectrum supported the structure of **9** by showing a doublet at δ 7.45 which integrated for one proton and corresponded to the amide proton CONH. The aromatic protons appeared as a multiplet at δ 7.34. In addition, the spectrum showed two singlet peaks at δ 6.92 and 5.02 assignable to the CONH<sub>2</sub> and PhCH<sub>2</sub> respectively. A quartet at δ 4.33 that integrated for one proton corresponded to H-2 of the asparaginyly moiety, which has moved slightly upfield from its position in the spectrum of L-asparagine because of the electron-withdrawing influence of the neighbouring carboxyl and amide functions. The <sup>13</sup>C NMR spectrum also displayed three peaks at δ 173.19, 171.17 and 155.82 corresponding to the carbonyl carbons COOH, CONH<sub>2</sub> and CONH respectively. The structure was further confirmed by the display of a peak at m/z = 289.0 consistent with [M+Na]<sup>+</sup> in the ES-mass spectrum.

The Fmoc-protected asparagine was similarly prepared by treating L-asparagine with 9-fluorenylmethyl chloroformate and yielded a white solid in 71% yield. However, this product was lost because of contamination with an unidentified compound before further analysis could be carried out.

### **3.3.2 Amide coupling of Z-asparagine (9) with methyl proline (1)**

In the preceding section, we discussed successful protection of N-terminus of asparagine. Since the Fmoc derivative had been lost, the objective of this section is to discuss coupling of Z-asparagine with **1** as shown in Scheme 3.11.



**Scheme 3.11.** Amide coupling of *Z*-asparagine with methyl prolinatate. Reagents and conditions: (b) DIPEA, EDC.HCl, HOBT, 0 °C to RT, stir (24 h).

The peptide bond formation was achieved in a single step *in situ* activation and coupling reaction using carbodiimides as discussed in section 3.2.2. In this approach, amide coupling of **9** with methyl prolinatate (**1**) in dichloromethane using EDC.HCl and stirring overnight produced the dipeptide **10** as a white solid in 77% yield. The <sup>1</sup>H NMR supported the product structure by showing the expected disappearance of COOH signal and downfield shift in the position of signals for α protons in both the asparaginyl and prolyl moieties to δ 5.03-4.92 when compared with the starting materials. This observation explicitly resulted from the deshielding effect of the adjacent amide and carboxyl groups. Similarly, the <sup>13</sup>C spectrum displayed four signals for carbonyl carbons as anticipated and the ES mass spectrum showed an ion with m/z = 378.1 corresponding to [MH]<sup>+</sup>.

### 3.3.3 Oxidative decarboxylation of *Z*-Asn-Pro-OMe (**10**).

In section 2.3.2, the result of successful preparation of *Z*-Ser-Pro-OMe (**6**) was presented. The objective of this section is to discuss preparation of its *N*-analogue [*Z*-(β-amino)Ala-Pro-OMe (**11**)] (Figure 3.3).

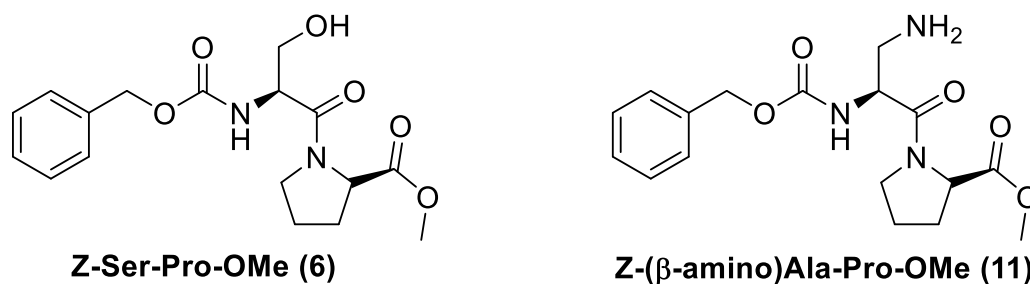
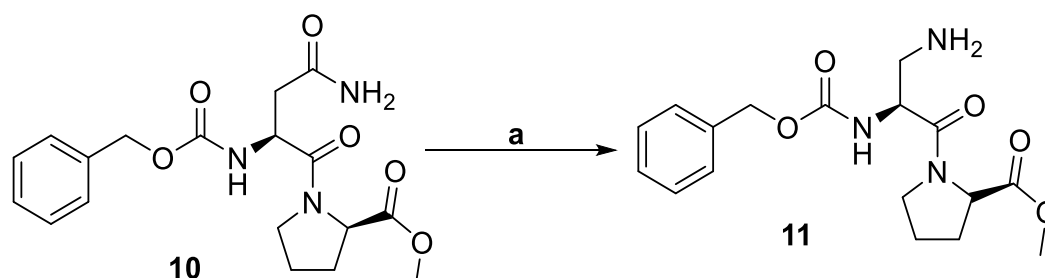


**Figure 3.3.** Structures of *Z*-Ser-Pro-OMe and its amino analogue

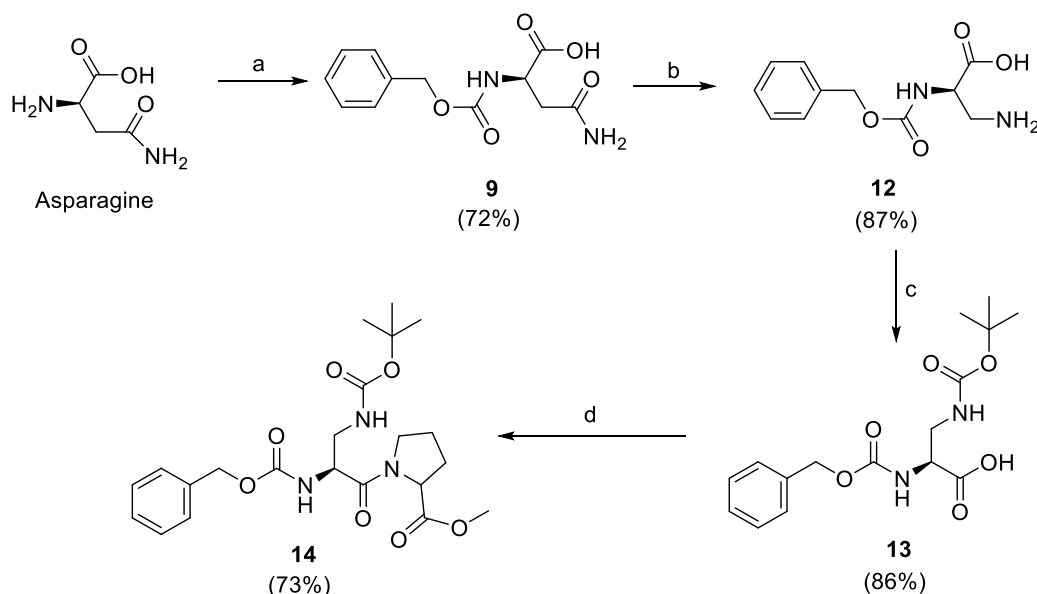
In subsections 3.3.1 and 3.2.2, we discussed the first two steps of the pathway followed for the preparation of the amino analogue of the Seryl-Prolyl motif (Scheme 3.8). The present subsection discusses the oxidative decarboxylation of compound **10** to compound **11** (Scheme 3.12).



**Scheme 3.12.** Oxidative decarboxylation of *Z*-Asn-Pro-OMe. Reagents and conditions: (a) PIDA, DMF-H<sub>2</sub>O; (1:1 v/v), 15 °C to RT.

Zhang et al have described oxidative decarboxylation of N<sup>α</sup>-protected asparagine using hypervalent iodine species such as phenyliodine (III) diacetate (PIDA) to produce β-aminoalanine derivatives.<sup>157</sup> Following this approach, a Hofmann-type rearrangement of **10** using PIDA in dimethyl formamide and water (DMF-H<sub>2</sub>O; 1:1, v/v) resulted in the formation of protected β-aminoalaninylproline methyl ester (**11**), containing the target motif. The product was obtained as a brown viscous liquid from which isolation of the pure compound was difficult. A repeat experiment using a mixture of lower boiling solvents than DMF (acetonitrile, ethyl acetate and water 2:2:1 v/v) resulted in a golden yellow liquid (2.9 g) from which also it was difficult to isolate the pure compound. Although the NMR and mass spectroscopic analyses confirmed the formation of the product (**11**), the NMR spectrum, however, showed *inter alia* some peaks attributable to impurities (solvent and by-products). These extraneous <sup>1</sup>H NMR peaks made the complete peak assignment a bit difficult. Consequently, only some characteristic proton peaks were assigned. Also the observed elemental analysis showed a lower percentage of key component elements (C, 49.23; H, 6.57; N, 8.48) than the calculated or expected values (C, 58.44; H, 6.64; N, 12.03) a fact indicative of the presence of impurities hence the non-determination of the percent yield of this crude product.

The unsuccessful isolation of the product prompted us to explore an alternative pathway as illustrated in Scheme 3.13.



**Scheme 3.13.** Synthetic pathway for *Z*-( $\beta$ -Boc-amino)Ala-Pro-OMe. Reagents and conditions: (a) benzyl chloroformate, 10% Na<sub>2</sub>CO<sub>3</sub>, 1,4-dioxane, 0 °C to RT; (b) PIDA, CH<sub>3</sub>CN/EtOAc/H<sub>2</sub>O (2:2:1 v/v), RT; (c) Di-*t*-butyldicarbonate, 10% Na<sub>2</sub>CO<sub>3</sub>, CH<sub>3</sub>CN, 0 °C to RT; (d) Pro-OMe, DIPEA, EDC, HOBT, 0 °C to RT.

In a repeat experiment, oxidative decarboxylation of **9** with PIDA in CH<sub>3</sub>CN, EtOAc and H<sub>2</sub>O (2:2:1 v/v) produced the corresponding amine **12** in 87% yield (Scheme 3.13). The structure of **12** was confirmed from the <sup>1</sup>H NMR showing a signal at  $\delta$  4.31 which integrated for one proton corresponding to the  $\alpha$ -H and two broad singlet signals at 3.25 and 3.04 ppm integrating for two protons corresponding to the  $\beta$ -methylene protons. Expectedly, the <sup>13</sup>C spectrum of **12** showed only two C=O signals with the disappearance of the signal at  $\delta$  171.17 for CONH<sub>2</sub> in **9** and the ES-MS displayed a peak at  $m/z = 238.9$  consistent with [MH]<sup>+</sup>.

Protection of the  $\beta$ -amino group by stirring a mixture of **12** and di-*tert*-butyl carbonate in 10% Na<sub>2</sub>CO<sub>3(aq)</sub> and 1,4-dioxane overnight resulted in the corresponding Boc-protected product **13** in 86% yield. The spectroscopic data of **13** confirmed the structure. In the <sup>1</sup>H NMR, the significant downfield shift of the  $\alpha$ -NH signal to  $\delta$  6.85 can be accounted for by the anisotropic and electron-withdrawing effects of the carboxyl group attached directly to the N atom. The

$^{13}\text{C}$  NMR displayed among other peaks signals for the three carbonyl carbons while the ES-MS displayed a signal at  $m/z = 361.1$  confirming  $[\text{M}+\text{Na}]^+$ .

Amide coupling of **13** with **1** in dichloromethane using EDC.HCl and stirring at room temperature overnight produced **14** in 73% yield. The structure of **14** was established from its  $^{13}\text{C}$  NMR spectrum which displayed four peaks at  $\delta$  172.21, 168.88, 155.91, and 155.73 corresponding to the four carbonyl carbons in the molecule. The mass spectrum further supported the structure by displaying a signal at  $m/z = 472.2$  which established  $[\text{M}+\text{Na}]^+$ .

A comparative study of Schemes 3.13 and 3.9 revealed the following: One, products in Scheme 3.13 were obtained as high purity solids whereas the final product in Scheme 3.9 was in liquid form and pure compound difficult to isolate from the crude product (iodosobenzene diacetate and solvents proving difficult to remove completely). Two, products in Scheme 3.13 have three protected sites that make for easy and selective structural transformation of the intermediate molecule whereas compounds in Scheme 3.9 had only two protected sites thus placing a limitation on the possible number of structural transformations. Three, the need to evaporate a mixture of solvents involving high boiling solvents like DMF (153 °C) in Scheme 3.9 was circumvented in Scheme 3.13. Four, the yield at each stage of the reaction in Scheme 3.13 was appreciably more than in Scheme 3.9.

Now that both the *O*- and *N*-derivatives of the target moiety had been successfully synthesized, the next task was to phosphorylate the hydroxyl group in the serine-proline motif and the beta-amino group in the *N*-derivative of the motif to obtain the corresponding *N*-phosphorylated peptides. However, attempts to phosphorylate these motifs was met with limited success. The factors that limited the success of the phosphorylation reactions are presented and discussed in section 3.4.

### **3.4 PHOSPHOESTERS OF SER-PRO AND RELATED DIPEPTIDES: THE PRODRUG APPROACH.**

Subsequent to development of the dipeptide motifs of the synthetic mimics of Pin1 substrate as earlier discussed in section 3.3, the focus switched to generating the phosphorylated products. Molecules containing phosphates are critical components of all living cells and essential for many biological

processes within the cell. In this work, it was particularly important to aim for a prodrug form, in order to give the products a chance of being able to cross the cell membrane, unlike the ionised phosphoryl peptides. A prodrug is a chemical entity that is inactive pharmacologically but produces a biologically active substance upon intracellular metabolism or chemical transformation. Chief among the disadvantages of the phosphate group is its polarity and aqueous solubility resulting from the imparted anionic charge at almost all physiological pH. This feature prevents it from penetrating the cell membrane thus resulting in low bioavailability of the orally administered phosphorylated compound. To overcome the challenge of crossing the membrane barrier, we aimed to protect the phosphoryl group with chemically labile lipophilic masking groups that can be activated within the cell. By this means, a non-charged compound with appropriate diffusability across the plasma membrane is formed. Within the the cell, the charged phosphate or phosphoramidate is regenerated by removal of the masking groups via enzymatic cleavage or chemical decomposition thereby rendering the molecule active biologically and unable to cross the membrane again. The subsequently charged compound consequent upon the rapid prodrug conversion by intracellular enzymatic hydrolysis is trapped and accumulate within the cell (Figure 3.4). Phosphate prodrugs promote aqueous solubility of the parent drug and therefore the approach has been used extensively in clinical practice for anticancer drugs such as taxol, pancratistatin and etoposide.<sup>158</sup>

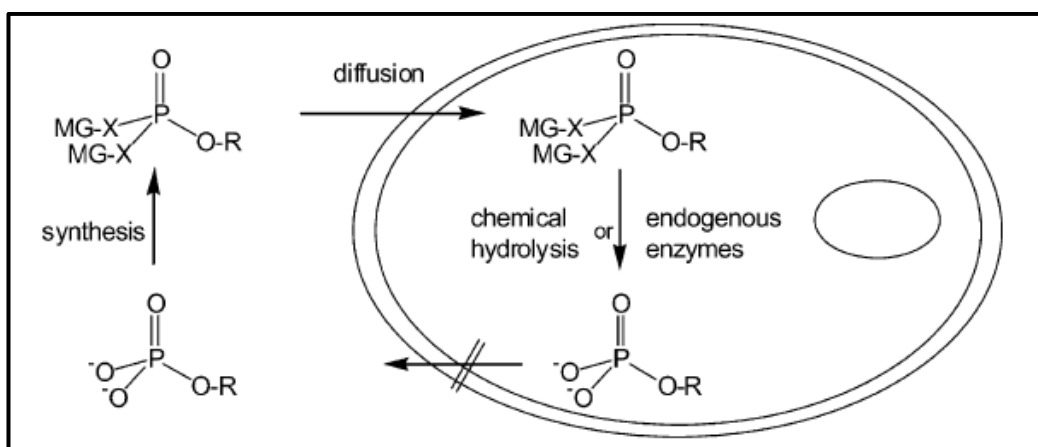


**Figure 3.4.** A diagram showing the concept of prodrug for phosphate esters. The masking groups (MG) enhance diffusion of molecule across the plasma membrane. Within the cell,



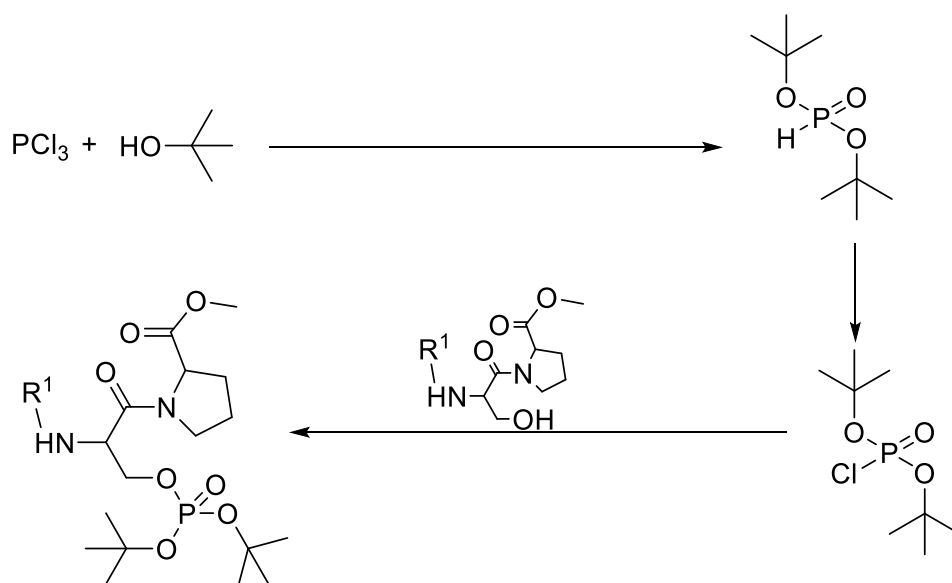
intracellular chemical or enzymatic hydrolysis regenerates the charged derivative thereby making it to be trapped and accumulate for bioactivity.  $X = O, N$  or  $C$  (adapted from Schultz<sup>159</sup>).

It is highly important that the masked molecule be sufficiently stable to ensure delivery to the target cells or tissues. Therefore it should be ensured that the design is in such a way that the protecting groups to be activated are not affected by enzymes in body fluids including blood, plasma and other biological fluids. Some of such masking groups used in this work include benzyl, ethyl, *tert*-butyl and allyl groups. Once inside the cells, the protecting groups of the phosphate-bearing molecules should undergo cleavage rapidly by endogenous intracellular enzymes including esterases, amidases, and phosphatases.

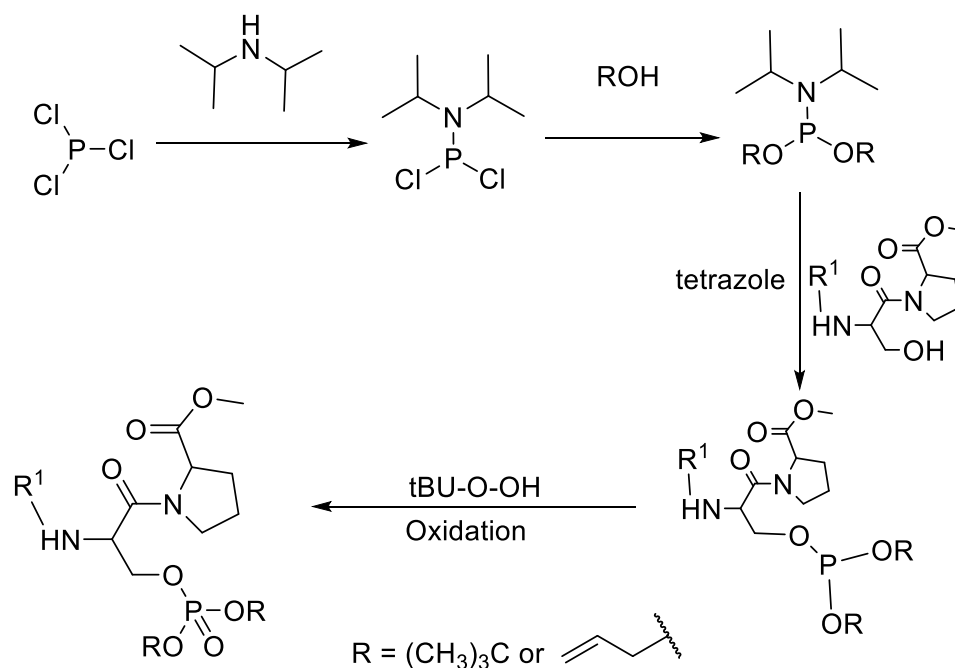
In this study, we proposed phosphorylating the synthesized Ser-Pro motif using di-*tert*-butylphosphorochloridate, diallyl- and di-*tert*-butyl *N,N*-diisopropylphosphoramidite. For the *N*-derivative, we proposed using dibenzyl phosphorochloridate, *N*-bis(9-fluorenylmethyl)phosphite, di-*tert*-butyl-, and bis(*S*-acetyl-2-thioethyl)-*N,N*-diisopropylphosphoramidite.

### 3.4.1 Proposed phosphoesters of Ser-Pro dipeptide

The following schemes represent the proposed reaction pathways for the *O*-phosphorylation of the Ser-Pro dipeptide. Scheme 3.14 represent the pathway involving di-*tert*-butylphosphorochloridate while Scheme 3.15 uses a phosphoramidite approach.



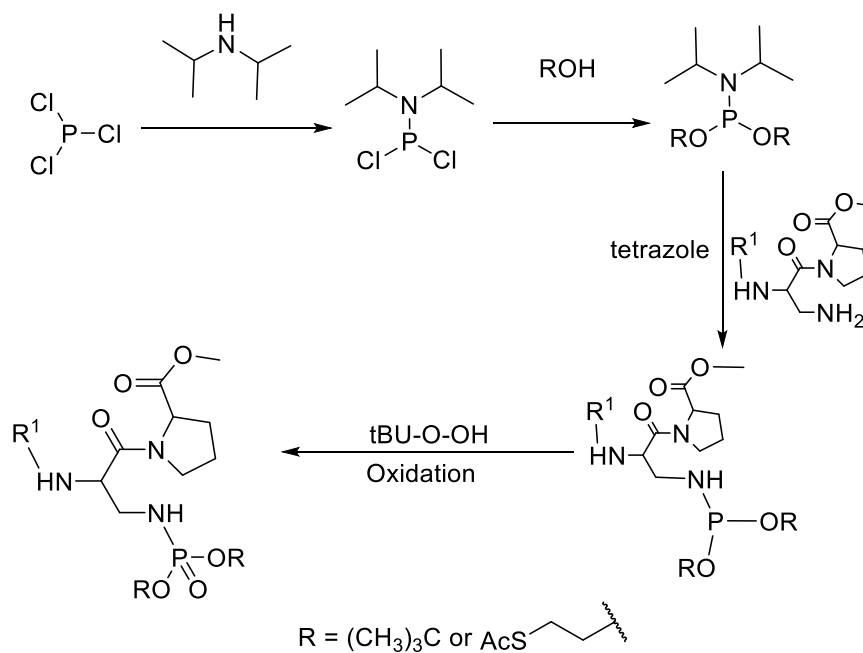
**Scheme 3.14.** Proposed preparation of phosphoester of Ser-Pro using di-tert-butylphosphorochloridate



**Scheme 3.15.** Preparation of phosphoester of Ser-Pro using the phosphoramidite approach.

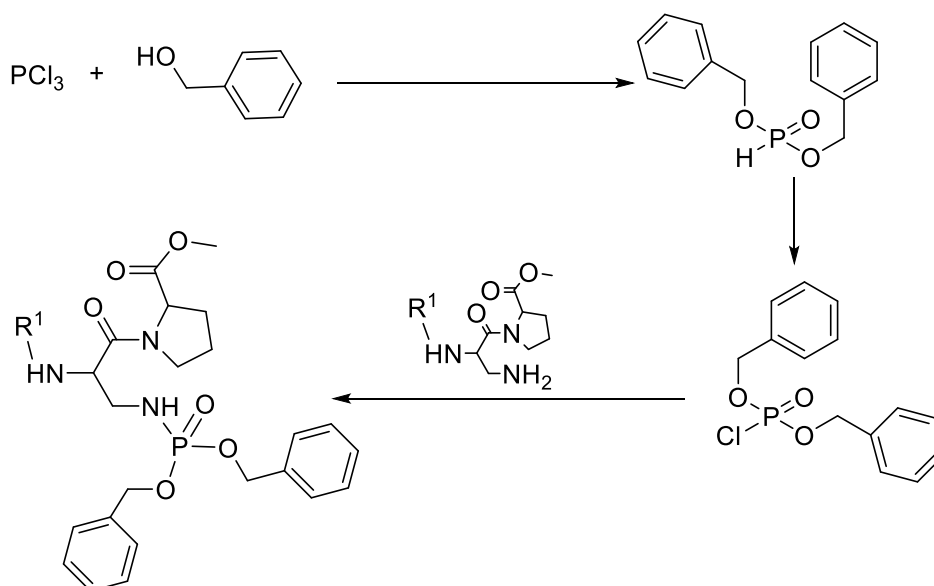
### 3.4.2 Proposed phosphoesters of amino analogues of the seryl-prolyl motif

Three approaches were proposed for the phosphorylation of the amino analogues of the seryl-prolyl motif. An approach employing phosphoramidites for phosphorylation (Scheme 3.16).

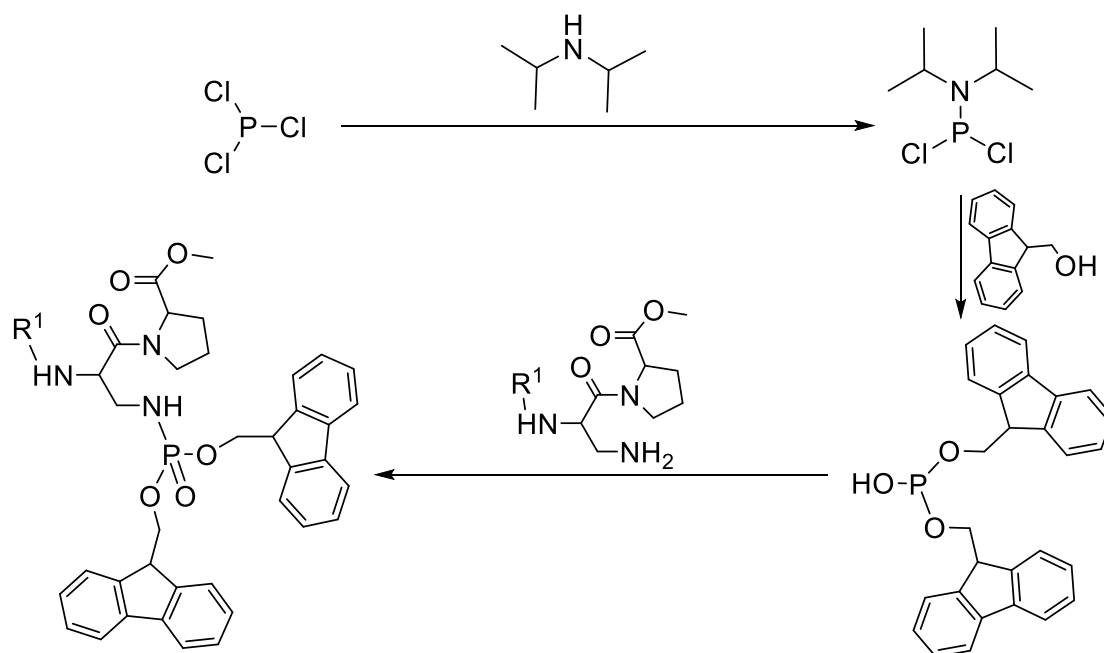


**Scheme 3.16.** Preparation of phosphoesters of  $\beta$ -aminoalanyl-proline using phosphoramidate approach.

The second involving dibenzylphosphorochloridate (Scheme 3.17) and the third involving *N*-bis-(9-fluorenylmethyl)phosphite as the phosphorylating agent (Scheme 3.18).



**Scheme 3.17.** Preparation of phosphoester of  $\beta$ -aminoalanylproline using dibenzylphosphorochloridate.



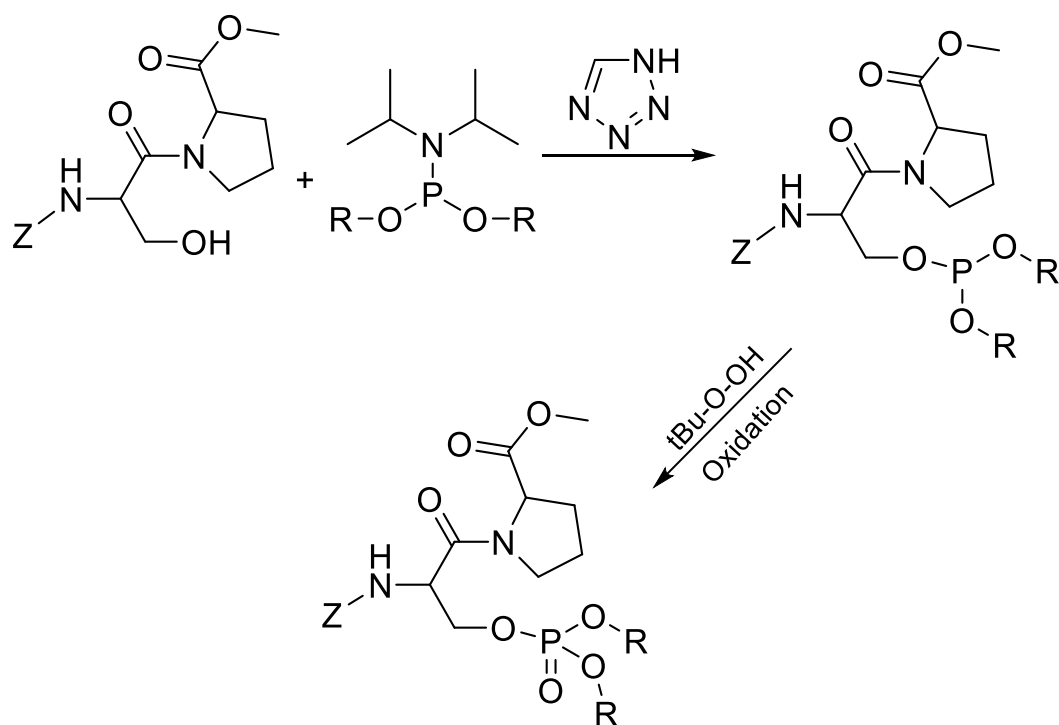
**Scheme 3.18.** Preparation of phosphoester of  $\beta$ -aminoalanylproline using bis(9-fluorenylmethyl)phosphite.

### 3.5 PHOSPHORYLATION OF SERYL-PROLINE DIPEPTIDE DERIVATIVES

In this section, we discuss the proposed and attempted methods of phosphorylating the synthesized molecules described in section 2.4.

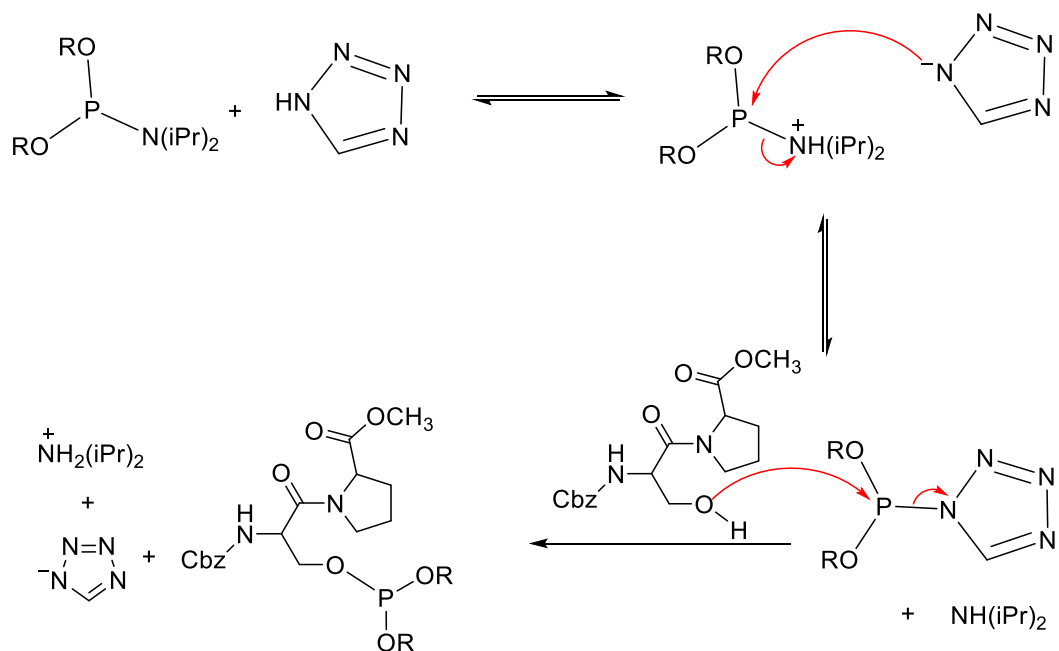
#### 3.5.1 Proposed O-phosphoryl serine-proline dipeptide by phosphoramidite approach

The use of phosphoramidites in phosphoamino and phosphopeptide synthesis as phosphitylation agents is a well-established synthetic method in the syntheses of several biological molecules including oligonucleotides and phospholipids. The proposed preparation of phosphoramidate derivatives of serine-proline motif in acetonitrile follows Scheme 3.19.



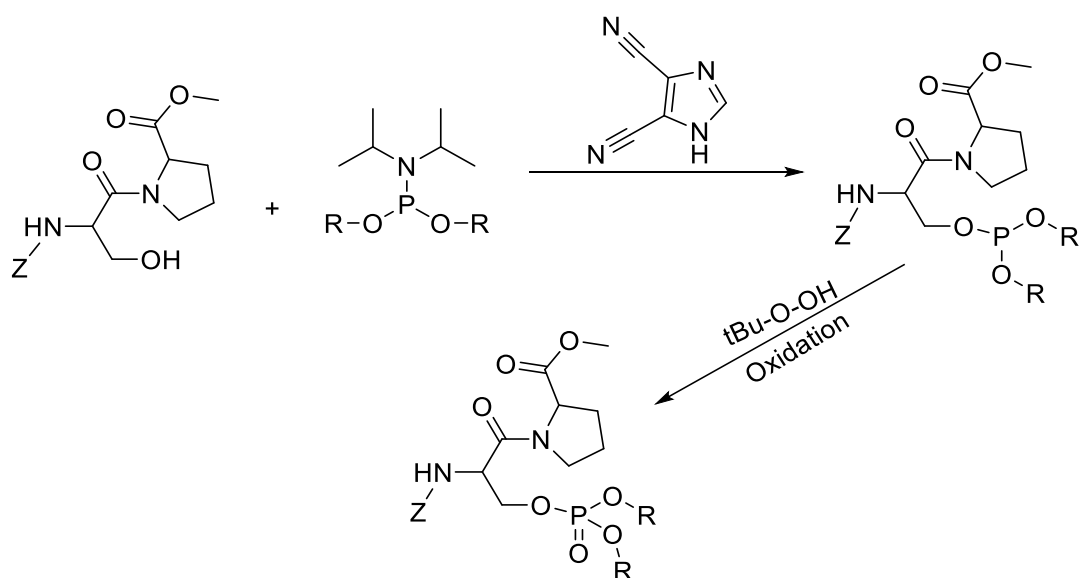
**Scheme 3.19.** Preparation of O-phosphoryl serine-proline dipeptide by phosphoramidite approach.

A catalyst is required for the displacement of the dialkylamino (*N,N*-diisopropylamino) ligand by the incoming hydroxyl group in the alcoholysis of phosphoramidites. Common catalysts include weak nitrogen acids, such as amine hydrohalides and azoles, particularly the most extensively used tetrazole. Studies on the mechanism of the phosphitylation reaction suggested that tetrazole plays a dual role. Firstly, it acts as an acid catalyst for the protonation of the nitrogen of the amine-leaving group. Secondly, it serves as a nucleophile by attacking the trivalent phosphorus thereby displacing the isopropylamine from the protonated amidite with consequent formation of the corresponding highly reactive tetrazolylphosphite intermediate. Then, the tetrazolylphosphite intermediate undergoes nucleophilic substitution by the peptidic alcohol to produce the phosphite triester (Scheme 3.20). Oxidation of the phosphite triester with *tert*-butyl hydroperoxide transforms it to the corresponding phosphoric triester (Scheme 3.19).



**Scheme 3.20.** Proposed mechanism of the tetrazole-catalysed O-phosphorylation of the serine-proline dipeptide.

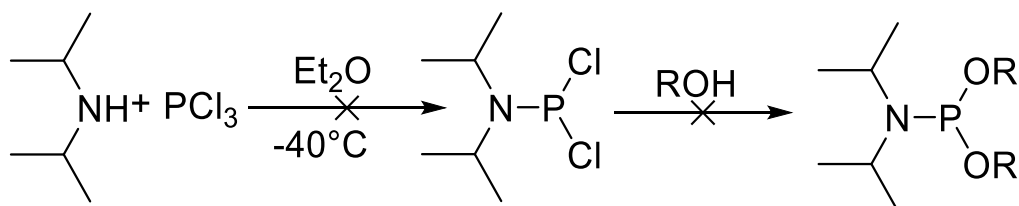
In view of the potential unstable (explosive) and toxic nature of 1H-tetrazole that call for care in its storage and handling, other substitutes including 4,5-dicyanoimidazole, pyridinium hydrochloride and trimethylsilyl chloride were considered. One of the major drawbacks of these substitutes is that they are not very effective on commercial scale. Since ours is a small scale preparation, we thought 4,5-dicyanoimidazole will be a perfect substitute activator (Scheme 3.21).



**Scheme 3.21.** Planned preparation of O-phosphoryl serine-proline dipeptide by phosphoramidite approach using 4,5-dicyanoimidazole.

### 3.5.2 Attempted preparation of O-phosphoryl serine-proline molecule

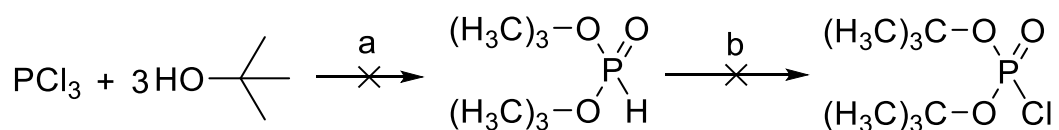
As the long term aim of this study was to make prodrug derivative(s), using non-commercially available reactants, we decided to practice making phosphoramidites 'from scratch', even if derivatives such as the dibenzyl- and diethyl phosphoramidites could be purchased. The available procedure for preparation of phosphoramidite<sup>160</sup> involves an initial preparation of *N,N*-diisopropylphosphoramidous dichloride and its subsequent conversion to dialkyl *N,N*-diisopropylphosphoramidite (Scheme 3.22).



**Scheme 3.22.** Attempted preparation of dialkyl *N,N*-diisopropylphosphoramidite.

In this method, a solution of diisopropylamine in dry diethyl ether was cautiously added in drops for more than 1 h to a solution of phosphorus trichloride in dry diethyl ether with vigorous stirring under nitrogen atmosphere, at -40 °C. The resulting mixture was stirred at 0 °C overnight, and then the precipitate was removed via canula filtering under dry inert atmosphere. The precipitate (diisopropylamine hydrochloride) was washed twice with dry diethyl ether. The diethyl ether was evaporated under a dry atmosphere to give the crude *N,N*-diisopropylphosphoramidous dichloride which failed to be vacuum distilled to give the pure product.

In this situation, we turned our attention to an alternative procedure described in section 2.4.1. This method involves an initial preparation of di-*tert*-butyl phosphonate and its subsequent transformation into di-*tert*-butyl phosphorochloridate (Scheme 3.23).



**Scheme 3.23.** Attempted preparation of di-*tert*-butyl phosphorochloridate. Reagents and conditions: (a) dry petroleum ether, (CH<sub>3</sub>)<sub>3</sub>N, stir RT (b)

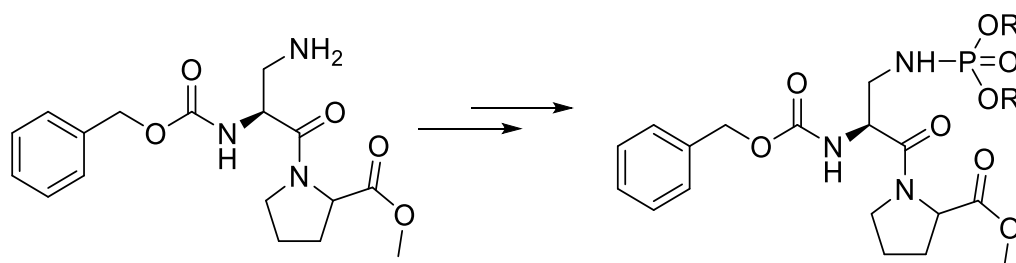
The former was prepared when a solution of phosphorus trichloride in dry petroleum ether was cautiously dropped over a period of 30 min into ice-methanol chilled solution (0 °C) of *t*-butyl alcohol and trimethylamine in petroleum ether. It was further stirred for 1 h without external cooling, after which time the suspension was filtered, the cake being washed well with additional petroleum ether. The solvent was evaporated using a rotary evaporator to obtain a yellow oil.

The resultant yellow oil residue should be rapidly distilled at 0.1 mmHg without fractionation and the resulting distillate distilled slowly. In this study, the attempted isolation of the product by distillation under high vacuum was unsuccessful, thus bringing the succeeding steps to a halt *via* this route.

### 3.6 PHOSPHORYLATED $\beta$ -AMINOALANYL-PROLINE DIPEPTIDES

Phosphoramidite route is one such method that has shown great efficiency in syntheses of biomolecules, examples include: phospholipids, oligonucleotides and sugars phosphates.

In this section we discuss methods proposed and attempted for phosphorylation of the  $\beta$ -aminoalanyl-proline dipeptides (Scheme 3.24).



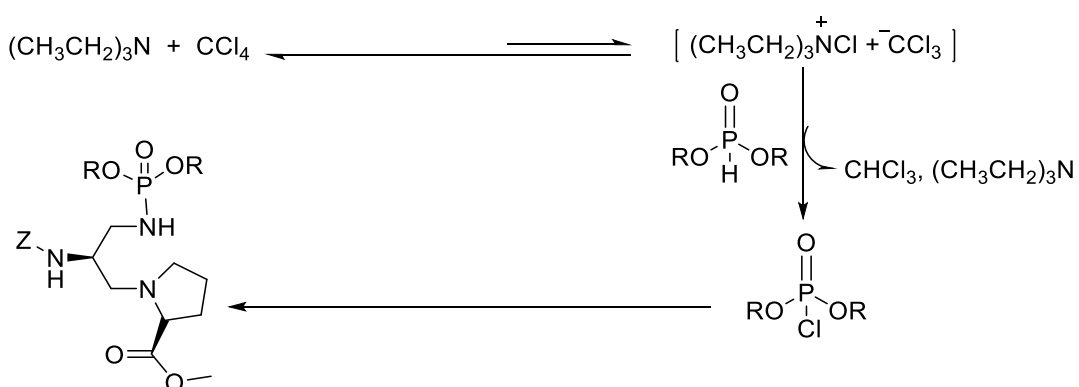
**Scheme 3.24.** Phosphorylation of the  $\beta$ -aminoalanyl-proline dipeptide.

#### 3.6.1 Proposed *N*-phosphoryl $\beta$ -aminoalanine-proline dipeptide

One proposed synthesis of the *N*-derivative of the target dipeptide uses the Atherton–Todd reaction of dialkyl phosphite and a primary amine. There are several suggested mechanisms for the Atherton–Todd reaction. In this study, we chose the mechanistic pathway shown in Scheme 3.25 being a plausible and more general mechanism for production of phosphoramidates from the reaction of primary or secondary amines with dialkylphosphite under basic conditions in carbon tetrachloride. It was suggested that carbon tetrachloride plays a double role in the reaction. It acts primarily as a solvent and secondarily

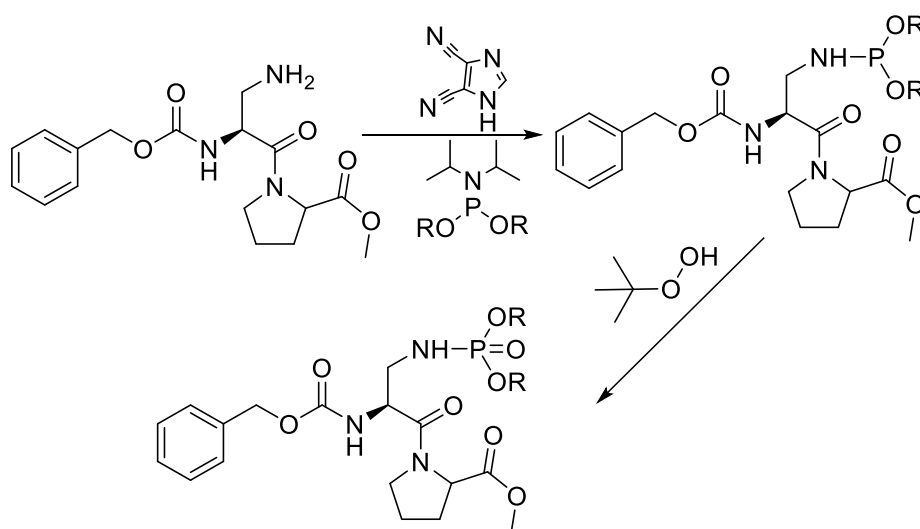


as a chlorinating agent to produce chlorophosphate *in situ* upon reacting with the phosphite. The reaction proceeds by a nucleophilic attack of the base (usually triethylamine) on carbon tetrachloride to form a salt  $[\text{R}_3\text{N}.\text{Cl}]^+\text{CCl}_3^-$ . The anion ( $\text{CCl}_3^-$ ) then deprotonates the dialkyl phosphite to give chloroform and the phosphonate anion, which reacts with chlorine cation to form dialkyl chlorophosphate. In the presence of an amine, the dialkyl chlorophosphate is transformed *in situ* into the corresponding dialkyl phosphoramidate.



**Scheme 3.25.** A proposed mechanism of the Atherton-Todd reaction for preparation of *N*-phosphoryl  $\beta$ -aminoalanine-proline derivative.

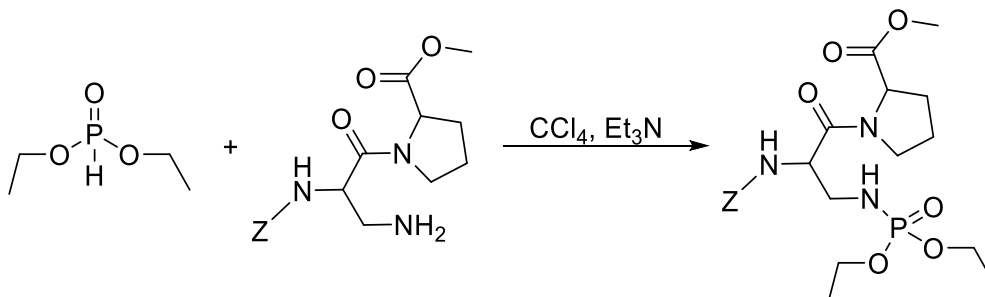
An alternative route involves using the phosphoramidite approach described already in section 3.5.1 according to Scheme 3.26.



**Scheme 3.26.** Phosphorylation of the  $\beta$ -aminoalanylproline dipeptide.

### 3.6.2 Attempted preparation of *N*-phosphoryl $\beta$ -aminoalanine-proline dipeptide

So as not to waste 'precious' dipeptides, model studies were undertaken with phenylalanine and *Z*- $\beta$ -aminoalanine for preparation of preparation of *N*-phosphoryl derivatives to test the methods and reagents made (Scheme 3.27).



**Scheme 3.27.** Attempted synthesis of *N*-phosphoryl- $\beta$ -aminoalanine-proline dipeptide.

Thus a mixture of diethylphosphite and carbon tetrachloride was added in drops to a solution of amino acid in triethylamine ( $\text{Et}_3\text{N}$ ) and ethanol solvent mixture cooled to  $0\text{ }^\circ\text{C}$ . The resultant mixture was stirred at  $20\text{ }^\circ\text{C}$  overnight, then the reaction mixture was acidified to pH2 with dilute HCl to stop the reaction. Following the extraction of the resulting mixture with ethyl acetate, it was dried with  $\text{MgSO}_4$ . Subsequent to the evaporation of the solvent, a colourless oily residue was obtained which was purified by crystallization from ethyl acetate-petroleum ether.

The reaction with phenylalanine was unsuccessful whereas some data were obtained for *N*-phosphoryl- $\beta$ -aminoalanine as presented in section 2.4.2. We also attempted with the crude *Z*-( $\beta$ -amino)Ala-Pro-OMe (**11**) (the amino derivative of the target molecule). This attempt yielded 2.7 g of a golden yellow oil, however, the NMR and mass spectroscopic analyses of this product did not show any diagnostic peaks to confirm the structure.

### 3.7 NEW DERIVATIVES OF A NON-PEPTIDE PIN1 INHIBITOR

Consequent to the limited success in phosphorylation of the synthetic mimics of Pin1 substrate discussed in sections 3.2 and 3.3, it seemed reasonable that we consider non-peptidic and non-phosphorylated small molecules capable of downregulating biomarkers of Pin1 activity. The search led to the identification of 2-methyl-5-(p-methoxyphenyl)-3-furoryl-3-(2-naphthyl)-D-alanine<sup>161</sup> (**30**) (Figure 3.5).

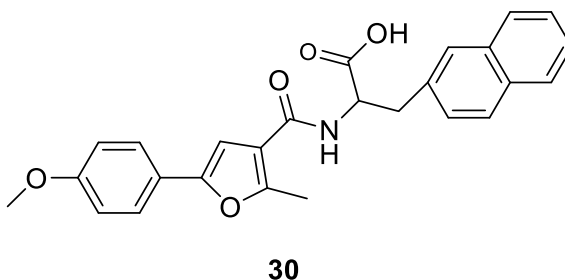


**Figure 3.5** Structure of the literature Pin1 inhibitor

The choice of this molecule was based first on its ability in cell-based assays to downregulate biomarkers of Pin1 activity. A report by Potter *et al.*<sup>161</sup> showed that in serum-free medium wherein Pin1 performs a significant function in proliferation and survival, treatment of PC3 prostate cancer cells with the identified compound (10  $\mu\text{M}$ ) resulted in reduction of cyclin D1 expression and blocking of proliferation of PC3 cells. This result phenocopied the effect of siRNA-transfected reduction of Pin1. The second reason for its choice was that as well as being a very efficient inhibitor of Pin1 ( $\text{IC}_{50}$  2.6  $\mu\text{M}$ ), it was one of only two from an array of structure-guided designed molecules with activity in cell-dependent assays. Subsequent to the identification of this molecule from the search, we proposed synthesis of some further derivatives of the 2-methyl-5-arylfuroic acid-based compound by replacing the 3-(2-naphthyl)-D-alanine moiety of the compound with other aromatic D-amino acids, with a view to evaluating their potency on TF and TF-mediated activities of TF-producing cells.

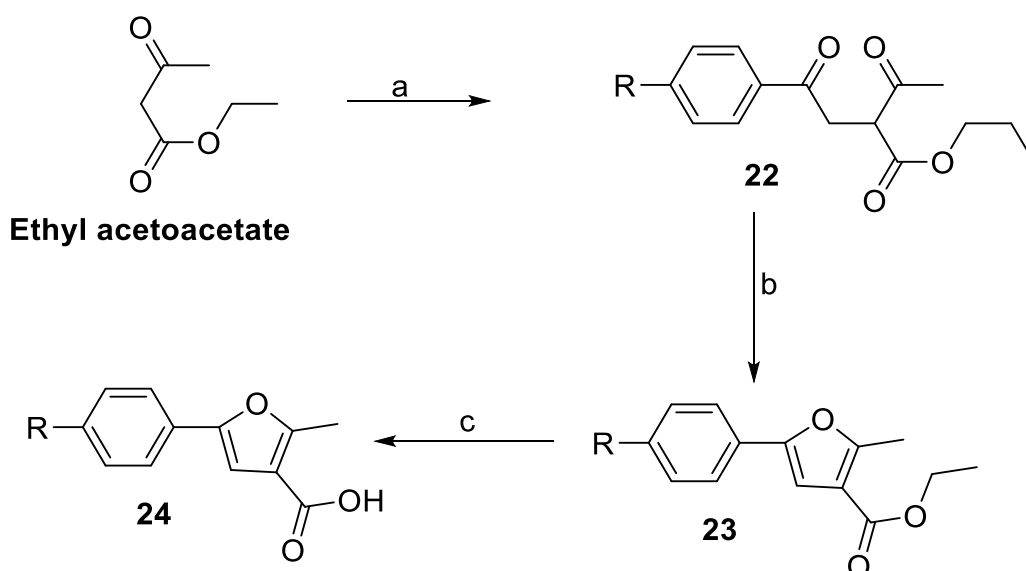
### 3.7.1 Aims

In this section, the various procedures used in the synthesis of the non-phosphorylated Pin1 inhibitor and its new derivatives are discussed. Thus, the objectives of the chapter include discussions on:

- Synthesis of 2-methyl-5-arylfuroic acid moiety.
- Amide coupling of the furoic acid fragment with some aromatic D-amino acids.

### 3.7.2 Synthesis of 2-methyl-5-arylfuroic acid

The pathway for the preparation of the 2-methyl-5-arylfuroic acid fragment (**24**) is illustrated in Scheme 3.28.

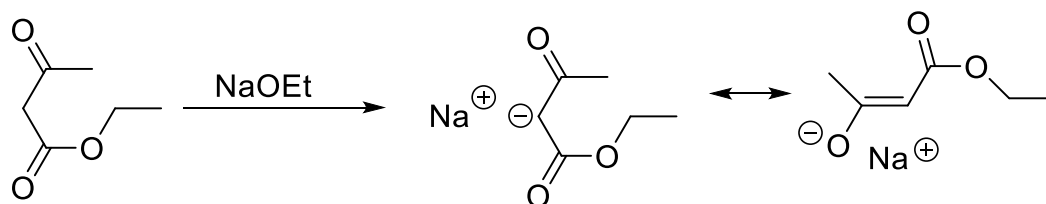


**Scheme 3.28.** Synthesis of 2-methyl-5-arylfuroic acid. Reagents and conditions: (a) Na chips, *p*-methoxyphenacyl bromide or phenacyl bromide, dry toluene, reflux 6 h; (b) Conc.HCl, reflux (under N<sub>2</sub> trap), 20 h; (c) 5% KOH, reflux, 2 h; R = OCH<sub>3</sub> or H

### 3.7.3 Preparation of ethyl phenacylacetate (**22**)

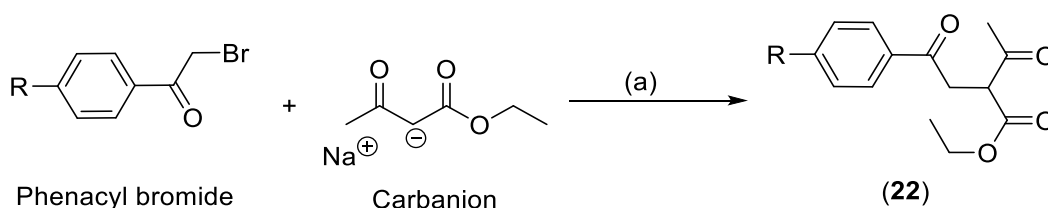
The synthesis of the non-peptide Pin1 inhibitor and its analogues was started first by generating an enolate from a reaction between ethyl acetoacetate and sodium metal. To generate the enolate ion, the procedure described by Wilds and Johnson<sup>147</sup> was followed first as described, by directly adding ethyl acetoacetate to sodium chips in toluene and heating under reflux. A modified approach involved an initial reaction of the sodium chips with dry ethanol to

generate sodium ethoxide, followed by evaporation of the solvent and then addition of the other reactants. This modification was born out of the fact that ethyl acetoacetate loses a proton from the alpha-carbon to form the corresponding conjugate base (a carbanion) when reacted with a base (e.g. sodium ethoxide) to form the corresponding sodium salt (Scheme 3.29). However, the modification did not produce a significant improvement in either the yield or reaction time.



**Scheme 3.29.** Formation of the enolate ion from ethyl acetoacetate.

The sodium salt of the ethyl acetoacetate was then alkylated by condensing it with the appropriate phenacyl bromide to give the intermediate ethyl phenacylacetoacetate (**22**) as shown in Scheme 3.30.



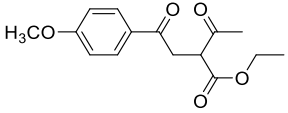
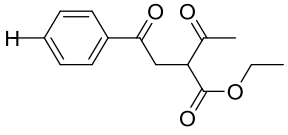
**22a:** R = OCH<sub>3</sub>; **22b:** R = H

**Scheme 3.30.** Preparation of alkylated ethyl acetoacetate. Reagents and reaction conditions:

(a) dry toluene, reflux, 6 h

The yield obtained for **22** was very low using the approach described by Wilds and Johnson. Product **22a** (R = OCH<sub>3</sub>) was obtained in 27% yield, whilst **22b** (R = H) was obtained in 18% yield. When sodium ethoxide was used the yield was further lowered; **22a** was obtained in 25% yield while **22b** was obtained in 15% yield Table 3.1. This observation is similar to the observation by Wilds and Johnson who experienced a drop in yield of **22a** to 60-75% when a small amount of absolute ethanol was combined with benzene.<sup>147</sup>

**Table 3.2.** Summary of product yield with or without sodium ethoxide.

Code	Structure	%Yield without EtONa	%Yield with EtONa
<b>22a</b>		27	18
<b>22b</b>		25	15

Attempts to optimize the yield by prolonging the reaction time using the method described by Wilds and Johnson was unsuccessful, therefore, an alternative approach suggested by Porretta et al.<sup>148</sup> was used with modifications. In this method, a mixture of sodium pellets suspension and ethyl acetoacetate in toluene was stirred at room temperature for three days. The resultant mixture after addition of phenacyl bromide was also stirred at room temperature for another three days resulting in a reddish-brown oily liquid produced in 88% yield for **22a** and 85% yield for **22b**.

The structure of these species was confirmed from the NMR data. In the <sup>1</sup>H NMR spectrum of **22a**, the diagnostic peak at  $\delta$  3.55 showing ABX pattern, which integrated for 2H ( $J = 18.3, 8.3, 6.0$  Hz), corresponded to the methylene group (c) of the phenacyl substituent on the  $\alpha$ -carbon of the alkylated ethyl acetoacetate (Figure 3.6). The upfield shift and change in multiplicity to ABX pattern from singlet of the corresponding signal in the spectrum of the starting phenacyl bromide confirmed the structural assignment. The upfield shift is justified by the loss of the electron-withdrawing bromine adjacent to the protons. The quartet signal at  $\delta$  4.20 integrating for three protons corresponded to the  $\alpha$ -H and methylene protons of acetoacetate moiety. The <sup>13</sup>C NMR spectrum showed among other peaks three carbon signals at  $\delta$  203.60, 195.80 and 169.60 consistent with the three carbonyl carbons.

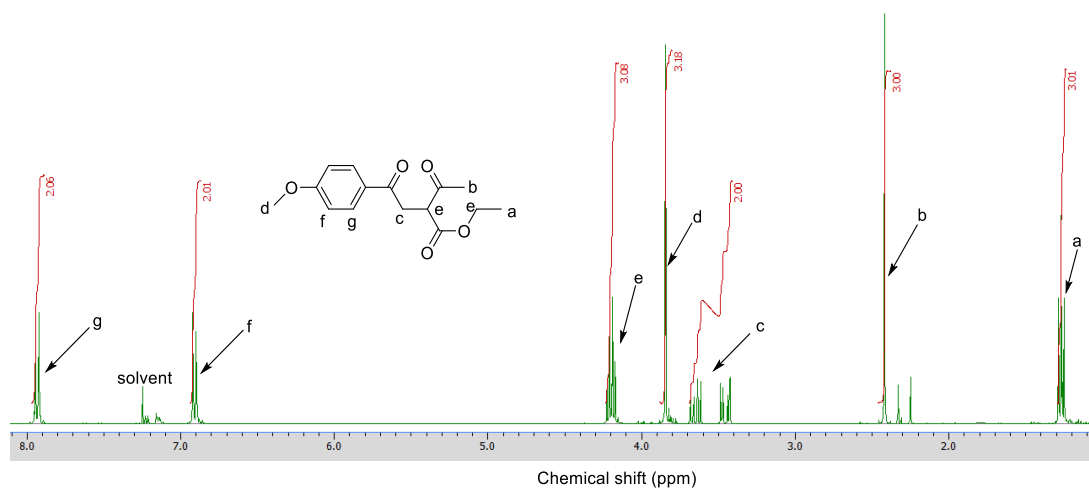


**Figure 3.6.**  $^1\text{H}$  NMR spectrum of **22a** in  $\text{CDCl}_3$ .

Similarly, in the  $^1\text{H}$  NMR spectrum of **22b** ( $\text{R} = \text{H}$ ), the phenacyl methylene protons resonated at 3.48-3.74 ppm as a multiplet while the methine and methylene protons of the acetoacetate moiety overlapped to give a multiplet signal that integrated for three protons at  $\delta$  4.18-4.24. Expectedly, the  $^{13}\text{C}$  NMR spectrum of this compound also displayed three carbonyl peaks.

#### 3.7.4 Preparation of Ethyl 2-methyl-5-aryl-3-furoate (**23**)

Using Wilds and Johnson's approach (method 1), treatment of **22** in ethanol with concentrated hydrochloric acid and heating under reflux for 20 h, with protection from air by means of a nitrogen trap, resulted in the cyclised product, ethyl 2-methyl-5-aryl-3-furoate (**23**). The product **23a** was obtained in 20% yield while the yield of **23b** was 23%. On the other hand, using method 2 (Porretta's approach) which involved heating a mixture of **22** and concentrated hydrochloric acid in ethanol under reflux for 24 h, the product yields obtained were 78% and 76% for **23a** and **23b** respectively.

The  $^1\text{H}$  NMR spectrum of **23a** (Figure 3.7) established successful cyclisation of the aliphatic dicarbonyl compound **22a** by the disappearance of the ABX-patterned peak in the spectrum of **22a** and appearance of a singlet at  $\delta$  6.93 that integrated for one proton assignable to H-4 furan among other peaks. In addition, the  $^{13}\text{C}$  NMR spectrum of **23a** showed presence of only one carbonyl signal at  $\delta$  159.32 and disappearance of both  $\text{C}_1$  and phenacyl carbonyl signals present in  $^{13}\text{C}$  NMR spectrum of the starting material **22a**. Also the presence of the molecular ion at  $m/z = 261.07$  for  $[\text{MH}]^+$  in the ES-MS further confirmed

the structure. Correspondingly, the  $^1\text{H}$  NMR spectrum of **23b** displayed a singlet peak at  $\delta$  6.88 consistent with the H-4 of the furan ring. Likewise the  $^{13}\text{C}$  NMR spectrum displayed a signal at 159.08 ppm corresponding to the carbonyl carbon.

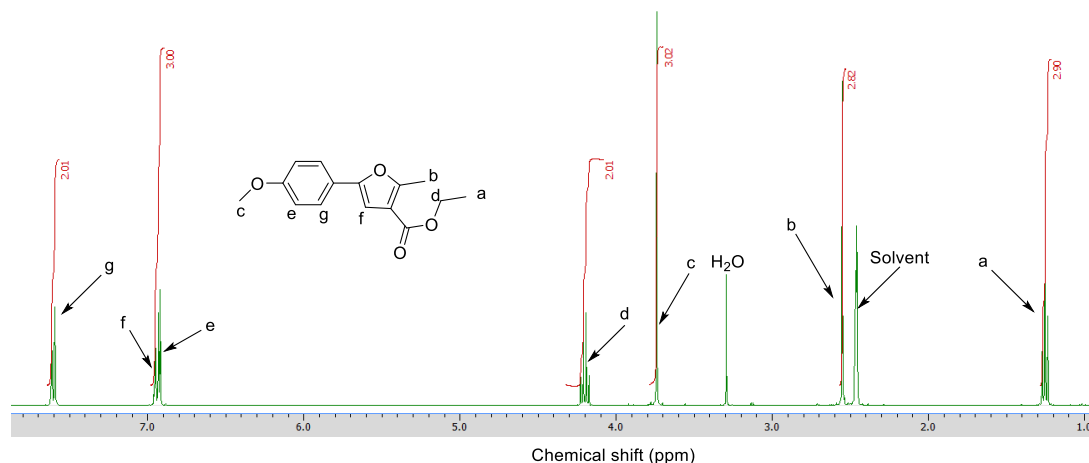
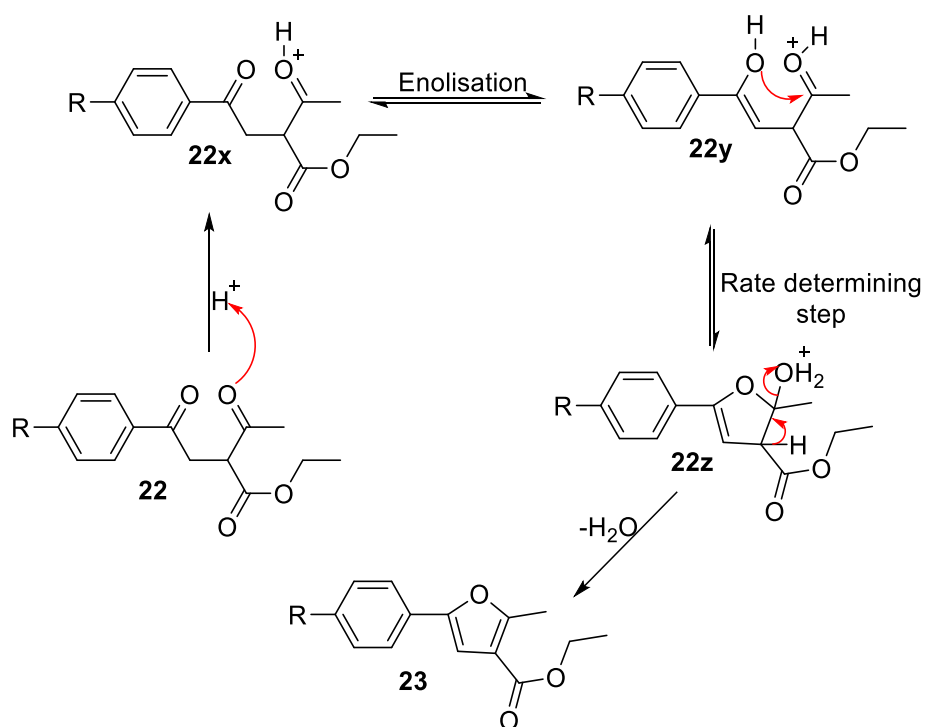


**Figure 3.7.**  $^1\text{H}$  NMR spectrum of **23a** in  $\text{DMSO-d}_6$ .

The conversion of this 1,4-dicarbonyl compound (**22**) was achieved through the acid-promoted dehydrative cyclization reaction involving the Paal-Knorr sequence to form the substituted furan ester **23** (Scheme 3.31).



**Scheme 3.31.** Cyclisation of the intermediate **22** (ethyl 2-(*p*-methoxyphenyl)acetoacetate) through Paal-Knorr synthesis.



### 3.7.5 Preparation of 2-Methyl-5-aryl-3-furoic acids (**24**)

Hydrolysis of the furan ester using method 1, which entailed heating a mixture of **23** and 5% potassium hydroxide solution in ethanol under reflux for 3 h produced the aryl furoic acid (**24**). Alternatively, using method 2 whereby a solution of sodium ethoxide and **23** was heated in ethanol under reflux overnight yielded the product; **24a** was yielded in 73% yield while **24b** was yielded in 79%. The structure of **24** was established from its spectroscopic data. Expectedly, no signal for the methyl and methylene protons was displayed in the  $^1\text{H}$  NMR spectra of **24a** (Figure 3.8) and **24b** compare to the  $^1\text{H}$  NMR spectrum of their corresponding esters **23a** and **23b**. Likewise, the  $^{13}\text{C}$  NMR spectrum of **24a** showed eleven carbon signals instead of thirteen in the  $^{13}\text{C}$  spectrum of **23a** while **24b** showed ten instead of twelve carbon environments in the  $^{13}\text{C}$  NMR spectrum of the starting material **23b** thereby corroborating the structure. The ES-mass spectrum of **24a** also showed an ion with  $m/z = 233.06$  which corresponded to  $[\text{MH}]^+$ .

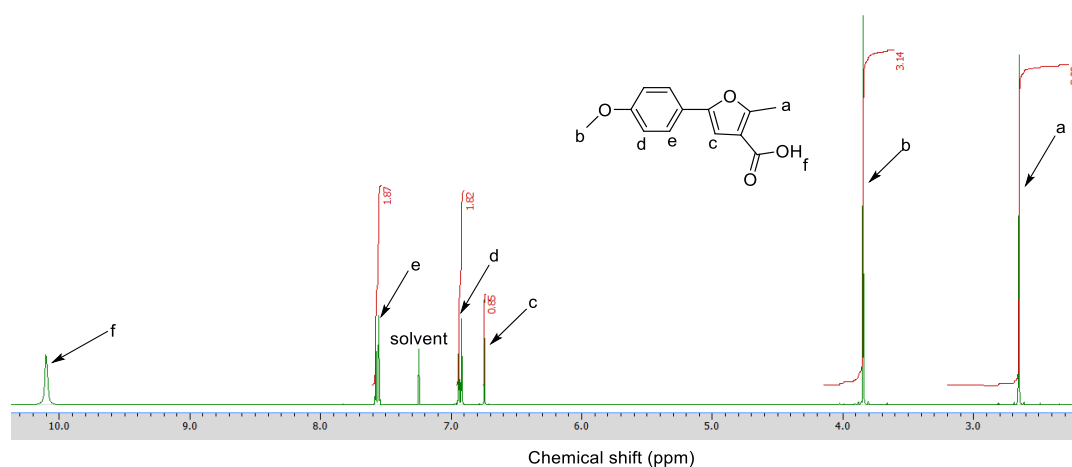


**Figure 3.8.**  $^1\text{H}$  NMR spectrum of **24a** in  $\text{CDCl}_3$

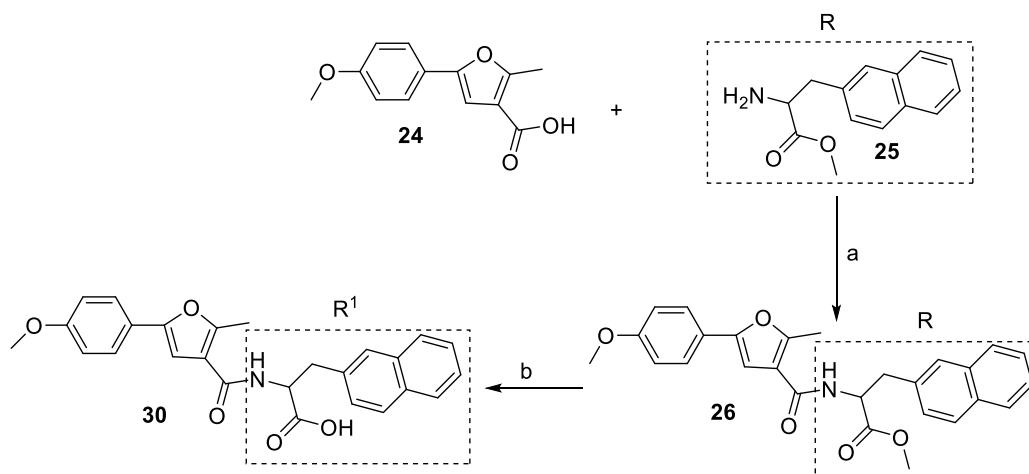
It is obvious that the method described by Porretta et al., gave better products and yields than that obtained using Wilds and Johnson's approach. The latter procedure involves heating under reflux at every stage of the reaction; this presumably led to decomposition of the product resulting in production of dark mixtures with difficult workup and low yield resulting from loss of more product in the workup process. In contrast, not all the stages of the reaction in the

Porretta's procedure involved heating, intermediate products were not dark mixtures and workup less difficult.

Now that the aryl furoic acid **24** had been prepared successfully, it was therefore available for amide coupling with different D-amino acids. The following section discusses only coupling with **24a**. Only the methoxy derivative (**24a**) was taken forward as it is the mimic for the literature compound and will be referred to simply as **24**; the unsubstituted derivative (**24b**) was just cheaper to do model/test reactions to make the furan acid.

### 3.8 AMIDE COUPLING OF (24) WITH AROMATIC D-AMINO ACIDS

The preparation of the target Pin1 inhibitors followed the same approach used for preparing the dipeptides **6-8** (Section 2.3.2). The aryl furoic acid **24** was coupled with some commercially available aromatic D-amino acids using EDC.HCl as shown in Scheme 3.32.



**Scheme 3.32.** Amide coupling of moieties of target Pin1 inhibitor. Reagents and conditions: (a) DIPEA, amino acid methyl ester hydrochloride, DCM, HOBt, EDC .HCl, stir at RT, 20 h; (b) 5% KOH, ethanol stir at RT.

#### 3.8.1 Preparation of methyl ester of 3-(2-naphthyl)-D-alanine (**25**)

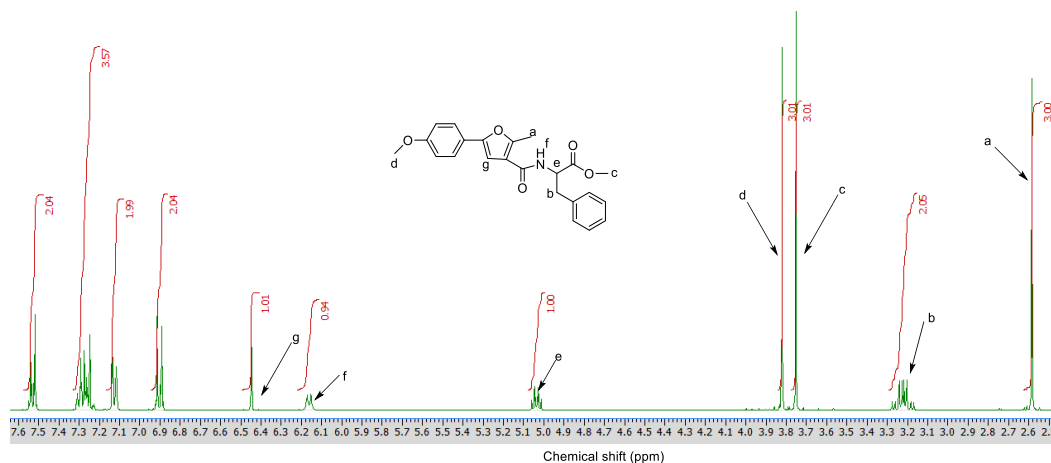
The 3-(2-naphthyl)-D-alanine methyl ester was not commercially available therefore the preparation of its methyl ester was first undertaken using the method described in section 2.3.1 whereby a mixture of the naphthylalanine, anhydrous methanol and thionyl chloride was heated under reflux leading to a white solid product **25** in 89% yield. Analysis of the  $^1\text{H}$  NMR spectrum of **25** confirmed the structure. It showed *inter alia*, a singlet that integrated for three

protons and corresponded to the  $-OCH_3$  group resonating slightly downfield from  $\delta$  3.48 in the  $^1H$  NMR of the starting material, methanol, to  $\delta$  3.63 in the spectrum of **25** because of the role of the adjacent carbonyl group as an electron-withdrawing species.

In the primary attempt at amide bond formation, aryl furoic acid **24** was coupled with the prepared methyl ester **25** (Scheme 3.6) to give the ester derivative of the literature Pin1 inhibitor **26** in 72% yield as a white solid. The structure of the amide-coupled ester **26** was established by the  $^1H$  NMR spectral analysis, which displayed a doublet at 6.20 ppm with  $J = 9.1$  Hz corresponding to the amide proton (CONH) and a singlet that integrated for one proton at  $\delta$  5.13 corresponding to the  $\alpha$ -H of the D-amino acid moiety.  $^{13}C$  NMR spectrum showed two carbonyl signals among others for the product to confirm the structural assignment. The ES-MS also showed the  $m/z$  value = 444.13 which is consistent with  $[MH]^+$ , the molecular ion of the product.

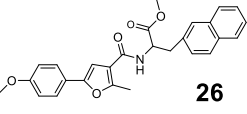
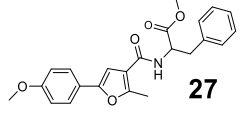
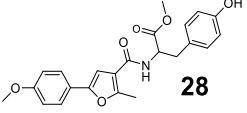
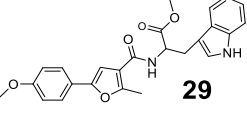
The first new derivative was similarly prepared from a coupling reaction between **24** and the methyl ester of D-phenylalanine using EDC.HCl and the product **27** obtained in 75% yield. The structural assignment was equally confirmed from the  $^1H$  NMR spectrum that displayed peaks including a doublet signal at  $\delta$  6.02 corresponding to amide proton (CONH) and an apparent quartet signal at  $\delta$  5.04 consistent with the  $\alpha$ -H of the D-amino acid moiety. The  $^{13}C$  NMR spectrum likewise displayed signals including two signals at 172.29 and 159.37 ppm corresponding to the carbonyl carbon atoms. In addition, the mass spectrum supported the structure by displaying an ion at  $m/z = 394.19$  consistent with  $[MH]^+$ . The structural assignment for this set of compounds is illustrated with the  $^1H$  NMR spectrum of a sample derivative **27** as presented in Figure 3.9 and a summary of important data given in Table 3.3. In repeat experiments, esters of two more new derivatives of the amide-coupled compound were similarly prepared by coupling **24** separately with commercially available D-tyrosine methyl ester hydrochloride and D-tryptophan methyl ester hydrochloride to produce **28** and **29** respectively. The amide proton of **28** in its  $^1H$  NMR spectrum, resonated as an apparent doublet at 6.62 ppm while the  $\alpha$ -H of the amino acid resonated as a quartet at 5.02 ppm. The  $^{13}C$  NMR displayed the carbonyl peaks at 159.54 and 173.00 while the mass spectrum displayed the molecular ion  $m/z = 410.18$  consistent with  $[MH]^+$ . In

the same vein, the amide proton and the  $\alpha$ -H of **29** appeared at 6.25 and 5.08 ppm respectively. The signals for the carbonyl carbons appeared at 159.41 and 172.49 ppm.



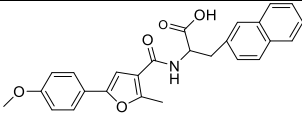
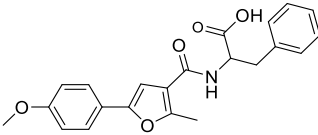
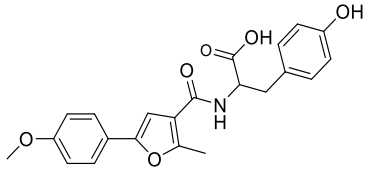
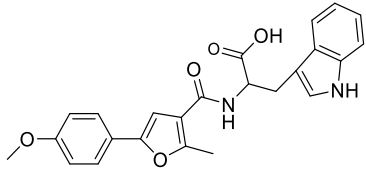
**Figure 3.9.**  $^1\text{H}$  NMR spectrum for **27** in  $\text{CDCl}_3$ . A sample illustration of the structural assignment of esters of synthesized derivatives of the literature Pin1 inhibitor.

**Table 3.3.** Summary of the characteristic  $^1\text{H}$  NMR and  $^{13}\text{C}$  NMR signals for the amide-coupled esters of the literature Pin1 inhibitor and its new derivatives.

Structure	Yield (%)	CONH (ppm)	$\alpha$ -H (ppm)	m/z for $[\text{MH}]^+$	C=O <sub>furan</sub> (ppm)	C=O <sub>ester</sub> (ppm)
 <b>26</b>	72	6.20	5.13	444.13	159.35	172.32
 <b>27</b>	75	6.16	5.04	394.19	159.37	172.29
 <b>28</b>	81	6.62	5.02	410.18	159.54	173.00
 <b>29</b>	76	6.25	5.08	433.19	159.41	172.59

Subsequent hydrolysis of the esters **26** by stirring a mixture of methanol solution of the sample and aqueous 5% KOH solution at ambient temperature overnight produced a white solid, the corresponding acid **30** (the non-peptide Pin1 inhibitor reported by Potter *et al.*<sup>161</sup>) in 55% yield. The structure of **30** was confirmed from both its <sup>1</sup>H and <sup>13</sup>C NMR spectra. The <sup>1</sup>H spectrum, displayed no signal for the methoxy protons of the ester function and the <sup>13</sup>C NMR spectrum likewise showed no signal corresponding to the methoxy carbon of the ester group compared to the NMR spectra of **26**. The ES-MS also supported the structure by displaying the expected signal at m/z = 430.14 consistent with [MH]<sup>+</sup>. Analysis of both <sup>1</sup>H and <sup>13</sup>C NMR spectra confirmed the structures of the new derivatives **31**, **32** and **33** by displaying no signals corresponding to the methoxy group labelled (c) in Figure 3.9. The ES-MS of each product displayed m/z value consistent with [MH]<sup>+</sup>. The summary of data is presented in Table 3.4.

**Table 3.4.** A summary of yield and molecular ion peaks of the new derivatives of the non-peptide inhibitor.

Code	Structure	Yield (%)	m/z for [MH] <sup>+</sup>
<b>30</b>		55	430.14
<b>31</b>		67	380.13
<b>32</b>		61	396.13
<b>33</b>		74	419.16

### 3.9 BIOLOGICAL EVALUATION OF SYNTHESIZED POTENTIAL PIN1 INHIBITORS

In biologically active molecules, phosphates act as functional units that generate regulated or controlled intracellular signals through prevention of intercellular chemical signal transmission. Since enzyme substrates found in nature are usually negatively charged, the inhibitors of these enzymes must necessarily carry one or more negative charges. However, it is difficult for small charged molecules to traverse the cell membrane except via endocytosis. For this reason, it was aimed at in this study to prepare the prodrug form of the pSer-Pro dipeptide. Since the success recorded in synthesizing the prodrug form of the pSer-Pro dipeptide molecule was limited, attention was shifted to the small molecule Pin1 inhibitors. The literature Pin1 inhibitor (**30**) and its new derivatives (**31**, **32** and **33**) were successfully synthesized in this study and investigated for their ability to: induce apoptosis using the TUNEL assay, cause nuclear localisation of p53 and induce Bax proteins expression.

It is worth mentioning here that the concentration used in the following experiments was the one optimized as described in section 2.7.7. Because there was no precedent for using these synthesised small compounds, the concentration optimised by Ettelaie et al., for small molecule inhibitor, Juglone, in a previous work<sup>81</sup> was used as a guide in choosing a range of concentration for the preliminary experiments.

#### 3.9.1 Examination of the influence of synthesized molecules on MDA-MB-231 cell proliferation

Inhibitory ability of the test agents towards cell proliferation was investigated by determining the cell numbers using the crystal violet staining assay. In 96-well plate, MDA-MB-231 cells ( $10^5$ /well) were cultured. Once adhered, a set of cells incubated with DMSO vehicle acted as negative control. Thereafter, cells were incubated for 24 h at 37 °C with test reagents **30**, **31**, **32** and **33** (100  $\mu$ M). The number of viable cells after treatment was estimated using the CVS assay and quantified from a previously constructed standard curve.

The result of the assay showed that all the reagents caused a reduction in the number of viable cells compared to the untreated cells (Figure 3.10). However,

compound **32** induced the highest reduction in cell numbers with compounds **30** and **33** showing moderate potencies. Compound **31** showed the least reduction in cell number.

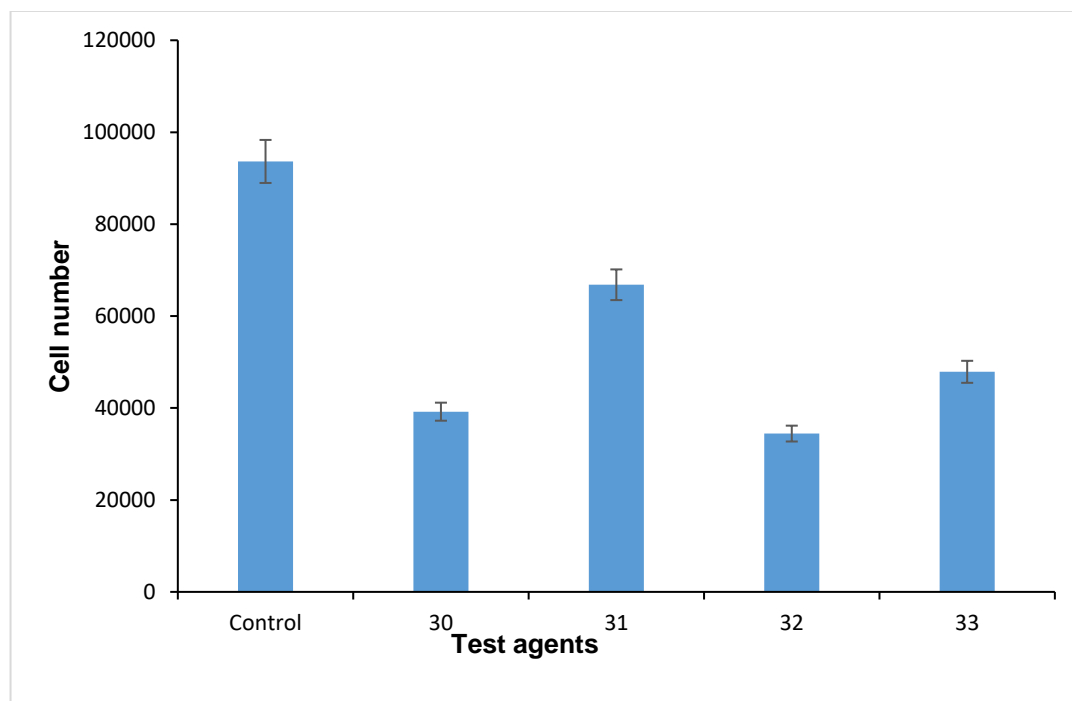


**Figure 3.10.** Assessment of reduction in cell number by the synthesized small molecules. MDA-MB-231 cells ( $10^5$ /well) were treated with synthetic molecules **30**, **31**, **32** and **33** ( $100 \mu\text{M}$ ) after seeding out in 96-well plates. Sets of cells were incubated with DMSO vehicle (control). The number of cells was then determined using the CVS assay and quantified from a previously constructed standard curve. (The data is the average of two independent experiments and expressed as  $\pm$  SD).

All the compounds show reduction in cell number, which probably suggests that they are potential death-inducing agents. However, one major drawback of the crystal violet assay is that it cannot differentiate between inhibition of proliferation and cell survival hence the need for a quantitative method to determine the cause of the observed reduction in cell number.

### 3.9.2 Cellular apoptosis measured 24 h post-treatment using TUNEL assay.

During apoptosis, endonucleases are activated resulting in the fragmentation of chromosomal DNA. In this study, DNA fragmentation resulting from

apoptosis of cells was measured using an apoptosis detection kit (TiterTACS™ Colorimetric Apoptosis Detection Kit). The ability of the test reagents to induce apoptosis in breast cancer cells was evaluated. Breast cancer (MDA-MB-231) cells ( $10^5$ /well) were seeded out in 24-well plates, incubated overnight and then incubated with synthetic molecules **30**, **31**, **32** and **33** (100  $\mu$ M) for 24 h. A set of cells were used untreated (negative control). The experimental data of the TUNEL assay used in this study to measure degradation of DNA showed significant induction of apoptosis in cells incubated with test agents **30** and **32** compared with the control, compound **33** showed moderate activity while **31** showed non-measurable apoptosis (Figure 3.11). The result suggests that TUNEL assay can assist in quantification of dead cells. However, one of the downsides of the TUNEL assay is its non-discriminatory staining of DNA damage by other events aside from apoptosis including necrosis and cells undergoing active cell repair. Therefore, to pursue the goal of elucidating the mechanisms involved in the induced apoptosis further, the influence of the synthesized molecules on key pro-apoptotic indicators including p53 and Bax protein was assessed.

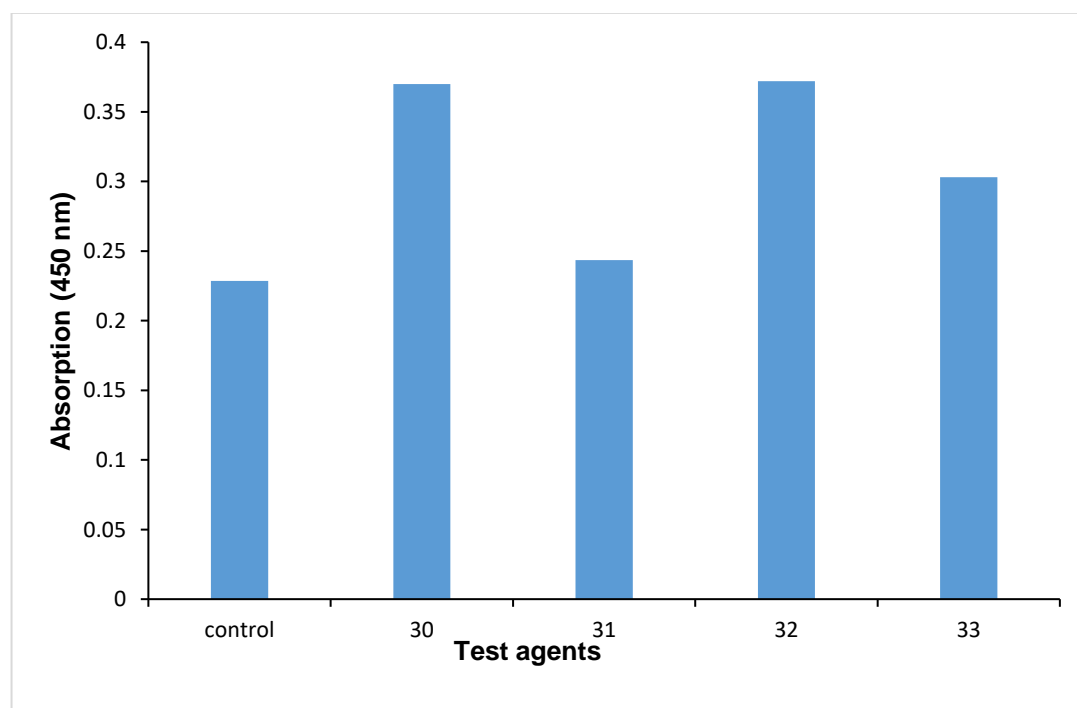


**Figure 3.11.** Measurement of induced cellular apoptosis by small molecule Pin1 inhibitors. MDA-MB-231 cells ( $10^5$ /well) were cultured in 24-well plates, incubated overnight, and then



incubated with the test reagents for 24 h. A set of cells were used untreated (negative control). Cellular apoptosis was measured after 24 h incubation and measured using a colorimetric TUNEL assay (n=1).

### 3.9.3 Analysis of nuclear localisation of p53 following treatment with synthesized molecules

The level of p53 nuclear localisation was examined by fluorescence microscopy. MDA-MB-231 cells ( $10^3$ /well) were cultured in 35 mm glass-bottom with 14 mm micro well dishes. Following incubation of cells for 4 h, they were treated with the synthesized molecules **30**, **31**, **32** and **33** (100  $\mu$ L). A set of cells without treatment acted as negative control and another set treated with TNF- $\alpha$  (10 ng/mL) acted as positive control. After 18 h of incubation, fixing and permeabilisation, the cells were probed with a p53 antibody. The cells were then labelled with DAPI to stain the nuclei and analysed using a fluorescence microscope. Subsequently, ImagePro Plus software was used to determine the p53 co-localisation within the nucleus. Cells treated with compound **32** showed significant p53 localisation to the nucleus compared to the control sample. Compounds **30** and **33** showed moderate localisation while compound **31** was largely ineffective (Figure 3.12).

One could draw a probable explanation for this observation perhaps from a previous study by Potter *et al.*<sup>161</sup> involving 2-methyl-5-(*p*-methoxyphenyl)-3-furoryl-3-(2-naphthyl)-D-alanine, the Pin1 inhibitor identified from the literature, which is the same as compound **30** in the present study (Figure 3.13). The study by Potter's group involved assessment of the ability of 2-methyl-5-(*p*-methoxyphenyl)-3-furoryl-3-(2-naphthyl)-D-alanine (**30**) to prevent the growth of serum-starved PC3 prostate cancer cells under conditions where Pin1 thrives as a modulator of subsistence and propagation.<sup>162</sup> It was reported that exposure of the PC3 cells to **30** under serum-free conditions suppressed cyclin D1 expression (a Pin1 activity biomarker) and prevented PC3 cells from multiplying.<sup>161</sup> The Potter's report presented evidence of compound **30** modulating biomarkers dependent upon Pin1 function including cyclin D1.

The first reason given for the efficiency of this compound in PPIase assay is its reduced polar surface area that enhanced its cell permeability. Another

reason adduced to explain its cell activity is its ligand potency, which is associated with its binding mode to the active site of Pin1.

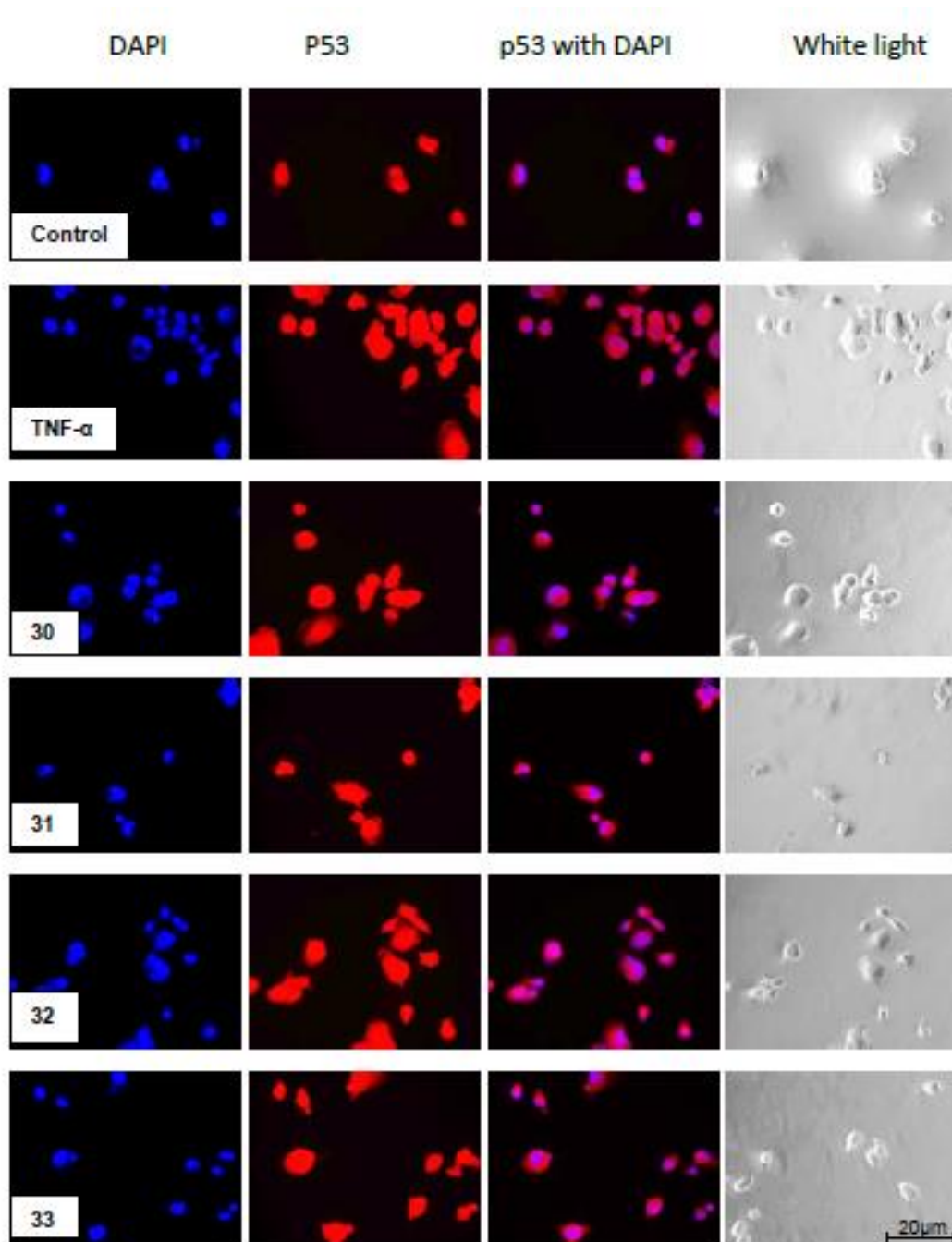


**Figure 3.12.** Analysis of the effect of the synthetic molecules on nuclear localisation of p53. MDA cells ( $10^3$ /well) were incubated for adherence for 4 h. Then treated with medium supplemented with test reagents **30**, **31**, **32** and **33** ( $100 \mu\text{M}$ ). An untreated set of cells represented the negative control and another set treated with TNF- $\alpha$  ( $10 \text{ ng/mL}$ ) acted as positive control. The cells were labelled 18 h post-treatment with p53 antibodies and DAPI and analysed using a fluorescence microscope ( $\times 40$ ) ( $n=2$ ).

It was suggested from the PPlase assay that the potency of the compound was in direct connection with the strong van der Waals interaction the furanoaryl moiety (Figure 3.13) makes with the hydrophobic pocket of the active site. It was suggested further that the carboxyl group interacts with Lys63 while the naphthyl substituent fixes into a 'shelf-like' hydrophobic plane surface positioned opposite to Cys113 as illustrated for a structurally similar molecule in Figure 3.14.

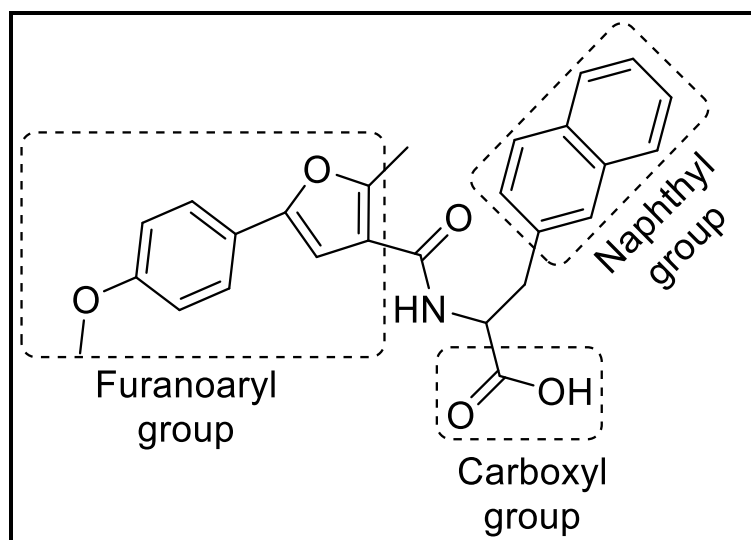


**Figure 3.13.** Molecular structure of compound 30

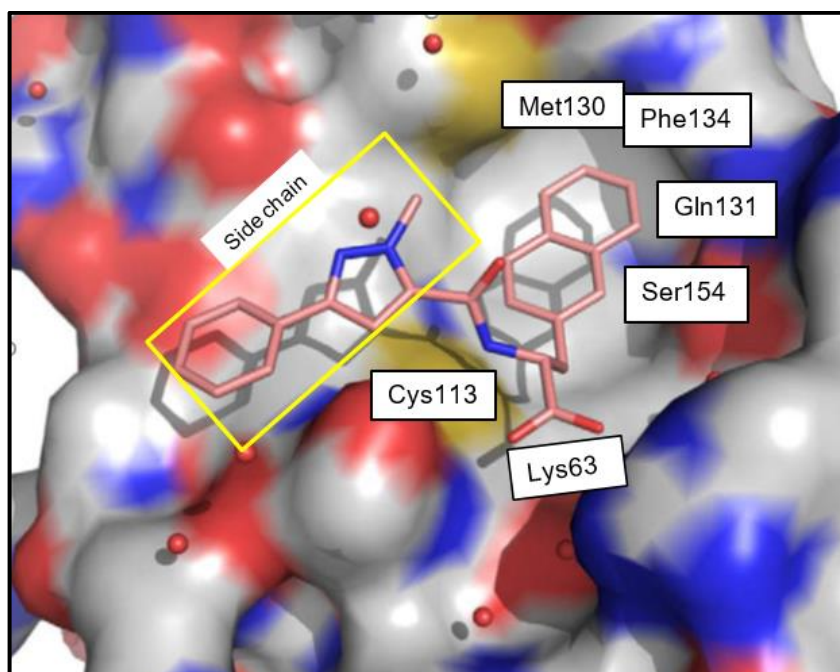


**Figure 3.14.** Crystal structure of a model molecule bound to Pin1 active site. The carboxyl group interacts with Lys63; the naphthyl substituent fixes into a 'shelf-like' hydrophobic plane

surface and the side chain makes a strong van der Waals contact with the hydrophobic pocket of the active site (Adapted from Potter et al.<sup>161</sup>).

Employing the same argument, the higher level of p53 nuclear localisation in the cells, shown by compound **32** (tyrosyl derivative) than compounds **30** and **33** (naphthyl and tryptophanyl derivatives respectively) may be due to additional H-bonding interaction of its OH group probably with some of the side chains in the 'shelf-like' flat hydrophobic surface in Pin1 active site. Conversely, the lack of measurable activity of compound **31** (the phenylalaninyl derivative) may be accounted for by the small size and non-polar nature of the phenyl group resulting probably in its hanging loosely over the flat hydrophobic surface.

#### 3.9.4 Synthesized molecules upregulate Bax protein expression in cancer cells

An attempted elucidation of the mechanisms by which the synthetic molecules trigger apoptotic cell death, led to examination of Bax protein expression in MDA-MB-231 cells using western blot (Figure 3.15a). Bax protein expression level was significantly higher in cells treated with compounds **30** and **32** than the control cells while it was lower in cells treated with compounds **31** and **33** than in the control (Figure 3.15b).

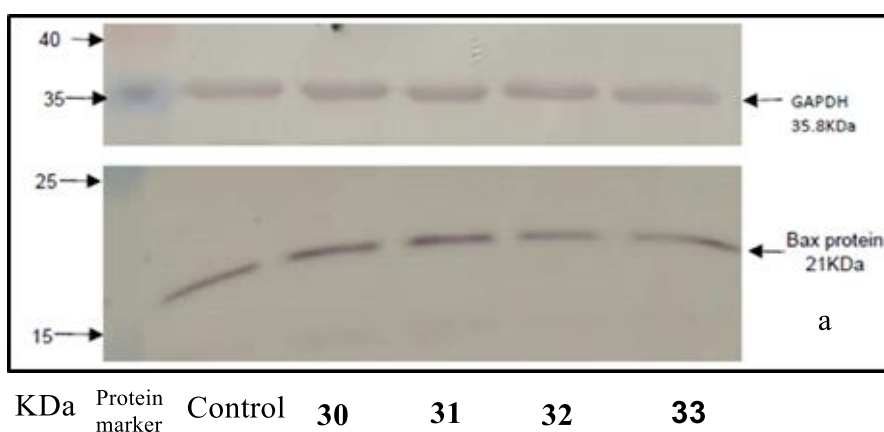


(Figure 3.15a)

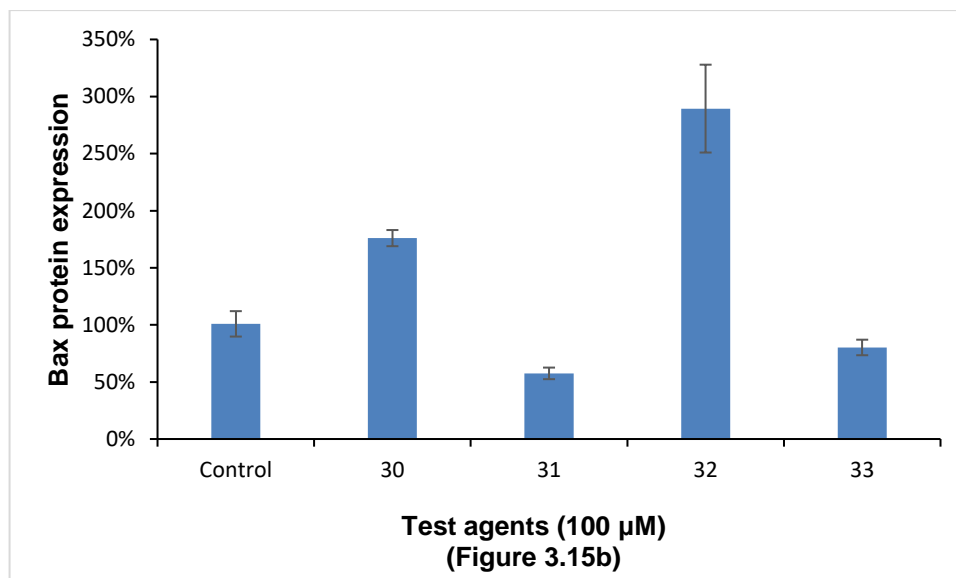


**Figure 3.15** Examination of expression of Bax protein in cells treated with compounds **30**, **31**, **32**, and **33**. MDA-MB-231 cells ( $10^5$ /wells) cultured in 12-well plates were treated with test reagents (100  $\mu$ M). The total protein was separated by SDS-PAGE. A mouse anti-human Bax antibody and anti-mouse HRP-conjugated antibody were used sequentially to probe the membranes for Bax protein. As loading control, the membrane was probed for GAPDH (see Figure 3.15a). The ImageJ program was used to normalise the amount of Bax protein against the corresponding GAPDH (Figure 3.15b). ( $n = 2$ ; expressed as  $\pm$  SD).

The Bax protein expression in cells treated with each of the molecules was measured by western blot 6 h post-treatment. Consequent to DNA damage or other stress stimuli, p53 protein upregulates expression of some genes involved in apoptotic pathways for regulation of apoptosis.<sup>163</sup> The proteins p21<sup>164</sup> and Bax<sup>165</sup>, are among the proteins upregulated by increase in p53 transcriptional activity. While p21 promotes arrest of cell cycle, Bax promotes apoptosis.

The following may explain the observation that expression of Bax protein in this study appeared to be increased in cells treated with compounds **30** and **32** while it decreased in those treated with compounds **31** and **33** compared to control cells (Figure 3.15b). Flores et al.<sup>166</sup> have lately unveiled a new understanding of the relationship between p53 and other related proteins including p63 and p73, in inducing apoptosis. Their investigation into the influence of the family members (p63 and p73) on p53 transcriptional activity

identified two distinct categories of target genes. While only p53 is enough to induce Mdm2 and p21, a cooperative action of p53, p63 and p73 is required to induce genes involved in cellular apoptosis such as *bax*, *nox*a and *PERP*. The report established that both p63 and p73 play a vital cooperative role with p53 in efficiently inducing p53-target apoptotic genes. Currently, the mechanism of the cooperative action of the triad is not known. Nonetheless, it might be suggested that all three proteins mutually promote complexation of the transcription complex to or stabilization on p53-target apoptotic genes.<sup>167</sup> The foregoing perhaps suggests that compounds **30** and **32** were able to induce considerable amount of p63 and p73 along with p53 while compounds **31** and **33** probably could not.

To validate the result of the Bax protein expression, the *bax* mRNA expression was examined by RT-PCR (the cycle graph is shown in Figure 3.16a). The *bax* mRNA expression in each sample was quantified from the PCR quantification data using the mathematical expression  $2^{-\Delta\Delta C_T}$  which represents the comparative  $C_T$  (threshold cycle) method<sup>149</sup> as shown in Table 3.5.

**Table 3.5.** Analysis of *bax* mRNA expression in samples treated with synthesized compounds

Treatment	$C_{T(bax)}$	$C_{T(\beta\text{-actin})}$	$\Delta C_T$ ( $C_{T(bax)} - C_{T(\beta\text{-actin})}$ )	$\Delta\Delta C_T$ ( $\Delta C_{T(\text{treated})} - \Delta C_{T(\text{control})}$ )	$2^{-\Delta\Delta C_T}$
<b>Control</b>	25.0	15.7	9.3	0	1
<b>30</b>	25.8	18.1	7.7	-1.6	3.03
<b>31</b>	22.2	18.2	4.0	-5.3	39.40
<b>32</b>	21.4	18.5	2.9	-6.4	84.44
<b>33</b>	26.2	18.8	7.4	-1.9	3.73

Expectedly, cells treated with compounds **30** and **32** showed significant *bax* mRNA expression (39 and 84 folds respectively) whereas in cells treated with **31** and **33** there was no appreciable *bax* mRNA expression compared to control cells (Figure 3.16b). This result shows that *bax* mRNA positively

correlates with p53, which suggests that p53 protein and *bax* gene are co-regulated in p53-mediated apoptosis.

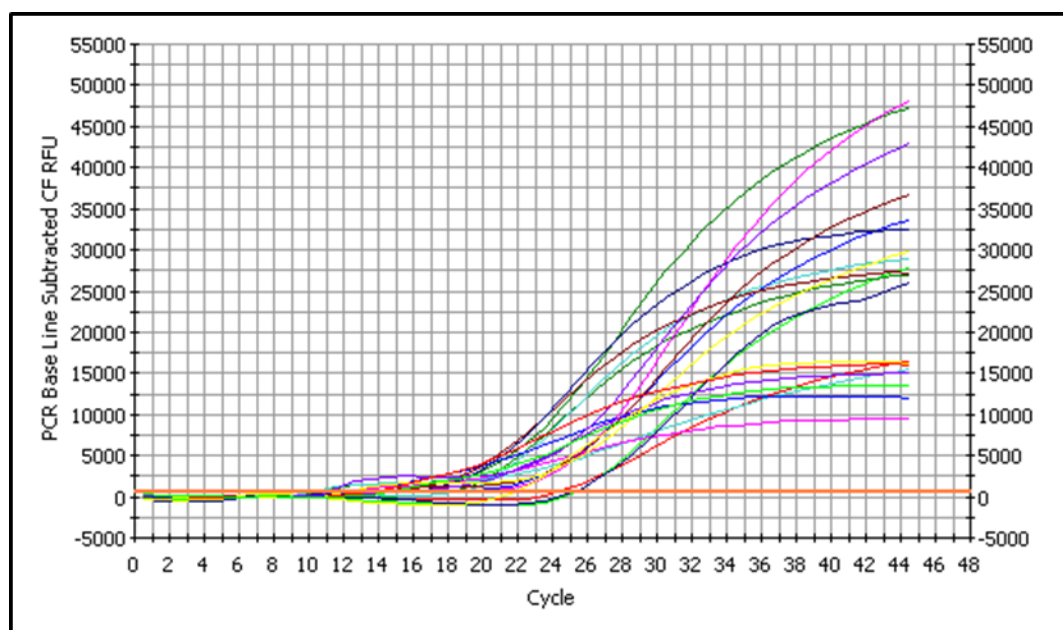


(Figure 3.16a)

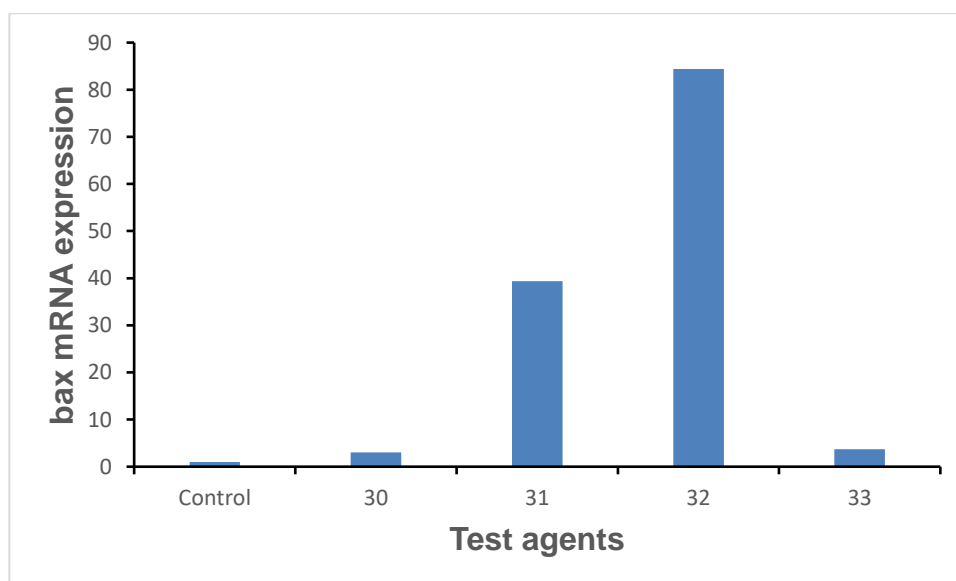


(Figure 3.16b)

**Figure 3.16.** Analysis of influence of test molecules on *bax* mRNA expression. MDA-MB-231 cells ( $10^5$ /well) cultured in 12-well plates were activated with the synthesized small molecule Pin1 inhibitors for 6 h. An untreated set of cells represented the negative control. Following isolation of total RNA 6 h post-activation, the relative *bax* mRNA expression was analysed by

*real time RT-PCR for Bax and  $\beta$ -actin amplification. The cycle graph shows PCR amplification of Bax and  $\beta$ -actin (Figure 3.16a). The cycle threshold ( $C_T$ ) values were normalised against the corresponding  $\beta$ -actin and the amount of bax mRNA expression in each sample was determined compared to the control cells (Figure 3.16b). (n = 1).*

Taken together, increased localisation of p53 to the nucleus was observed in MDA-MB-231 cells treated separately with the synthesized molecules **30**, **32** and **33**. Compounds **30** and **32**, caused an increase in bax protein expression with corresponding upregulation of *bax* mRNA expression by these compounds. However, cells treated with compounds **31** and **33** did not show measurable expression for both parameters.

### **3.10 CONCLUSION**

This study aimed to prepare synthetic metabolically stable mimics of pSer-Pro motif and to explore the ability of the molecules to inhibit Pin1. Previous studies identified transfection of cancer cells by the last eighteen amino acid residue of TF cytoplasmic domain (RKAGVGQSKENWSPLNVS) as capable of preventing cellular release of TF.<sup>80</sup> The resultant effect of this caused an accumulation of TF within the cell with consequential initiation of mechanisms that induce cell death.<sup>168</sup> It was further suggested that Ser253 and Ser258 phosphorylation in TF cytoplasmic domain regulates TF release while Pin1 was recognized to be the modulator of the phosphorylation in TF cytoplasmic domain.<sup>81</sup> A recent study also demonstrated that Pin1 enhances expression of TF by activating NF- $\kappa$ B and AP-1 signalling pathways in addition to interacting directly with TF through phosphorylated Ser258-Pro259 within the TF cytoplasmic domain.<sup>117</sup> These reports therefore prompted an investigation into inhibition of Pin1 with synthetic mimics of its specific substrate, pSer-Pro peptide. It was then hypothesized that inhibiting Pin1 with these synthetic mimics will prevent release of TF and consequently induce apoptosis. This strategy may result in novel intervention approaches for cancer therapy. Consequently, the initial step of this work involved preparation of methyl ester of proline using methanol and thionyl chloride approach, which resulted in methyl ester hydrochloride of proline and its analogues (**1 - 5**). Subsequent



coupling of the methyl ester **1** with serine analogues using amide coupling synthetic strategy resulted in dipeptides **6**, **7**, and **8**. However, preparation of Ser-Pro dipeptides with highly functionalised derivatives such as Boc-O-benzyl-L-Ser-Pro-OMe, and *N-Z-O-tert-butyl-L-Ser-Pro-OMe* was unsuccessful.

An attempt was made to prepare phosphoryl derivatives of the seryl-prolyl motif with electronegative atoms other than oxygen, such as nitrogen, with a view to producing comparatively stable phosphoamino acids at human physiological pH. Therefore, the N-analogue of serine was prepared using Zhang strategy<sup>157</sup>, which involved preparation of  $\beta$ -aminoalanine through a Hoffmann-type rearrangement of *N*<sup>z</sup>-protected asparagine, which was eventually coupled with proline ester (**1**) to give the dipeptide **14**. Unfortunately, all attempts to phosphorylate the dipeptides (particularly **6** and **14**) were unsuccessful. This therefore led to exploring synthetic strategies for preparation of a small molecule non-peptide Pin1 inhibitor **30** and establishment of three new derivatives (**31**, **32** and **33**) of the compound.

A preliminary investigation into the ability of the non-peptide small molecules to induce apoptosis was carried out using crystal violet staining (CVS) assay to determine the influence of the test compounds on cell proliferation. All the synthesized non-peptide molecules were capable of reducing cell number. Next, quantitative determination of cellular apoptosis based on fluorescent labelling of fragments of DNA (TUNEL assay) was analysed. In this study, incubation of cells with each of compounds **30-33** (100  $\mu$ M) for 24 h revealed that compounds **30** and **32** significantly induced apoptosis, **33** displayed moderate apoptotic cell death whereas **31** exhibited non-quantifiable apoptosis.

Localisation of p53 within the nucleus is crucial to the protein's transcriptional activity where it transactivates certain pro-apoptotic genes. Therefore, the effect of the synthesized molecules in promoting p53 localisation to the nucleus was examined. Activation of MDA-MB-231 cells with **32** resulted in significant nuclear localisation; **30** and **33** caused moderate localisation while **31** showed no detectable effect. In addition, the influence of the test compounds on Bax protein expression was assessed. Cells treated with compounds **30** and **32** expressed significantly higher level of Bax protein

whereas cells treated with **31** and **33** showed lower level of expression of the protein than the control cells. The expression of *bax* mRNA analysed by RT-PCR showed positive correlation with Bax protein expression because cells treated with **30** and **32** expressed significant *bax* mRNA while those treated with **31** and **33** showed insignificant *bax* mRNA expression compared to control cells.

Taken together, the result of the biological investigation revealed that **32** exhibited highest reduction in cell number, increase in p53 localisation within the nucleus and Bax protein expression relative to the control cells. Both **30** and **33** demonstrated lesser activity concerning the investigated cellular characteristics, however, **31** was mainly inactive.

It has been established that p53 is the chief regulator of arrest of cell cycle or apoptosis consequent to DNA damage; it plays a crucial role in preventing damaged DNA replication. During transition to G1-S phase or mitosis, p53 induces p21 to inhibit CDK activity for cell cycle arrest or activates caspases by proapoptotic proteins such as BAX and PUMA to induce apoptosis.<sup>169</sup> In addition, a body of research suggests that consequent upon DNA damage, Pin1 modulates functions of p53 through Pin1-catalysed isomerization to induce cell cycle checkpoints during cell cycle progression.<sup>170,171</sup> However, convincing evidence has demonstrated that the function of Pin1 is dependent on the level of its expression. Although its normal expression produce cell cycle arrest by increasing p53 transactivation activity and level of CDK inhibitor p21 protein, over-expression of Pin1 promotes cell proliferation and tumor progression.<sup>172</sup> Particularly in cancer, Pin1 is over-expressed because many cancers frequently deregulate the Rb-E2F pathway involved in regulating its expression.<sup>173</sup> Therefore, in cancer where overexpression of Pin1 results in cell proliferation and malignant growth, depletion of Pin1 both prevent tumor growth and promote tumor apoptosis. It was demonstrated in previous sections of this study that some of the synthesized non-peptide molecules moderate expression of p53 and other proapoptotic proteins to induce apoptosis through a mechanism believed to inhibit transcriptional activity of Pin1. Thus, this study has demonstrated successful synthesis of new derivatives of a known Pin1 inhibitor that can function probably as potential small molecule Pin1 inhibitor

and may prove to be beneficial in moderating TF procoagulant function and restraining the resulting increased tumor cell growth.

To take the study forward, further investigation into establishment of the ligand potency and binding mode of the synthesized molecules to Pin1 could be carried out using standard Mercedes-Camacho Pin1 binding assay methodology.<sup>174</sup> In addition, confirmation of the role Pin1 plays in phosphorylation of specific seryl-prolyl motifs within TF could be investigated using Pin1 mRNA-targeted siRNA; measurement of the phosphorylation of the specified motifs, TF release and apoptotic cell death. Furthermore, assessment of the ability of the synthesized molecules to interfere with mechanisms specific to cancer cells will be necessary.

# Bibliography

---

1 J. M. Bauca, E. Martinez-Morillo and E. P. Diamandis, *Clin. Chem.*, 2014, **60**, 1052-1061.

2 A. Eisenreich, A. Zakrzewicz, K. Huber, H. Thierbach, W. Pepke, P. Goldin-Lang, H. Schultheiss, A. Pries and U. Rauch, *Oncol. Rep.*, 2013, **30**, 462-470.

3 J. L. Yu, L. May, V. Lhotak, S. Shahrzad, S. Shirasawa, J. I. Weitz, B. L. Coomber, N. Mackman and J. W. Rak, *Blood*, 2005, **105**, 1734-1741.

4 F. Masoudkibir, N. Sarrafzadegan, C. Gotay, A. Ignaszewski, A. D. Krahn, M. K. Davis, C. Franco and A. Mani, *Atherosclerosis*, 2017, **263**, 343-351.

5 C. Tsai and R. Nussinov, *Sem. Cancer Bio.*, 2013, **23**(4), 235-242.

6 V. Lavanya, A. Mohamed Adil, N. Ahmed, A. Rishi and S. Jamal, *Integr. Cancer Sci. Therap.*, 2014, **1**, 39-46.

7 L. M. Merlo, J. W. Pepper, B. J. Reid and C. C. Maley, *Nat. Rev. Cancer*, 2006, **6**, 924-935.

8 M. Olivier, A. Petitjean, V. Marcel, A. Petre, M. Mounawar, A. Plymoth, C. De Fromentel and P. Hainaut, *Cancer Gene Ther.*, 2009, **16**, 1-12.

9 G. M. Cooper and R. E. Hausman, *The Cell: A Molecular Approach*. Sunderland (MA) 4<sup>th</sup> Edn., 2000.

- 10 S. J. Elledge, *Science*, 1996, **274**, 1664-1672.
- 11 S. L. Robbins and R. S. Cotran, *Pathologic Basis of Disease*, Saunders, New Delhi, 2004
- 12 D. Hanahan and R. A. Weinberg, *Cell*, 2000, **100**, 57-70.
- 13 D. Hanahan and R. A. Weinberg, *Cell*, 2011, **144**, 646-674.
- 14 E. Witsch, M. Sela and Y. Yarden, *Physiology*, 2010, **25**, 85-101.
- 15 M. Malumbres and M. Barbacid, *Nat. Rev. Cancer*, 2009, **9**, 153-166.
- 16 G. I. Evan and K. H. Vousden, *Nature*, 2001, **411**, 342-348.
- 17 J. Lopez and S. Tait, *Br. J. Cancer*, 2015, **112**, 957-962.
- 18 J. Koff, S. Ramachandiran and L. Bernal-Mizrachi, *Int. J. Mol. Sci.*, 2015, **16**, 2942-2955.
- 19 P. A. Perez-Mancera, A. R. Young and M. Narita, *Nat. Rev. Cancer*, 2014, **14**, 547-558.
- 20 J. W. Shay and W. E. Wright, *Nat. Rev. Mol. Cell Biol.*, 2000, **1**, 72-76.
- 21 C. Günes and K. L. Rudolph, *Cell*, 2013, **152**, 390-393.
- 22 J. Folkman, *N. Engl. J. Med.*, 1971, **285**, 1182-1186.
- 23 D. Hanahan and J. Folkman, *Cell*, 1996, **86**, 353-364.
- 24 G. Bergers and L. E. Benjamin, *Nat. Rev. Cancer*, 2003, **3**, 401-410.
- 25 J. E. Talmadge and I. J. Fidler, *Cancer Res.*, 2010, **70**, 5649-5669.

- 26 J. Massagué and A. C. Obenauf, *Nature*, 2016, **529**, 298-306.
- 27 M. G. Vander Heiden, L. C. Cantley and C. B. Thompson, *Science*, 2009, **324**, 1029-1033.
- 28 R. J. DeBerardinis and N. S. Chandel, *Fundamentals of cancer metabolism. Sci Adv* 2: e1600200, 2016.
- 29 N. N. Pavlova and C. B. Thompson, *Cell metabolism*, 2016, **23**, 27-47.
- 30 R. G. Jones and C. B. Thompson, *Genes Dev.*, 2009, **23**, 537-548.
- 31 M. Burnet, *Br. Med. J.*, 1957, **1**, 779-786
- 32 K. Malmberg, *Cancer Immunol. Immunother.*, 2004, **53**, 879-892.
- 33 J. Kravchenko, E. Corsini, M. A. Williams, W. Decker, M. H. Manjili, T. Otsuki, N. Singh, F. Al-Mulla, R. Al-Temaimi and A. Amedei, *Carcinogenesis*, 2015, **36**, S111-S127.
- 34 J. B. Gutiérrez and de Cerain Salsamendi, Adela López, *Fundamentos de ciencia toxicológica*, Ediciones Díaz de Santos, 2001.
- 35 W. K. Lutz, *Toxicol. Lett.*, 2002, **126**, 155-158.
- 36 T. Minamoto, M. Mai and Z. Ronai, *Cancer Detect. Prev.*, 2000, **24**, 1-12.
- 37 H. Ohshima, M. Tatemichi and T. Sawa, *Arch. Biochem. Biophys.*, 2003, **417**, 3-11.
- 38 H. Ohshima, H. Tazawa, B. S. Sylla and T. Sawa, *Mutation Research/Fundamental and Molecular Mechanisms of Mutagenesis*, 2005, **591**, 110-122.

- 39 W. M. Haschek, C. G. Rousseaux, M. A. Wallig, B. Bolon and R. Ochoa, *Haschek and Rousseaux's handbook of toxicologic pathology*, Academic Press, 2013.
- 40 P. A. Oliveira, A. Colaço, R. Chaves, H. Guedes-Pinto, P. De-La-Cruz, F. Luis and C. Lopes, *Anais da academia brasileira de ciências*, 2007, **79**, 593-616.
- 41 R. N. Proctor, *Nat. Rev. Cancer*, 2001, **1**, 82-86.
- 42 J. H. Weisburger and G. M. Williams, *Science*, 1981, **214**, 401-407.
- 43 J. Miller, *Origins of human cancer*, 1977, 605-627.
- 44 F. P. Guengerich, *Carcinogenesis*, 2000, **21**, 345-351.
- 45 B. K. Park, N. R. Kitteringham, J. L. Maggs, M. Pirmohamed and D. P. Williams, *Annu. Rev. Pharmacol. Toxicol.*, 2005, **45**, 177-202.
- 46 S. Mitchell and R. Smith, *Xenobiotica*, 2010, **40**, 301-305.
- 47 S. M. Cohen and L. L. Arnold, *Toxicol. I Sci.*, 2010, **120**, S76-S92.
- 48 A. Rundle, *Mutat. Res.*, 2006, **600**, 23-36.
- 49 S. M. Cohen, *Int. J. Toxicol.*, 1998, **17**, 129-142.
- 50 S. Kawanishi, Y. Hiraku, M. Murata and S. Oikawa, *Free Radical Biol. Med.*, 2002, **32**, 822-832.
- 51 Q. Zhang, K. Salnikow, T. Kluz, L. C. Chen, W. C. Su and M. Costa, *Toxicol. Appl. Pharmacol.*, 2003, **192**, 201-211.
- 52 J. E. Trosko, *Molecular Carcinogenesis: Published in cooperation with the University of Texas MD Anderson Cancer Center*, 2001, **30**, 131-137.

- 53 Y. Liu, T. Yin, Y. Feng, M. M. Cona, G. Huang, J. Liu, S. Song, Y. Jiang, Q. Xia, J. V. Swinnen, G. Bormans, U. Himmelreich, R. Oyen and Y. Ni, *Quant. Imaging Med. Surg.*, 2015, **5**, 708-729.
- 54 J. E. Trosko, *BMB Reports*, 2003, **36**, 43-48.
- 55 E. Shacter and S. A. Weitzman, *oncology-Williston Park then Huntington-*, 2002, **16**, 217-229.
- 56 L. A. Loeb and K. C. Cheng, *Mutat. Res.*, 1990, **238**, 297-304.
- 57 J. W. Grisham, W. K. Kaufmann and D. G. Kaufman, *Pathol. Immunopathol. Res.*, 1983, **1**, 49-66.
- 58 A. Luch, *Nat. Rev. Cancer*, 2005, **5**, 113-125.
- 59 J. E. Klaunig and L. M. Kamendulis, *Annu. Rev. Pharmacol. Toxicol.*, 2004, **44**, 239-267.
- 60 A. Poland, E. Glover and A. S. Kende, *J. Biol. Chem.*, 1976, **251**, 4936-4946.
- 61 D. W. Nebert, A. Puga and V. Vasiliou, *Ann. N. Y. Acad. Sci.*, 1993, **685**, 624-640.
- 62 J. Mimura and Y. Fujii-Kuriyama, *Biochim. Biophys. Acta (BBA)-Gen. Subj.*, 2003, **1619**, 263-268.
- 63 F. W. Frueh, K. C. Hayashibara, P. O. Brown and J. P. Whitlock Jr, *Toxicol. Lett.*, 2001, **122**, 189-203.
- 64 K. Dixon and E. Koprass, *Sem. Cancer Bio.* 2004.**14**(6), 441-448.
- 65 T. Hawighorst, P. Velasco, M. Streit, Y. K. Hong, T. R. Kyriakides, L. F. Brown, P. Bornstein and M. Detmar, *EMBO J.*, 2001, **20**, 2631-2640.
- 66 K. Golka, S. Kopps and Z. W. Myslak, *Toxicol. Lett.*, 2004, **151**,



203-210.

67 T. Wang, C. Chiou and Y. Chang, *Mutagenesis*, 1998, **13**, 405-408.

68 E. A. Lock, C. J. Reed, J. M. McMillan, J. E. Oatis Jr and R. G. Schnellmann, *Toxicology*, 2007, **230**, 234-243.

69 H. Shi, L. G. Hudson and K. J. Liu, *Free Radical Biol. Med.*, 2004, **37**, 582-593.

70 A. Hartwig, M. Asmuss, I. Ehleben, U. Herzer, D. Kostelac, A. Pelzer, T. Schwerdtle and A. Burkle, *Environ. Health Perspect.*, 2002, **110 Suppl 5**, 797-799.

71 M. Costa, Y. Yan, D. Zhao and K. Salnikow, *J. Environ. Monit.*, 2003, **5**, 222-223.

72 C. Wild, R. Garner, R. Montesano and F. Tursi, *Carcinogenesis*, 1986, **7**, 853-858.

73 R. Hasegawa, M. Futakuchi, Y. Mizoguchi, T. Yamaguchi, T. Shirai, N. Ito and W. Lijinsky, *Cancer Lett.*, 1998, **123**, 185-191.

74 C. Milsom, N. Magnus, B. Meehan, K. Al-Nedawi, D. Garnier and J. Rak, *Arterioscler. Thromb. Vasc. Biol.*, 2009, **29**, 2005-2014.

75 D. Garnier, C. Milsom, N. Magnus, B. Meehan, J. Weitz, J. Yu and J. Rak, *Thromb. Res.*, 2010, **125**, S44-S50.

76 M. Guan, J. Jin, B. Su, W. W. Liu and Y. Lu, *Clin. Biochem.*, 2002, **35**, 321-325.

77 M. Åberg and A. Siegbahn, *J. Thromb. Haemost.*, 2013, **11**, 817-825.

78 B. M. Mueller and W. Ruf, *J. Clin. Invest.*, 1998, **101**, 1372-1378.

- 79 W. Ruf, *Tissue factor signaling in hemostasis*, Amer Soc Hematology 1200 19th ST, NW, STE 300, Washington, DC 20036-2422 USA, 1999.
- 80 M. E. Collier and C. Ettelaie, *J. Biol. Chem.*, 2011, **286**, 11977-11984.
- 81 C. Ettelaie, M. E. Collier, S. Featherby, J. Greenman and A. Maraveyas, *Biochim. Biophys. Acta (BBA)-Mol. Cell Res.*, 2018, **1865**, 12-24.
- 82 M. M. Fiore, P. F. Neuenschwander and J. H. Morrissey, *J. Biol. Chem.*, 1994, **269**, 143-149.
- 83 E. K. Spicer, R. Horton, L. Bloem, R. Bach, K. R. Williams, A. Guha, J. Kraus, T. C. Lin, Y. Nemerson and W. H. Konigsberg, *Proc. Natl. Acad. Sci. U. S. A.*, 1987, **84**, 5148-5152.
- 84 A. J. Chu, *Int. J. Inflam.*, 2011, **201**, 1-30.
- 85 M. Clauss, M. Gerlach, H. Gerlach, J. Brett, F. Wang, P. C. Familletti, Y. C. Pan, J. V. Olander, D. T. Connolly and D. Stern, *J. Exp. Med.*, 1990, **172**, 1535-1545.
- 86 T. Ueno, M. Toi, M. Koike, S. Nakamura and T. Tominaga, *Br. J. Cancer*, 2000, **83**, 164-170.
- 87 I. Depasquale and W. Thompson, *Histopathology*, 2008, **52**, 500-509.
- 88 A. A. Khorana, S. A. Ahrendt, C. K. Ryan, C. W. Francis, R. H. Hruban, Y. C. Hu, G. Hostetter, J. Harvey and M. B. Taubman, *Clin. Cancer Res.*, 2007, **13**, 2870-2875.
- 89 S. Seto, H. Onodera, T. Kaido, A. Yoshikawa, S. Ishigami, S. Arii and M. Imamura, *Cancer: Interdisciplinary Int. J. Am. Cancer Soc.*, 2000, **88**, 295-301.

- 90 B. Sanchez-Solana, M. Motwani, D. Q. Li, J. Eswaran and R. Kumar, *J. Biol. Chem.*, 2012, **287**, 39291-39302.
- 91 M. Hojjat-Farsangi, *Int. J. Mol. Sci.*, 2014, **15**, 13768-13801.
- 92 M. Hojjat-Farsangi, *J. Drug Target.*, 2016, **24**, 192-211.
- 93 M. Shabani and M. Hojjat-Farsangi, *Curr. Drug Targets*, 2016, **17**, 1687-1703.
- 94 K. Imai and A. Takaoka, *Nat. Rev. Cancer*, 2006, **6**, 714-727.
- 95 P. Gill, A. Grothey and C. Loprinzi, in *Oncology*, ed. A. E. Chang, Springer, 2006, p. 1482-1496.
- 96 R. Roskoski Jr, *Pharmacol. Res.*, 2015, **100**, 1-23.
- 97 B. Escudier and M. Gore, *Drugs in R & D*, 2011, **11**, 113-126.
- 98 J. E. Cortes, D. W. Kim, H. M. Kantarjian, T. H. Brummendorf, I. Dyagil, L. Griskevicius, H. Malhotra, C. Powell, K. Gogat, A. M. Countouriotis and C. Gambacorti-Passerini, *J. Clin. Oncol.*, 2012, **30**, 3486-3492.
- 99 H. Y. Zou, Q. Li, J. H. Lee, M. E. Arango, S. R. McDonnell, S. Yamazaki, T. B. Koudriakova, G. Alton, J. J. Cui, P. P. Kung, M. D. Nambu, G. Los, S. L. Bender, B. Mroczkowski and J. G. Christensen, *Cancer Res.*, 2007, **67**, 4408-4417.
- 100 P. J. Houghton, *Clin. Cancer Res.*, 2010, **16**, 1368-1372.
- 101 M. H. Cohen, G. A. Williams, R. Sridhara, G. Chen and R. Pazdur, *Oncologist*, 2003, **8**, 303-306.
- 102 M. H. Cohen, G. Williams, J. R. Johnson, J. Duan, J. Gobburu, A. Rahman, K. Benson, J. Leighton, S. K. Kim, R. Wood, M. Rothmann, G. Chen, K. M. U, A. M. Staten and R. Pazdur, *Clin. Cancer Res.*, 2002, **8**, 935-942.

- 103 B. Moy, P. Kirkpatrick, S. Kar and P. Goss, *Nat. Rev. Drug Discov*, 2007, **6**, 431-432.
- 104 E. Weisberg, P. Manley, J. Mestan, S. Cowan-Jacob, A. Ray and J. Griffin, *Br. J. Cancer*, 2006, **94**, 1765.
- 105 P. Schöffski, *Expert Rev. Anticancer Ther*, 2012, **12**, 711-723.
- 106 L. Lang, *Gastroenterology*, 2008, **134**, 379-379.
- 107 R. C. Kane, P. F. Bross, A. T. Farrell and R. Pazdur, *Oncologist*, 2003, **8**, 508-513.
- 108 J. R. Berenson, J. D. Hilger, O. Yellin, R. Dichmann, D. Patel-Donnelly, R. V. Boccia, A. Bessudo, L. Stampleman, D. Gravenor and S. Eshaghian, *Leukemia*, 2014, **28**, 1529.
- 109 S. Wojtowicz-Praga, J. Low, J. Marshall, E. Ness, R. Dickson, J. Barter, M. Sale, P. McCann, J. Moore and A. Cole, *Invest. New Drugs*, 1996, **14**, 193-202.
- 110 B. Fingleton, *Curr. Pharm. Des.*, 2007, **13**, 333-346.
- 111 D. Bissett, K. J. O'Byrne, J. Von Pawel, U. Gatzemeier, A. Price, M. Nicolson, R. Mercier, E. Mazabel, C. Penning and M. H. Zhang, *J. Clin. Oncol*, 2004, **23**, 842-849.
- 112 N. B. Leighl, L. Paz-Ares, J. Douillard, C. Peschel, A. Arnold, A. Depierre, A. Santoro, D. C. Betticher, U. Gatzemeier and J. Jassem, *J. Clin. Oncol*, 2005, **23**, 2831-2839.
- 113 M. Konopleva, J. Watt, R. Contractor, T. Tsao, D. Harris, Z. Estrov, W. Bornmann, H. Kantarjian, J. Viallet, I. Samudio and M. Andreeff, *Cancer Res.*, 2008, **68**, 3413-3420.
- 114 H. Xiong, R. S. Pradhan, A. Nada, A. P. Krivoshik, K. D. Holen, J. W. Rhodes, G. B. Gordon, R. Humerickhouse and W. M. Awani,

*Anticancer Res.*, 2014, **34**, 3739-3746.

115 G. Patry, H. Hovington, H. Larue, F. Harel, Y. Fradet and L. Lacombe, *Int. J. cancer*, 2008, **122**, 1592-1597.

116 H. Chand and W. Kisiel, *J. Thromb. Haemost*, 2007, **5**, 640-641.

117 K. Kurakula, D. S. Koenis, M. A. Herzik Jr, Y. Liu, J. W. Craft Jr, P. B. van Loenen, M. Vos, M. K. Tran, H. H. Versteeg, M. T. H. Goumans, W. Ruf, C. J. M. de Vries and M. Sen, *Haematologica*, 2018, **103**, 1073-1082.

118 H. H. Versteeg, J. W. Heemskerk, M. Levi and P. H. Reitsma, *Physiol. Rev.*, 2013, **93**, 327-358.

119 U. Schönbeck, F. Mach, G. K. Sukhova, M. Herman, P. Graber, M. R. Kehry and P. Libby, *Am. J. Pathol.*, 2000, **156**, 7-14.

120 C. Behrsin, M. Bailey, K. Bateman, K. Hamilton, L. Wahl, C. Brandl, B. Shilton and D. Litchfield, *J. Mol. Biol.*, 2007, **365**, 1143-1162.

121 G. Wulf, G. Finn, F. Suizu and K. P. Lu, *Nat. Cell Biol.*, 2005, **7**, 435-441.

122 A. Amirkhosravi, T. Meyer, J. Chang, M. Amaya, F. Siddiqui, H. Desai and J. L. Francis, *Thromb. Haemost*, 2002, **87**, 930-936.

123 K. P. Lu, G. Finn, T. H. Lee and L. K. Nicholson, *Nat. Chem. Biol.*, 2007, **3**, 619-629.

124 K. P. Lu, S. D. Hanes and T. Hunter, *Nature*, 1996, **380**, 544-547.

125 R. Ranganathan, K. P. Lu, T. Hunter and J. P. Noel, *Cell*, 1997, **89**, 875-886.

- 126 M. Zhang, X. J. Wang, X. Chen, M. E. Bowman, Y. Luo, J. P. Noel, A. D. Ellington, F. A. Etzkorn and Y. Zhang, *ACS Chem. Biol.*, 2012, **7**, 1462-1470.
- 127 J. W. Werner-Allen, C. J. Lee, P. Liu, N. I. Nicely, S. Wang, A. L. Greenleaf and P. Zhou, *J. Biol. Chem.*, 2011, **286**, 5717-5726
- 128 S. F. Göthel and M. Marahiel, *Cell. Mol. Life Sci.*, 1999, **55**, 423-436.
- 129 Y. Zhang, S. Daum, D. Wildemann, X. Z. Zhou, M. A. Verdecia, M. E. Bowman, C. Lücke, T. Hunter, K. Lu and G. Fischer, *ACS Chem. Biol.*, 2007, **2**, 320-328.
- 130 X. Tan, F. Zhou, J. Wan, J. Hang, Z. Chen, B. Li, C. Zhang, K. Shao, P. Jiang and S. Shi, *Cancer Biol. Ther.*, 2010, **9**, 111-119.
- 131 L. Bao, A. Kimzey, G. Sauter, J. M. Sowadski, K. P. Lu and D. Wang, *Am. J. Pathol.*, 2004, **164**, 1727-1737.
- 132 T. Sasaki, A. Ryo, H. Uemura, H. Ishiguro, Y. Inayama, S. Yamanaka, Y. Kubota, Y. Nagashima, M. Harada and I. Aoki, *Pathol. Res. Pract.*, 2006, **202**, 357-364.
- 133 K. Leung, C. Tsai, M. Hsiao, C. Tseng, L. Ger, K. Lee and P. Lu, *Oncol. Rep.*, 2009, **21**, 1097-1104.
- 134 H. Miyashita, T. Uchida, S. Mori, S. Echigo and K. Motegi, *Oncol. Rep.*, 2003, **10**, 1045-1048.
- 135 J. D. Moore and A. Potter, *Bioorg. Med. Chem. Lett.*, 2013, **23**, 4283-4291.
- 136 M. Hidaka, K. Kosaka, S. Tsushima, C. Uchida, K. Takahashi, N. Takahashi, M. Tsubuki, Y. Hara and T. Uchida, *Biochem. Biophys. Res. Commun.*, 2018, **499**, 681-687.

- 137 L. Hennig, C. Christner, M. Kipping, B. Schelbert, K. P. Rücknagel, S. Grabley, G. Küllertz and G. Fischer, *Biochemistry*, 1998, **37**, 5953-5960.
- 138 T. Uchida, M. Takamiya, M. Takahashi, H. Miyashita, H. Ikeda, T. Terada, Y. Matsuo, M. Shirouzu, S. Yokoyama and F. Fujimori, *Chem. Biol.*, 2003, **10**, 15-24.
- 139 X. J. Wang, B. Xu, A. B. Mullins, F. K. Neiler and F. A. Etzkorn, *J. Am. Chem. Soc.*, 2004, **126**, 15533-15542.
- 140 S. Wei, S. Kozono, L. Kats, M. Nechama, W. Li, J. Guarnerio, M. Luo, M. You, Y. Yao and A. Kondo, *Nat. Med.*, 2015, **21**, 457-466.
- 141 L. Dong, J. Marakovits, X. Hou, C. Guo, S. Greasley, E. Dagostino, R. Ferre, M. C. Johnson, E. Kraynov and J. Thomson, *Bioorg. Med. Chem. Lett.*, 2010, **20**, 2210-2214.
- 142 A. Potter, V. Oldfield, C. Nunns, C. Fromont, S. Ray, C. J. Northfield, C. J. Bryant, S. F. Scrace, D. Robinson and N. Matossova, *Bioorg. Med. Chem. Lett.*, 2010, **20**, 6483-6488.
- 143 J. Marsolier, M. Perichon, J. DeBarry, B. Villoutreix, J. Chluba, T. Lopez, C. Garrido, X. Zhou, K. Lu and L. Fritsch, *Nature*, 2015, **520**, 378-382.
- 144 D. V. Urusova, J. H. Shim, D. J. Kim, S. K. Jung, T. A. Zykova, A. Carper, A. M. Bode and Z. Dong, *Cancer. Prev. Res. (Phila)*, 2011, **4**, 1366-1377.
- 145 S. M. Jones, J. E. Urch, M. Kaiser, R. Brun, J. L. Harwood, C. Berry and I. H. Gilbert, *J. Med. Chem.*, 2005, **48**, 5932-5941.
- 146 L. Audrieth and M. Sveda, *J. Org. Chem.*, 1944, **9**, 89-101.
- 147 A. L. Wilds and T. L. Johnson, *J. Am. Chem. Soc.*, 1945, **67**,

286-290

148 G. C. Porretta, M. Scalzo, F. Chimenti, A. Bolasco, M. Biava, M. Fischetti and F. Riccardi, *Farmaco Sci.*, 1987, **42**, 629-639.

149 K. J. Livak and T. D. Schmittgen, *Methods*, 2001, **25**, 402-408.

150 C. Ettelaie, M. E. Collier, S. Featherby, N. E. Benelhaj, J. Greenman and A. Maraveyas, *Thromb. J.*, 2016, **14**, 2.

151 G. C. Barrett, *R. S. C. Publications: London*, 1996, **27**, 1.

152 G. A. Pher, G. David and T. David, *J. Org. Chem.*, 1997, **62**, 7364-7375.

153 M. J. Simon, E. U. Jonathan, K. Marcel, B. Reto, L. H. John, B. Colin and H. G. Ian, *J. Med. Chem.*, 2005, **48**, 5932-5941.

154 J. Li and Y. Sha, *Molecules*, 2008, **13**, 1111-1119.

155 A. Williams and I. T. Ibrahim, *Chem. Rev.*, 1981, **81**, 589-636.

156 B. Duclos, S. Marcandier and A. J. Cozzone, in *Methods in enzymology*, ed. Academic Press, Elsevier, 1991, p. 10-21.

157 L. Zhang, G. S. Kauffman, J. A. Pesti and J. Yin, *J. Org. Chem.*, 1998, **63**, 10085.

158 A. K. Sinhababu and D. R. Thakker, *Adv. Drug Deliv. Rev.*, 1996, **19**, 241-273.

159 C. Schultz, *Bioorg. Med. Chem.*, 2003, **11**, 885-898.

160 J. W. Perich and R. Johns, *Synthesis*, 1988, **1988**, 142-144.

161 A. J. Potter, S. Ray, L. Gueritz, C. L. Nunns, C. J. Bryant, S. F. Scrace, N. Matassova, L. Baker, P. Dokurno and D. A. Robinson, A. E. Surgenor, B. Davis, J. B. Murray, C. M. Richardson and J. D.



- Moore, *Bioorg. Med. Chem. Lett.*, 2010, **20**, 586-590.
- 162 A. Ryo, H. Uemura, H. Ishiguro, T. Saitoh, A. Yamaguchi, K. Perrem, Y. Kubota, K. P. Lu and I. Aoki, *Clin. Cancer Res.*, 2005, **11**, 7523-7531
- 163 J. Chipuk and D. Green, *Cell Death Differ.*, 2006, **13**, 994-1002.
- 164 A. J. Levine, *Cell*, 1997, **88**, 323-331
- 165 W. S. El-Deiry, T. Tokino, V. E. Velculescu, D. B. Levy, R. Parsons, J. M. Trent, D. Lin, W. E. Mercer, K. W. Kinzler and B. Vogelstein, *Cell*, 1993, **75**, 817-825.
- 166 E. R. Flores, K. Y. Tsai, D. Crowley, S. Sengupta, A. Yang, F. McKeon and T. Jacks, *Nature*, 2002, **416**, 560-564.
- 167 M. Urist and C. Prives, *Cancer Cell*, 2002, **1**, 311-313.
- 168 A. Pradier and C. Ettelaie, *J. Vasc. Res.*, 2008, **45**, 19-32
- 169 M. Fischer, *Oncogene*, 2017, **36**, 3943-3956.
- 170 M. Berger, N. Stahl, G. Del Sal and Y. Haupt, *Mol. Cell. Biol.*, 2005, **25**, 5380-5388.
- 171 P. Zacchi, M. Gostissa, T. Uchida, C. Salvagno, F. Avolio, S. Volinia, Z. Ronai, G. Blandino, C. Schneider and G. Del Sal, *Nature*, 2002, **419**, 853-857.
- 172 C. Cheng, A. K. Chow, R. Pang, E. W. Fok, Y. Kwong and E. Tse, *Am. J. pathol.*, 2013, **182**, 765-775.
- 173 Y. Tong, H. Ying, R. Liu, L. Li, J. Bergholz and Z. Xiao, *Cell death & disease*, 2015, **6**, e1640-e1652.
- 174 A. Y. Mercedes-Camacho and F. A. Etzkorn, *Anal. Biochem.*, 2010, **402**, 77-82

